



**HAL**  
open science

## Structural studies of the *Staphylococcus aureus* ribosome

Iskander Khusainov

► **To cite this version:**

Iskander Khusainov. Structural studies of the *Staphylococcus aureus* ribosome. Biophysics. Université de Strasbourg, 2015. English. NNT : 2015STRAJ071 . tel-01403855

**HAL Id: tel-01403855**

**<https://theses.hal.science/tel-01403855>**

Submitted on 28 Nov 2016

**HAL** is a multi-disciplinary open access archive for the deposit and dissemination of scientific research documents, whether they are published or not. The documents may come from teaching and research institutions in France or abroad, or from public or private research centers.

L'archive ouverte pluridisciplinaire **HAL**, est destinée au dépôt et à la diffusion de documents scientifiques de niveau recherche, publiés ou non, émanant des établissements d'enseignement et de recherche français ou étrangers, des laboratoires publics ou privés.

**ÉCOLE DOCTORALE des Sciences de la Vie et de la Santé**

**IGBMC - CNRS UMR 7104 - Inserm U 964**

**THÈSE** présentée par :

**Iskander KHUSAINOV**

soutenue le : **27 Novembre 2015**

pour obtenir le grade de : **Docteur de l'université de Strasbourg**

Discipline/ Spécialité : **Biophysique et biologie structurale**

(Biophysics and Structural biology)

**Structural studies of the  
*Staphylococcus aureus* ribosome**

**Etudes structurales du ribosome de  
*Staphylococcus aureus***

**THÈSE dirigée par :**

**M. YUSUPOV Marat**

**Mme. YUSUPOVA Gulnara**

Directeur de recherche, Université de Strasbourg

Directeur de recherche, Université de Strasbourg

**RAPPORTEURS :**

**M. JENNER Lasse B.**

**M. MECHULAM Yves**

Associate Professor, Aarhus University (Denmark)

Directeur de recherche, École Polytechnique (Paris)

---

**AUTRES MEMBRES DU JURY :**

**M. GEISSMANN Thomas**

**M. MARZI Stefano**

Chargé de recherches, ENS de Lyon (Lyon)

Chargé de recherches, Université de Strasbourg

## ACKNOWLEDGEMENTS

First of all I would like to thank all jury members, Dr. Yves Mechulam, Dr. Lasse Bohl Jenner, Dr. Thomas Geissmann and Dr. Stefano Marzi who agreed to evaluate my PhD work. I am extremely thankful to meet them in Strasbourg and to discuss.

I would like to express my sincere gratitude to my advisors, Gula and Marat for their constant support and patience, for their motivation, advice and confidence. I am thankful to them for giving me the opportunity to learn many different methods of biochemistry and structural analysis in the laboratory. Every single day I learn something new here. Working in Marat's and Gula's laboratories is a priceless experience.

This work would not be complete without electron microscopy involvement. I express my gratitude to our collaborator Yaser Hashem with whom we obtained the first structure of Staphylococcus ribosome; and to Alex Myasnikov for his significant contribution in cryo-EM data collection and helpful discussions. Special regards to Dr. Pascale Romby. It is always a pleasure to discuss with her and to get a fresh view on the project.

I am thankful to the structural biology platform of IGBMC: Catherine, Pierre and Alastair, who taught me a lot of techniques of biophysics and crystallization. In addition, I thank Prof. Richard Beckett and Dr. Farida Minibayeva for patiently correcting my thesis and bringing it to its presentable form.

Now it is a good time to thank all of my colleagues who made me feel comfortable here. First, I want to cordially thank two people: Sergey, whose endless enthusiasm and striking erudition inspired me to move forward from day to day; and Natasha, who helped me to not get lost in the ribosome world during my first year. Gracias/Grazie to my eEF2 team Eduardo and Simone. These two people present an unbelievable combination of experience, knowledge, curiosity, diligence, belief and reasonable skepticism that make them extremely nice companions. And particular credits to Alexey of course. Always strict, always straightforward, sometimes sarcastic but never disingenuous, he made our synchrotron trips very special. Many thanks to our French teammates Justine, Mélanie, David. Thanks to them, I knew more about French culture, cuisine, and most importantly, they were always helpful with the French language and administration duties. And many thanks to all the present and former members of our lab, Irina, Yuzuru, Marie, Daniya, Muminjon, Jean-Paul, Raphaël, Nico, Sylvie, Lasse, Liudmila, for their support and friendly atmosphere in the laboratory.

Besides work in the laboratory, we had a great time outside IGBMC. First, I would like to thank our Eastern Union team Anna and Kate. We met here during the interview and kept the friendship over the whole PhD. I appreciate the hospitality of Ben and Damien, who showed us Strasbourg and helped with integration into the French life during first year. I am grateful to Nico and Claire, Firas and Irene, Marie and G erald, Irina, Anna, Kate, Karima, Heena, Shilpy, Alexey, Vova, Grigory, Valerio, Xavi, Ismail, Xieyang and others for the unforgettable moments and adventures that we had together: *via ferrata* in Jura, opera in Dijon, ski in the Alps, board games at Alexey's place, crazy night bike trip along the Rhine and many others. I would like to thank all the members of SPB and personally Michel who always gave me a hand when I asked. Many thanks to my friends in Kazan - Aidar, Igor, Sergey and Olga. It is always a pleasure to come to the hometown and meet them there.

Most importantly, I would like to thank my family. I am very grateful to my parents Rezeda and Shamil who accepted my wish to come to France with understanding. To my aunt Farida, who showed me the beauty of science and biology when I was child; and to my grandmother Jasmina, who patiently listens to all my stories about synchrotrons, diffraction and gives a good advice when I need one. I am also grateful to my brother Farid and my niece Rushaniya with whom we spent a great time in Saint-Petersburg this year. I am very happy to have such an adorable family!

My PhD thesis has been possible only because of constant support and participation of all the people mentioned above. I've never walked alone. Thank you very much!

## TABLE OF CONTENTS

<b>ACKNOWLEDGEMENTS</b> .....	2
<b>TABLE OF CONTENTS</b> .....	4
<b>TABLE OF FIGURES AND TABLES</b> .....	6
<b>SUMMARY</b> .....	8
<b>RÉSUMÉ DE THÈSE</b> .....	12
<b>ABBREVIATIONS</b> .....	22
<b>INTRODUCTION</b> .....	22
<b>THE RIBOSOME</b> .....	25
Core of the ribosome.....	25
Specifications of bacterial and eukaryotic ribosome .....	26
Protein synthesis .....	27
Structural studies of the ribosome .....	29
<b>STAPHYLOCOCCUS AUREUS</b> .....	34
Main characteristics of <i>S. aureus</i> .....	34
Virulence determinants.....	35
<i>S. aureus</i> - superbug .....	38
Antibiotic resistance of <i>S. aureus</i> .....	39
Mechanisms of antibiotics action and bacterial resistance. ....	40
Current drugs used in treatment of <i>S. aureus</i> diseases .....	44
<i>S. aureus</i> ribosome as a target for new antibiotics .....	49
<b>TRANSLATION ELONGATION FACTORS</b> .....	50
Translation elongation cycle.....	50
eEF2 is a potential target for drug development .....	54
<b>PROJECT OUTLINE</b> .....	55
<b>RESEARCH PROJECT 1. STRUCTURE DETERMINATION OF <i>S. AUREUS</i> RIBOSOME</b> .....	51
<b><i>S. AUREUS</i> CELL GROWTH</b> .....	58
<i>S. aureus</i> strain .....	58
Cells preparation .....	58
<b>RIBOSOMES PURIFICATION</b> .....	59
Buffers .....	60
Lysis .....	60
PEG precipitation and sucrose cushion .....	61
Sucrose density gradient centrifugation .....	61

Ribosome concentration and storage .....	62
<b>RIBOSOMES CHARACTERIZATION</b> .....	63
One- and two-dimensional polyacrylamide gel electrophoresis (PAGE).....	63
Agarose gel electrophoresis .....	64
Analytical sucrose density gradient centrifugation.....	64
Analytical ultracentrifugation.....	67
Mass spectrometry.....	67
<b>CRYSTALLOGRAPHIC STUDIES OF <i>S. AUREUS</i> RIBOSOME</b> .....	70
Why x-rays and why crystals?.....	70
Macromolecular crystallization in theory.....	71
Macromolecular crystallization in practice .....	73
Crystallization of <i>S. aureus</i> ribosome .....	76
Post-crystallization treatment .....	82
Post-crystallization treatment of <i>S. aureus</i> ribosome crystals.....	83
X-ray data collection.....	86
<b>CRYO-EM STRUCTURE DETERMINATION OF <i>S. AUREUS</i> RIBOSOME</b> .....	89
Latest improvements in cryo-EM .....	89
Electron microscope organization.....	90
Sample preparation and data collection .....	92
Image processing for single particle cryo-EM .....	94
<b>RESEARCH PROJECT 1: SUMMARY</b> .....	105
<b>RESEARCH PROJECT 2. PURIFICATION AND CRYSTALLIZATION OF HUMAN eEF2</b> .....	100
<b>PURIFICATION AND CRYSTALLIZATION OF HUMAN eEF2 PROTEIN</b> .....	107
HeLa cells preparation.....	107
Purification of native eEF2.....	107
Characterization of human eEF2. ....	110
Crystallization of human eEF2. ....	112
Diffraction experiment .....	113
Cloning of human eEF2.....	114
<b>RESEARCH PROJECT 2: SUMMARY</b> .....	119
<b>DISCUSSION</b> .....	121
<b>PERSPECTIVES</b> .....	125
<b>REFERENCES</b> .....	126

**TABLE OF FIGURES AND TABLES**

FIGURES:

**Figure 1.** Structural organization and functional sites of the ribosome ..... 25

**Figure 2.** Composition of bacterial and eukaryotic ribosomes and the common core, based on x-ray studies..... 27

**Figure 3.** Schematic diagram of bacterial protein synthesis ..... 28

**Figure 4.** Regulation network of production of virulence factors in *S. aureus*..... 36

**Figure 5.** Rnalll secondary structure ..... 38

**Figure 6.** Antibacterial resistance mechanisms ..... 41

**Figure 7.** Antibiotics targeting sites during protein synthesis ..... 43

**Figure 8.** Antibiotics susceptibility profiles of *S. aureus*.. ..... 51

**Figure 10.** The structures of apo eEF2, ef-g in complex with GDP, sordarin, enterotoxin a ..... 53

**Figure 11.** Sucrose gradient profile of *S. aureus* ribosome sample ..... 62

**Figure 12.** One-dimensional and two-dimensional SDS-PAGE, agarose gel of *S. aureus* ribosome sample.. ..... 64

**Figure 13.** Characterization of *S. aureus* ribosomes sample by sucrose density gradient centrifugation ..... 66

**Figure 14.** Sedimentation profile of *S. aureus* ribosome sample. .... 67

**Figure 15.** Schematic representation of diffraction experiment..... 71

**Figure 16.** Schematic phase diagram of protein crystallization. .... 72

**Figure 17.** Idealized phase diagrams showing the trajectories of three different crystallization methods, vapour-diffusion, batch and liquid-diffusion ..... 75

**Figure 18.** Crystals of *S. aureus* 70S ribosome..... 81

**Figure 19.** Scheme of post-crystallization treatment ..... 85

**Figure 20.** Crystals cracked during post crystallization treatment. .... 85

**Figure 21.** Diffraction patterns of different crystals ..... 88

**Figure 22.** Schematic representation of basic composition of an electron microscope..... 91

**Figure 23.** Scattering of the electrons by atom. .... 91

**Figure 24.** Representation of the cryo-EM grid at different scales ..... 92

**Figure 25.** Electron micrograph of the vitrified *S. aureus* 70S ribosome sample taken on the F-30 polara microscope.. ..... 93

**Figure 26.** Processing of *S. aureus* ribosome cryo-EM images taken at different defocus ..... 96

**Figure 27.** Schematic and idealized representation of particle extraction and 3D reconstruction .. 97

**Figure 28.** Schematic representation of 3D classification of *S. aureus* ribosome dataset..... 98

**Figure 29.** Resolution curve of cryo-em structure reconstruction after 3D auto-refinement and post-processing ..... 99

**Figure 30.** Local resolution map of *S. aureus* ribosome ..... 100

**Figure 31.** Cryo-em structure of *S. aureus* ribosome..... 101

**Figure 32.** Comparison of cryo-EM structures of *B. subtilis* ribosome and *S. aureus* ribosome ..... 102

**Figure 33.** Examples of the comparative analysis of secondary structure elements of the rRNAs from different organisms. .... 103

**Figure 34.** X-ray structure of *t. thermophilus* ribosome fitted into *S. aureus* ribosome structure . 104

**Figure 35.** Purification of human eEF2 protein..... 109

**Figure 36.** MALLS profiles of two independent experiments ..... 111

**Figure 37.** Crystals of eEF2 protein obtained by robotic screening..... 113

**Figure 38.** Diffraction pattern of eEF2 crystals in MRC 2drop crystallization plate. .... 113

**Figure 39.** Two strategies of eEF2 cloning experiment. ....115  
**Figure 40.** Agarose gel of amplified fragments of eEF2 DNA .....116  
**Figure 41.** Secondary structures of *S. aureus* and *S. cerevisiae* rRNA .....122

TABLES:

**Table 1.** Mechanisms of action and resistance mechanisms of selected ribosome-targeting antibiotics 44  
**Table 2.** Several antimicrobial agents and their therapeutic utilization 47  
**Table 3.** List of ribosomal proteins found in *S. aureus* 70S ribosome sample 68  
**Table 4.** List of non-ribosomal proteins found in *S. aureus* ribosome sample 69  
**Table 5.** Published crystal conditions for 70S ribosomes 77  
**Table 6.** Mass spectrometry results of eEF2 protein sample 112  
**Table 7.** Primers used for amplification of human eEF2. 114

## SUMMARY

The high-resolution structures of ribosomes and ribosomal subunits obtained by crystallography and electron microscopy have revolutionized the field of protein translation. Knowledge of the precise positions of residues in the ribosome in various states has led to a deeper understanding of the complex mechanisms of protein synthesis. Crystal structures of ribosomal complexes with antibiotics and antifungal compounds have provided unparalleled insight into their mechanisms of action, and they also facilitate the design of more effective drugs (Garreau de Loubresse et al., 2014; see for review Wilson, 2014). It was discovered that most of translation inhibitors bind to the conserved regions of the ribosomes (PTC, tRNA-binding sites, protein exit tunnel, etc). However, the effects of the same drug on different organism can vary from species to species. An excellent example is provided by the drug-resistant bacteria, which are tolerant to many of commonly used antibiotics. Among them is *Staphylococcus aureus* (*S. aureus*), an aggressive pathogen that causes numerous infections in humans. This bacterium is rather unique and thus, requires individual approach for treatment.

*S. aureus* is responsible for severe nosocomial and community-acquired infections. It can cause a variety of life-threatening diseases in humans. Deeply penetrating infections of *S. aureus* include endocarditis, peritonitis, necrotizing pneumonia, bacteremia, meningitis, osteomyelitis, septic arthritis, and infections of bones, joints and organs. Some skin conditions caused by staphylococcal exfoliative toxins include blisters, skin loss, pimples, furuncles, impetigo, folliculitis, abscesses, poor temperature control, fluid loss, and secondary infection. Certain strains of *S. aureus* produce the superantigen TSST-1, which is responsible for toxic shock syndrome (TSS) (Murray et al., 2002), from which mortality is very high; death can occur within two hours (Chen et al., 2007).

Another focus area in *S. aureus* research is its increasing resistance to antibiotics. A 2014 report by World Health Organization (WHO) reveals that antimicrobial resistance, including antibiotic resistance is no longer a prediction for the future, it is occurring now in every region of the world and has the potential to affect anyone, of any age, in any country. Antibiotic resistance is now a major threat to public health. According to the report, as many as 60% of *S. aureus* infections are determined to be methicillin-resistant (MRSA) in Europe. This value was 90% in the WHO Region of Americas, 80% in African Region, 80% in Western Pacific Region. In the Eastern Mediterranean Region 50% of *S. aureus* infections were reported to be methicillin-resistant, while this value was more than 25% in some parts of South-East Asia.

The resistance to the ribosome binding antibiotics is provided by the small modifications (mainly methylation) of the rRNA in the antibiotic binding sites. These modifications do not affect the process of protein synthesis, but prevent the binding of the drug. Solving the structure of the ribosome from *S. aureus* will be the first step in understanding precise mechanism of its resistance and will facilitate the design of new antistaphylococcal compounds.

### *Research project 1.*

The project dedicated to solving the structure of 70S ribosome of *S. aureus* was initiated in 2011. By that time the structures of *Thermus thermophilus* and *Escherichia coli* ribosomes had already been solved by X-ray crystallography. However, the structure of any Gram-positive or any pathogenic bacteria ribosome was still unidentified. It is known that some aspects of protein synthesis differ between Gram-negative and Gram-positive bacteria. Additionally, pathogenic bacteria have evolved complex mechanisms of translation regulation, that provide high degree of pathogenesis and facilitate survival in stressful conditions. Moreover, many pathogenic bacteria (including *S. aureus*) show extremely high resistance to ribosome-targeting antibiotics. The structure of the ribosome from the Gram-positive multi-resistant pathogenic bacterium *Staphylococcus aureus* would enable us to understand the peculiar structural features of its translation machinery, leading to a better understanding of the specific features of how this bacterium regulates protein synthesis, and how it can survive stress. Most importantly, the structure of the ribosome will serve as a model system for developing new anti-staphylococcal drugs.

We first focused on the crystallographic studies of the *S. aureus* 70S ribosome. This involved:

- preparing the cells: growing, harvesting, breaking;
- developing a purification protocol for obtaining pure and stable ribosomes that are suitable for crystallization;
- crystallization and post-crystallization treatment: searching for crystallization conditions, growing big crystals and preparation for diffraction analysis;
- developing the strategy of data collection at the synchrotron;
- solving the structure: processing the data and building the model.

A protocol for the efficient purification of *S. aureus* 70S ribosomes using a minimal amount of cells was developed. It is based on the protocols used for the bacterium *Thermus thermophilus* (Gogia et al., 1986, Yusupov et al., 2001) and the yeast *Saccharomyces cerevisiae* (Ben-Shem et al., 2011). Lysis procedures, ionic conditions, magnesium and polyethylene glycol (PEG) concentrations, sucrose gradients, etc. were optimized during the development of the purification protocol.

Ribosomes were shown to be pure, stable and capable of being crystallized. The size of the crystals of *S. aureus* 70S ribosome was sufficient for X-ray analysis ( $200 \times 80 \times 20 \mu\text{m}$ ); however the diffraction of these crystals after post-crystallization treatment reached a maximum resolution of 17.5 Å.

As we experienced specific difficulties with the diffraction of the crystals and because of time constraints, we used a cryo-EM technique to determine the structure of the *S. aureus* ribosome. The purity of the sample and recent advances in cryo-EM field gave us a hope that we would be able to obtain a high-resolution structure. The data were collected using the latest generation microscope (Titan Krios, installed at the Centre de Biologie Intégrative (CBI, Illkirch, France)). After image processing, the first structure of *S. aureus* 70S ribosome was obtained at 3.9 Å resolution. The structure at this resolution allows visualization of the side chains of the ribosomal proteins, base-pairing of the nucleotides of *S. aureus* rRNA, and other fine details of the structure, however, does not give us the ability to analyse the mechanisms of binding of the antibiotics. Therefore, the resolution will be further improved by performing several additional steps of image processing. At the same time my colleagues continue crystallographic studies of 70S ribosome from *S. aureus*.

The results I have obtained during my PhD will be discussed in details in the next chapters.

### *Research project 2.*

One of the scientific goals of our laboratory is the crystal structure determination of the human 80S ribosome. During our development of the protocol for human 80S ribosome purification we discovered that most of the ribosomes co-purify with translation elongation factor 2 (eEF2) protein. The same observation was reported in the recent cryo-EM study of human 80S ribosome: the sample of vacant 80S ribosome contained some fraction of 80S ribosome complex with eEF2 (Anger, et al., 2013). Thus, the part of my work was devoted to the determination of the crystal structure of human eEF2.

It is well known that eEF2 is one of the major regulators of translation in eukaryotes, and it is often involved in cell stress response and cancer. Determination of the structure of human eEF2 can clarify some aspects of regulation and repression of protein synthesis in humans. The eEF2 protein is known to be a target of specific protein synthesis inhibitors, and therefore the knowledge of the structure of human eEF2 could also help to discover potential anti-cancer compounds.

The project on eEF2 started by developing a protocol to purify the native eEF2 protein using the ribosome-free cytosolic fraction of HeLa cells. The protocol of purification was developed and first crystals of native eEF2 protein were obtained. However, purification of native protein gave a

very low yield, not suitable for large scale crystallization experiments. Therefore, we switched to the recombinant production of the protein in bacteria. The gene of human eEF2 protein was amplified from the cDNA library of HeLa cells and first cloning experiments were performed.

The results and current state of this project will be discussed in details in the next chapters.

## RÉSUMÉ DE THÈSE

La biosynthèse protéique est un processus fondamental, retrouvé au sein de toutes les cellules, qui permet d'assurer le décodage de l'information génétique. Ce mécanisme de traduction implique de nombreux partenaires, protéines et acides nucléiques, et nécessite une parfaite coordination de leurs actions afin d'assurer la fidélité du transfert de l'information génétique. Le ribosome est l'acteur central de ce processus de traduction. Abondant dans les cellules et conservé au cours de l'évolution, celui-ci est composé de deux sous-unités, une petite et une grande, combinant des protéines et des acides nucléiques qui s'associent au cours de la traduction pour former un ribosome fonctionnel. Dans cet état, le ribosome est capable de catalyser l'addition séquentielle des acides aminés de la chaîne peptidique en cours de synthèse en utilisant l'ARN messager (ARNm) comme matrice et les ARN de transfert aminoacylés (aa-ARNt) comme substrats. Les deux sous-unités présentent des fonctions bien distinctes. Le décodage de l'information génétique contenu dans l'ARNm est assuré par la petite sous-unité tandis que la grande sous-unité catalyse la réaction de transpeptidation permettant la formation d'une liaison peptidique entre chaque acide aminé. Une dizaine de facteurs protéiques se lient successivement au ribosome afin de catalyser les différentes étapes de la traduction, à savoir: l'initiation, l'élongation, la terminaison et le recyclage. Bien que la synthèse des protéines conservée parmi tout les domaines du vivant, tous les organismes ont des spécificités. Soit, les bactéries Gram positives et Gram négatives ont leurs propres spécificités concernant la régulation et l'organisation de la machinerie traductionnelle.

Les structures à haute résolution des ribosomes et sous-unités ribosomales obtenues par cristallographie aux rayons X et microscopie électronique ont révolutionnées le domaine de la traduction des protéines. La connaissance des positions précises des résidus dans le ribosome dans divers états a conduit à une meilleure compréhension des mécanismes complexes de la synthèse des protéines. Les structures de complexes ribosomiaux avec des antibiotiques et des composés antifongiques ont fourni un aperçu sans précédent de leurs mécanismes d'action et facilitent également la conception de médicaments plus efficaces (Garreau de Loubresse et al, 2014; revue Wilson, 2014). Il a été découvert que la plupart des inhibiteurs de la traduction se lient aux régions conservées des ribosomes (centre de peptidyltransférase, les sites de liaison d'ARNt, tunnel de sortie de la protéine, etc.). Cependant, les effets d'un même médicament sur des espèces différentes peuvent varier. Un excellent exemple est fourni par les bactéries résistantes à de

nombreux antibiotiques couramment utilisés. Parmi celles-ci, *Staphylococcus aureus* (*S. aureus*), un agent pathogène qui provoque de graves et nombreuses infections chez l'homme. Cette bactérie est assez unique et donc, requiert une approche individuelle pour le traitement.

*S. aureus* est responsable des infections nosocomiales et infections sévères et peuvent causer une variété de maladies potentiellement mortelles chez l'homme. Ces infections comprennent l'endocardite, la péritonite, pneumonie nécrosante, la bactériémie, la méningite, l'ostéomyélite, l'arthrite septique, et les infections des os, des articulations et des organes (Fridkin et al, 2005).

*S. aureus* est un pathogène majeur d'une importance croissante en raison de sa haute résistance aux antibiotiques (Lowy, 1998). Un rapport par l'Organisation mondiale de la Santé (OMS) révèle que la résistance aux antimicrobiens, y compris la résistance aux antibiotiques n'est plus une prédiction pour l'avenir, elle se passe maintenant dans toutes les régions du monde et a le potentiel de toucher tout le monde, de tout âge, dans tous les pays. La résistance aux antibiotiques est maintenant une menace majeure pour la santé publique. Selon ce rapport, pas moins de 60% des infections à *S. aureus* sont déterminées comme résistantes à la méthicilline (SARM) en Europe (World Health Organization, 2015).

Les gènes responsables de la résistance sont souvent transmis par des éléments génétiques mobiles tels que les plasmides et, par conséquent, populations bactériennes peuvent acquérir une résistance très rapidement. Divers mécanismes de résistance aux antibiotiques sont indiqués sur la Fig I. Les bactéries peuvent empêcher la pénétration de l'antibiotique dans la cellule (a), le retirer de la cellule en utilisant une pompe d'efflux (b), de dégrader (h) ou modifier l'antibiotique (g). Alternativement les bactéries peuvent muter (c), modifier (d) ou protéger (f) les cibles des antibiotiques. La conception de nouveaux agents antimicrobiens est fortement requise pour le traitement des maladies causées par *S. aureus*.

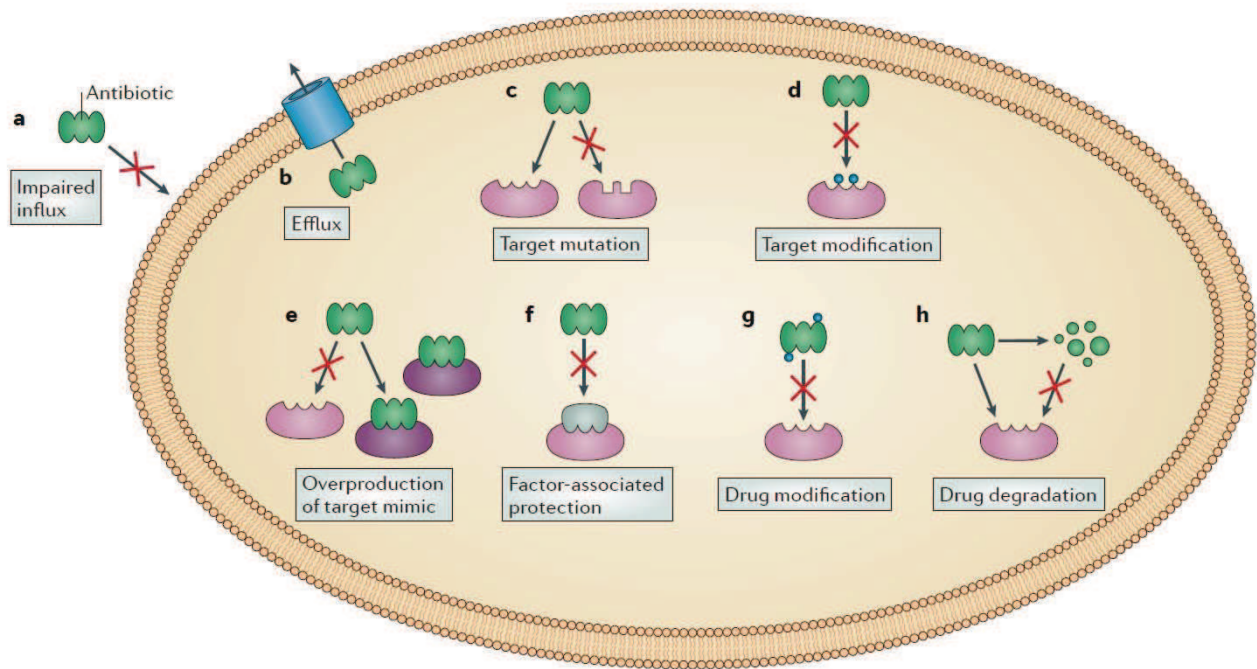


**Fig I.** Mécanismes de résistance antibactérienne (adapté de Wilson, 2014).

Pour comprendre les aspects structurels de la résistance aux antibiotiques nous avons besoin de connaître la structure de leur cible. Par conséquent nous nous sommes concentrés sur la structure du ribosome, qui est la principale cible des antibiotiques les plus couramment utilisés. La résolution de la structure du ribosome de *S. aureus* sera la première étape vers la compréhension du mécanisme précis de sa résistance aux antibiotiques et facilitera la conception de nouveaux composés antistaphylococciques.

### *Projet de recherche 1.*

Le projet dédié à la résolution de la structure du ribosome de *S. aureus* a été initié en 2011. À cette époque, les structures des ribosomes de *Thermus thermophilus* et *Escherichia coli* avaient déjà été résolues par cristallographie aux rayons X. Cependant, la structure d'un ribosome de toute bactérie Gram positif ou tout ribosome pathogène restait manquante. Hors, il est connu que certains aspects de la synthèse des protéines diffèrent entre les bactéries à Gram négatif et à Gram positif. En outre, les bactéries pathogènes ont développé des mécanismes complexes de régulation de la traduction, qui offre un rendement élevé de la pathogenèse et facilite la survie de la bactérie dans des conditions stressantes. En outre, de nombreuses bactéries pathogènes (y compris *S. aureus*) montrent une très haute résistance aux antibiotiques ciblant spécifiquement les

ribosomes. Cette résistance est souvent due à des modifications au sein du ribosome lui-même. La structure du ribosome de la bactérie pathogène multi-résistante à Gram positif *Staphylococcus aureus* révélerait les caractéristiques structurelles particulières de machinerie de traduction nous permettant ainsi de mieux comprendre les spécificités de la régulation de la synthèse des protéines, et de la survie de cet agent pathogène. Plus important encore, elle servira comme un système modèle pour le développement de nouveaux médicaments contre *Staphylococcus*.

Nous avons d'abord mis l'accent sur les études cristallographiques du ribosome de *S. aureus*.

Cela a impliqué:

- la préparation des cellules: culture, la récolte, lyse ;
- l'élaboration d'un protocole de purification qui fournira des ribosomes purs et stables, propices à la cristallisation ;
- la mise au point de conditions de cristallisation optimales permettant d'obtenir des cristaux dans grande taille et en quantité suffisante
- la mise au point de traitements de post-cristallisation nécessaires pour l'analyse par diffraction aux rayons X;
- l'élaboration de la stratégie de collecte de données au synchrotron;
- la résolution de la structure: le traitement des données et de la construction du modèle.

J'ai développé le protocole de purification des ribosomes *S. aureus* efficace utilisant une quantité minimale de cellules. Il est basé sur les protocoles utilisés pour les bactéries *Thermus thermophilus* (Gogia et al., 1986, Yusupov et al., 2001) et les levures *Saccharomyces cerevisiae* (Ben-Shem et al., 2011). La procédure de lyse, les conditions ioniques, des concentrations de magnésium et de polyethylene glycol (PEG), des gradients de saccharose, etc. ont été optimisés au cours du développement du protocole de purification. L'échantillon purifié a été caractérisé en utilisant plusieurs méthodes biophysiques et biochimiques. Des gels SDS ont confirmé la pureté de l'échantillon (Fig II, A et B); gel d'agarose a montré le caractère intact de l'ARNr (Fig II, C) ultracentrifugation analytique a démontré que l'échantillon contenait principalement des particules 70S (Fig II, D). L'analyse par spectrométrie de masse a révélé l'absence de protéines ribosomiques S1 et L9. La stabilité du ribosome sous différentes concentrations  $Mg^{2+}$  a été analysée par centrifugation en gradient de saccharose. La concentration minimale de  $Mg^{2+}$  qui permet de garder les sous-unités associées a été déterminée et les conditions pour la dissociation des 70S dans en sous-unités 50S et 30S ont été trouvées.

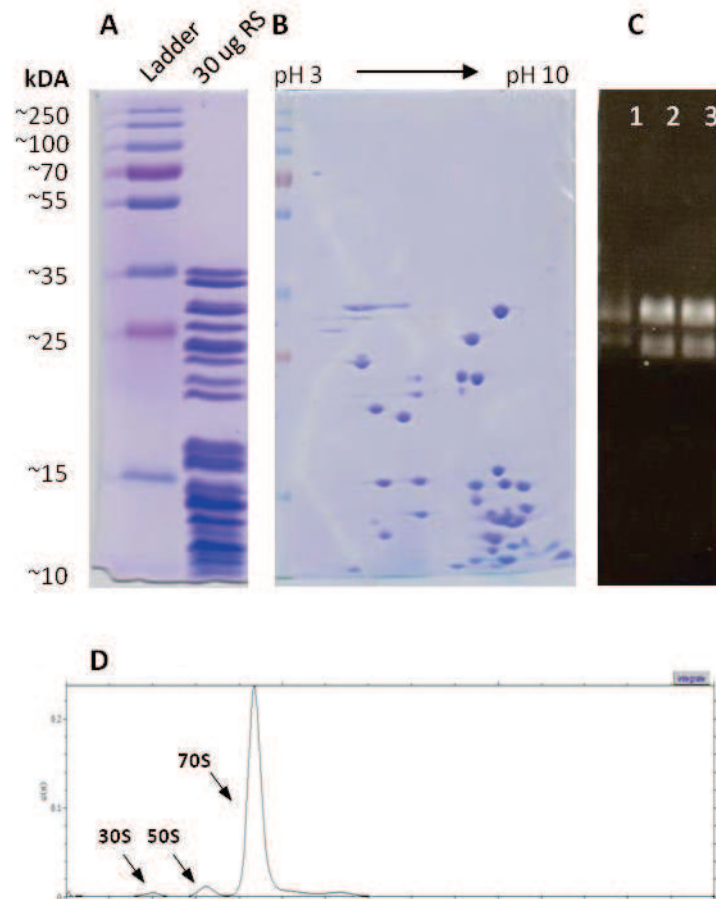


**Fig II.** SDS-PAGE (électrophorèse sur gel de polyacrylamide en présence de dodécylsulfate de sodium) unidimensionnel (A) et bidimensionnel (B) de l'échantillon du ribosome de *S. aureus*. Électrophorèse sur gel d'agarose des ribosomes (C): 1 - *T. thermophilus* 70S (5 µg), 2 et 3 - 70S de *S. aureus* (15 µg). Les bandes supérieure et inférieure correspondent à des ARNr 23S et 16S, respectivement. Profil de sédimentation de l'échantillon du ribosome de *S. aureus* (D).

Particules cristallines initiales de ribosome 70S de *S. aureus* ont été obtenues en utilisant une recherche robotique. Après plusieurs étapes d'optimisation de cristallisation, de grands cristaux tridimensionnels ont été obtenus. Typiquement, les cristaux sont apparus de façon reproductible dans les 7 - 10 jours et ont atteint leur taille moyenne (200 × 80 × 20 µm) après deux semaines supplémentaires (Fig III). La taille des cristaux de ribosome de *S. aureus* est suffisante pour l'analyse par diffraction aux rayons X. Les conditions de déshydratation et de cryo-refroidissement ont été optimisées pour les cristaux obtenus. Les premières données de diffraction de cristaux du ribosome 70S de *S. aureus* ont été recueillies. La diffraction de ces cristaux atteint au maximum 17.5 Å, le groupe de l'espace a été déterminée comme P4<sub>2</sub>2<sub>1</sub>2 et la taille de l'unité asymétrique était: 450 × 450 × 280 Å.

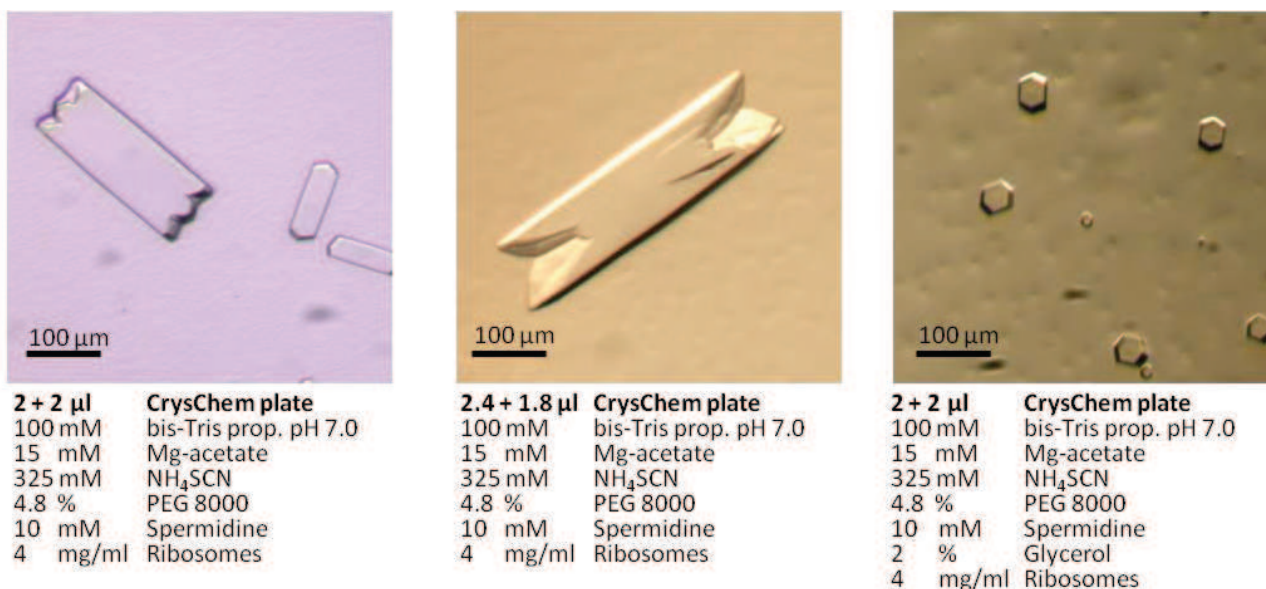


**Fig III.** Les cristaux du ribosome 70S de *S. aureus*.

En raison de difficultés avec qualité de la diffraction des cristaux, nous avons choisi d'utiliser la technique de cryo-microscopie électronique (cryo-ME) pour déterminer la structure du ribosome de *S. aureus*. La pureté de l'échantillon et de sérieux progrès dans le domaine de la cryo-ME au cours des dernières années a donné un espoir d'obtenir la structure à haute résolution grâce à cette technique. Les données ont été recueillies en utilisant la dernière génération de microscope (Titan Krios, installé au Centre de Biologie Intégrative (CBI, Illkirch, France)).

Les conditions appropriées pour la préparation de la grille cryo-ME et de la collecte de données ont été trouvées pour l'échantillon du ribosome 70S de *S. aureus* (Fig IV, A). Le traitement des images cryo-ME a été réalisé avec Scipion workflow et les algorithmes intégrés (Fig IV, B). Après le traitement des images, la structure à une résolution de 3.9 Å a été obtenue. La structure à cette résolution permet de voir les chaînes latérales des protéines ribosomales, la base-azotée des nucléotides de l'ARNr de *S. aureus*, etc (Fig IV, C). Cette résolution donne également la possibilité d'analyser la liaison des antibiotiques et, en combinaison avec les connaissances biochimiques, de développer des composés antimicrobiens efficaces contre *S. aureus*.

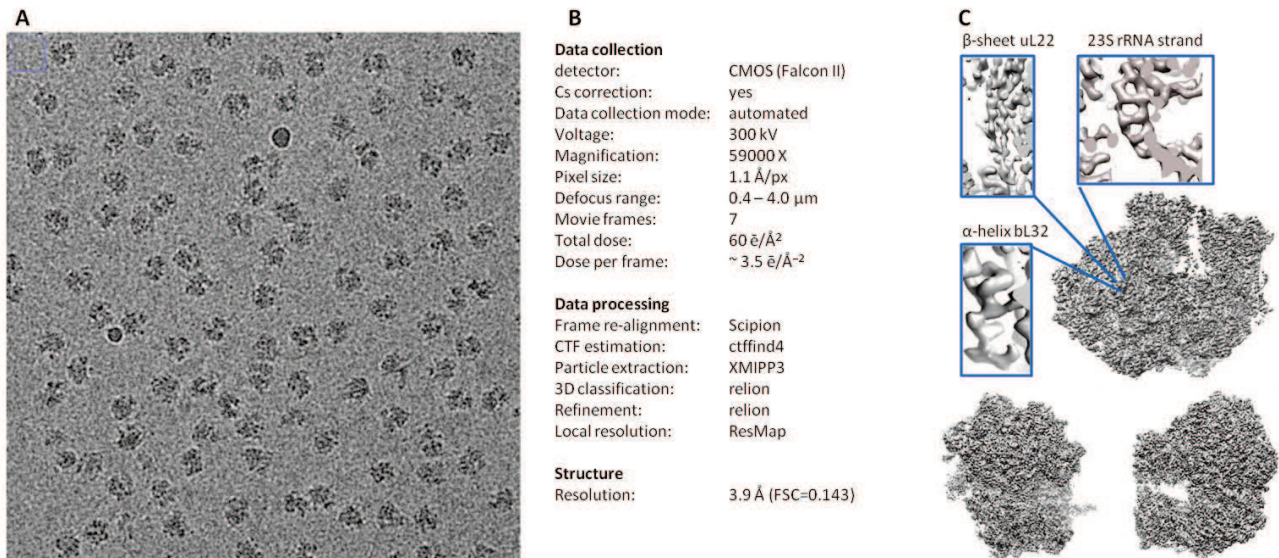


**Fig IV.** A. Micrographie électronique du ribosome 70S de *S. aureus*. L'échantillon a été vitrifié en éthane liquide et prélevé sur le Polara F-30 microscope. Agrandissement 59000X, tension 300 kV, détecteur CCD eagle 4Kx4K. La structure Cryo-ME de *S. aureus* ribosome. B. Paramètres de collection de données sur Titan Krios microscope et de traitement des image.

Nous avons effectué une analyse comparative du ribosome de *S. aureus* et des objets de modèle structures cristallines du ribosomes 70S de *T. thermophilus* (Jenner et al, 2010) et de *E. coli* (Schuwirth et al., 2005) et la structure cryo-ME du ribosome 70S de *B. subtilis* (Sohmen et al., 2015). Le ribosome de *T. thermophilus* est le ribosome plus structurellement étudiée, le ribosome de *E. coli* est le plus étudié biochimiquement et la bactérie *Bacillus* est phylogénétiquement l'organisme le plus proche du genre *Staphylococcus*. Plusieurs hélices d'ARN ont été trouvées pour être étendues dans la structure de *S. aureus* (Fig V). Certaines des extensions sont conservées par *E. coli* (H26, H44, H27, H68, H79), ou *T. thermophilus* (h9, H15, H63), tandis que d'autres sont spécifiques des bactéries à Gram-positif *S. aureus*, ou *B. subtilis* (H6, H10, H17, H25, H54).

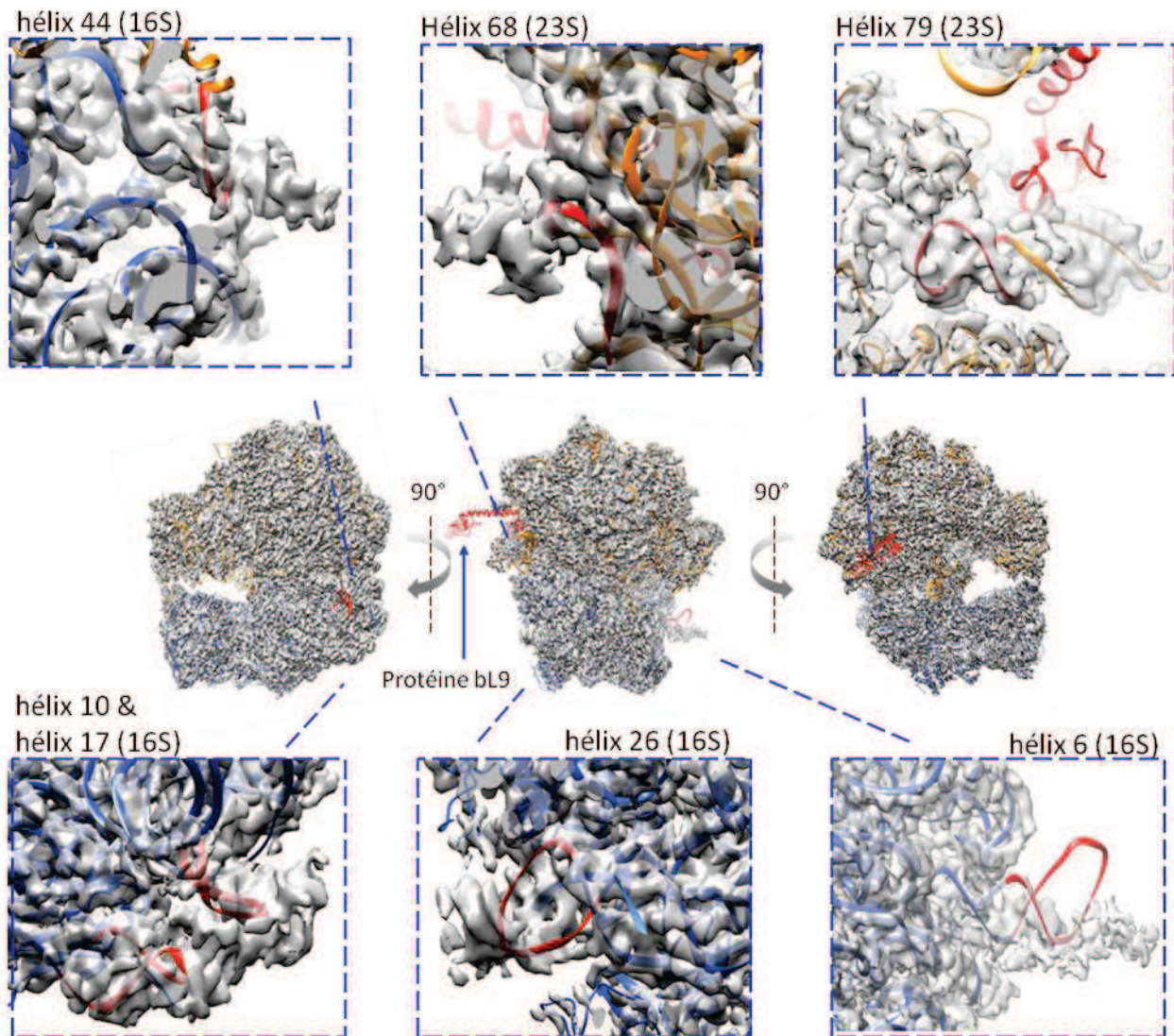


**Fig V.** La structure cristalline du ribosome de *T. thermophilus* (Code PDB 4V4F) monté dans la structure du ribosome de *S. aureus* comme corps rigide: sous-unité 30S est colorée en bleu, sous-unité 50S est colorée en or. Les extensions de certaines hélices d'ARNr et les protéines ribosomiques sont colorées en rouge.

Un autre détail important observé dans la structure de *S. aureus* est l'absence de protéines ribosomiques S1 et L9. Protéine S1 est la protéine ribosomique la plus grande et la plus acide, et son rôle est de faciliter l'adaptation de l'ARNm de la sous-unité 30S lors de l'initiation de la traduction dans les bactéries. La protéine S1 d'*E. coli* ou de *T. thermophilus* se compose d'environ 550 acides aminés se pliées en six domaines, et il se lie au ribosome relativement faiblement. La protéine S1 de *S. aureus* est constituée de 391 acides aminés se pliées en quatre domaines et ne se lie pas au ribosome. Le mécanisme d'interaction de la protéine S1 avec le ribosome de *S. aureus* reste difficile à déterminer. La protéine L9 est également une spécificité bactérienne. Elle située sur la périphérie très proche de tige L1 dans le domaine V de l'ARNr et se trouve sur le côté du ribosome bactérien. La position de la protéine L9 près de la voisine ribosome 5'-amont dans polysomes top-to-top suggère qu'il pourrait contribuer à

la régulation inter-ribosome. (Dunkle et Cate, 2011). D'autre part, la protéine ribosomale L9 n'est pas essentiel dans *E. coli* ou *T. thermophilus*, mais elle est conservée dans d'autres bactéries.

Tous les résultats obtenus dans ces travaux, faciliteront la description à l'échelle atomique du ribosome de *S. aureus* et ses complexes fonctionnels' dans un futur proche. La combinaison des méthodes de cristallographie aux rayons X et de cryo-ME aidera à atteindre cet objectif. Les résultats obtenus serviront de base pour le développement de nouveaux composés contre la bactérie pathogène et extrêmement résistante qu'est *S. aureus*.

### *Projet de recherche 2.*

Une autre partie de mon travail a été consacrée à la détermination de la structure tridimensionnelle par radio-cristallographie du facteur d'élongation humain de type 2 (eEF2). Cette protéine a été jugée plutôt étroitement lié aux ribosomes 80S humains lors de la purification effectuée au sein de notre laboratoire. Il est bien connu que eEF2 est le principal régulateur de la traduction chez les eucaryotes et est souvent impliqué dans la réponse au stress cellulaire et dans le développement du cancer (revue White-Gilbertson, 2009). La détermination de la structure de eEF2 humaine permettrait de clarifier certains aspects de la régulation et de la répression de la synthèse des protéines chez l'homme. La protéine eEF2 est connue pour être une cible d'inhibiteurs spécifiques de la synthèse des protéines, de sorte que la structure de eEF2 humaine pourrait aussi aider à découvrir des composés anticancéreux potentiels.

Le travail a commencé avec l'élaboration du protocole de purification de la protéine native eEF2 utilisant comme source la fraction cytosolique libre des ribosomes des cellules HeLa. La pureté, l'homogénéité et la stabilité de la protéine purifiée a été analysée par SDS-PAGE, diffusion dynamique de la lumière, diffusion de la lumière multiangle, essai de décalage thermique et la spectrométrie de masse. Les premiers cristaux ont été obtenus par recherche robotique (Fig VI). L'analyse par diffraction de ces cristaux au synchrotron s'est avéré être des cristaux de protéine. Cependant, la qualité de la diffraction ne suffit pas à collecter les données.

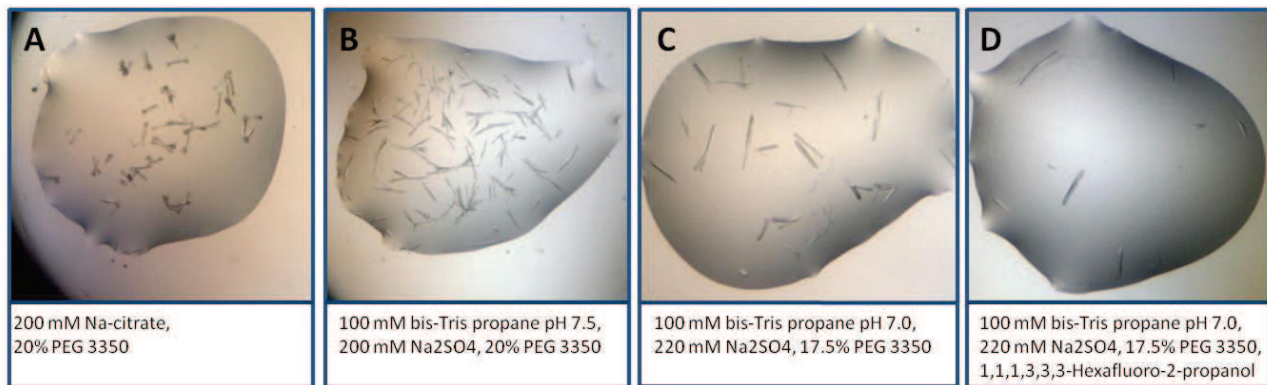


**Fig VI.** Les cristaux de protéine eEF2 obtenus par recherche robotique.

En outre l'optimisation de la cristallisation d'eEF2 était impossible en raison du manque de matériel. La purification de la protéine native requise de nombreuses cellules humaines, qui sont coûteux. Nous avons donc décidé de cloner et exprimer la protéine hétérologue. Initialement, car elle offre la plus facile, la moins chère et le plus rapide système d'expression, *E. coli* a été sélectionnée.

Cependant, nous avons choisi de poursuivre par la purification de la protéine eEF2 recombinante dans des bactéries. Pour le moment, le travail est à l'étape de clonage de la région codante de la protéine eEF2 dans un vecteur d'expression bactérien pET-15b (His-tag, la thrombine site de clivage, résistance à l'ampicilline, IPTG inducible). La gène complet d'eEF2 humain ou ses fragments ont été amplifiés en utilisant la bibliothèque HeLa ADNc incorporée dans un bactériophage. Le travail est toujours en cours.

## ABBREVIATIONS

### Ribosome:

aa-tRNA	aminoacyl-tRNA
A-site	aminoacyl site, (A-tRNA – A-site tRNA)
EF	elongation factor (eEF – eukaryotic EF)
E-site	exit site (E-tRNA – E-site tRNA)
IF	initiation factor (eIF – eukaryotic IF)
mRNA	messenger ribonucleic acid
PTC	peptidyl transferase centre
P-site	peptidyl site, (P-tRNA – P-site tRNA)
RF	release factor (eRF – eukaryotic RF)
RP	ribosomal proteins
RRF	ribosome recycling factor
rRNA	ribosomal ribonucleic acid
SD	Shine-Dalgarno
tRNA	transfer ribonucleic acid

### Methods:

NMR	nuclear magnetic resonance
Cryo-EM	cryo-electron microscopy
LC-MS/MS	liquid chromatography coupled mass spectrometry
DLS	dynamic light scattering
MALLS	multiangle laser light scattering
MALDI	matrix assisted laser desorption/ionization
PCR	polymerase chain reaction
PAGE	polyacrylamide gel electrophoresis

### *S. aureus*:

<i>B. subtilis</i>	<i>Bacillus subtilis</i>
<i>E. coli</i>	<i>Escherichia coli</i>
MRSA	methicillin-resistant <i>S. aureus</i>
mrMRSA	multi resistant MRSA
MSSA	methicillin-susceptible <i>S. aureus</i>
nmrMRSA	non-multi resistant MRSA
PBPs	penicillin binding proteins
<i>S. aureus</i>	<i>Staphylococcus aureus</i>
<i>T. thermophilus</i>	<i>Thermus thermophilus</i>
TSS	toxic shock syndrome
VISA	vancomycin-intermediate <i>S. aureus</i>
VRSA	vancomycin-resistant <i>S. aureus</i>
WHO	World Health Organization
$\sigma^A$	sigma factor A
$\sigma^B$	sigma factor B

### Cryo-electron microscopy:

CMOS	complementary metal-oxide semiconductor
------	---

CTF	contrast transfer function
DDD	direct detector device
DQE	detective quantum efficiency
FEG	field emission gun
FSC	Fourier shell correlation
SNR	signal-to-noise ratio
TEM	transmission electron microscopy

**Reagents:**

DMSO	dimethyl sulfoxide
DTT	dithiothreitol
EDTA	ethylenediaminetetraacetic acid
EG	ethyloene glycol
GDP	guanosine diphosphate
GTP	guanosine triphosphate
LB	lysogeny broth
MPD	3-methyl,1, 5-pentenediol
PBS	phosphate-buffered saline
PEG	polyethylene glycol
PMSF	phenylmethylsulfonyl fluoride
SDS	sodium dodecyl sulfate

---

## Introduction

---

## THE RIBOSOME

Protein synthesis is performed by the ribosome in all living organisms. It is one of the most conserved biological processes. The central dogma of molecular biology states that DNA is transcribed into RNA and RNA is subsequently translated into proteins. Ribosome is macromolecular machine which translates the nucleotides-based language of the mRNA into amino acid-based language of proteins. The ribosome is a major link between genes and proteins and it is made of nucleic acid (ribosomal RNA, or rRNA) and protein (ribosomal proteins, or RP) components.

### Core of the ribosome

Structurally ribosomes in all living cells are composed of two subunits, called small ribosomal subunit (SSU) and large ribosomal subunit (LSU). Both are composed of rRNA(s) and proteins with average ratio of 2:1 RNA to protein (the exceptions are mitochondrial and chloroplast ribosomes which have ratios 1:2 and 3:2 respectively (see for review Sharma and Agrawal, 2012). The ribosome is an asymmetric macromolecular complex and each subunit has particular structural and functional organization, thus carries out different functions in translation (Figure 1).

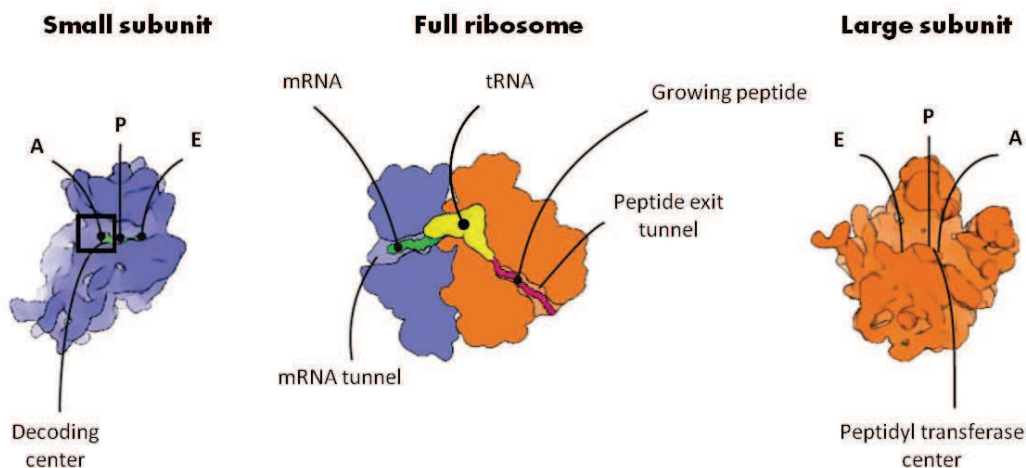


**Figure 1.** Structural organization and functional sites of the ribosome. The two ribosomal subunits (left and right) assemble together to form the full ribosome (center). Main functional sites and natural ligands (mRNA, tRNA) are annotated (adapted from Melnikov et al., 2012).

The small subunit is responsible for the decoding process where aminoacyl-tRNA (aa-tRNA) is selected according to the mRNA sequence. Its major functional sites are the mRNA path used to conduct mRNA during translation, the decoding center responsible for decoding, and the tRNA

binding sites (A, P and E). The A-site serves to bind aminoacyl-tRNA as it enters into the ribosome during protein synthesis, the P-site holds tRNA carrying the nascent polypeptide chain (peptidyl-tRNA), and the E-site (exit) is where tRNA dissociates from the ribosome. During translation, tRNAs are translocated from the A to the P-site and from the P to the E-site. The large subunit catalyzes peptide bond formation. Its major functional sites are the tRNA binding sites (A, P and E), the peptide exit tunnel that extends through the body of the large subunit, and the peptidyl transferase centre (PTC). The PTC is responsible for peptide bond formation and is located at the entrance to the peptide tunnel in a conserved region on the interface that is mainly composed of rRNA. As a result of peptide bond formation in the PTC, the nascent polypeptide chain is transferred from the peptidyl-tRNA in the P- site to the aa-tRNA in the A-site, thus extending the nascent chain by one amino acid.

### **Specifications of bacterial and eukaryotic ribosome**

Despite the universal conservation of the core, ribosome composition varies between domains of life, taxonomic subgroups, organelles and even within a single individual, although to a smaller extent. Ribosomes may contain their own set of specific moieties: specific proteins, insertions and extensions of conserved proteins and expansion segments of rRNAs.

Major differences in ribosome composition are observed between domains of life. Apart from the core, the bacterial ribosome (*E. coli* or *T. thermophilus*) contains 21 bacteria-specific proteins, a few extensions of the conserved proteins and of ribosomal RNA. The eukaryotic ribosome (*S. cerevisiae*) contains 46 eukaryote-specific proteins (800 kDa) and extensions and insertions in most of the proteins of the core (200 kDa), and the rRNA harbors several extensions in the conserved rRNA chains (about 800 nucleotides that account for 350 kDa) (Ben-Shem et al., 2011; Melnikov et al., 2012). Sedimentation coefficients are used to characterize and to name isolated or associated subunits. Hence, association of the small subunit (30S in bacteria, 40S in eukaryotes) with the large subunit (50S in bacteria, 60S in eukaryotes) results in the full ribosome – 70S in bacteria and 80S in eukaryotes.

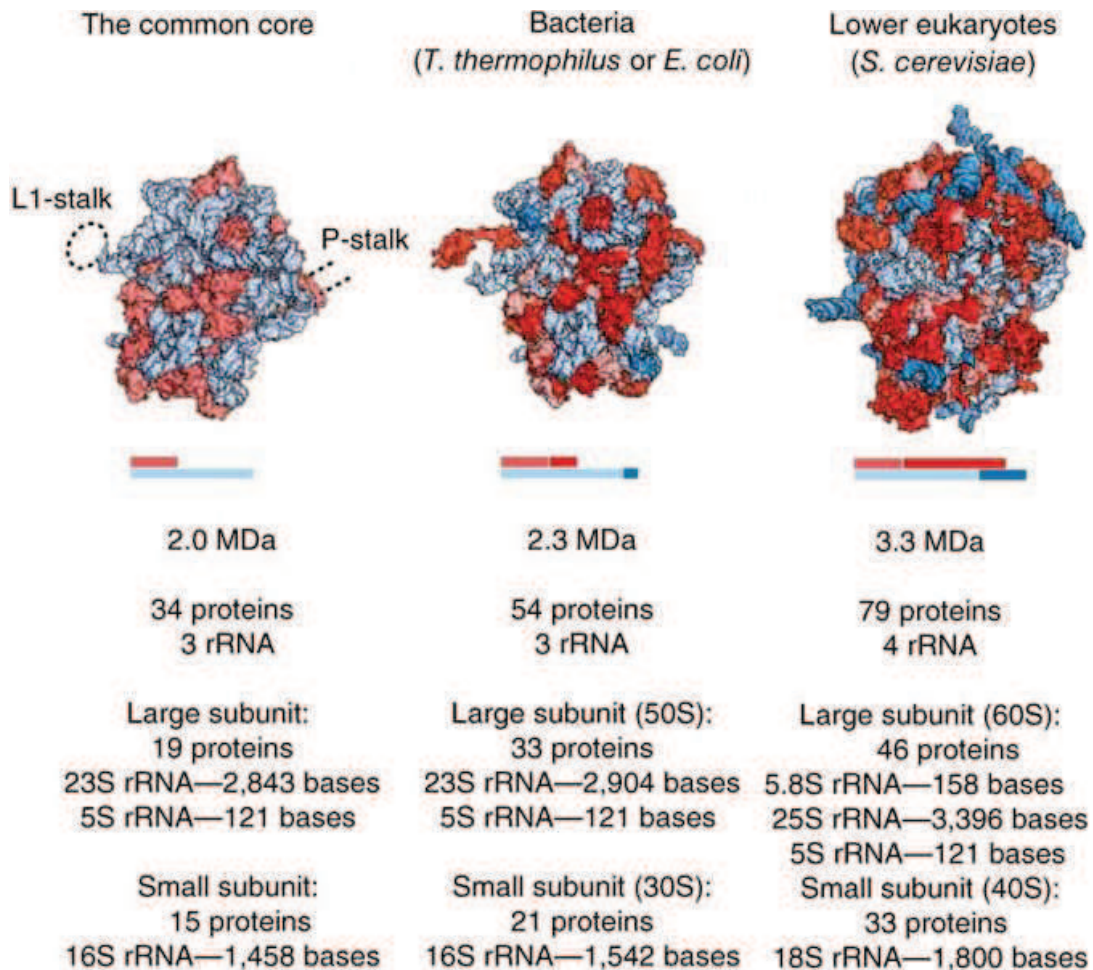


**Figure 2.** Composition of bacterial and eukaryotic ribosomes and the common core, based on X-Ray studies. Bacterial and eukaryotic ribosomes share a conserved core composed of RNA (light blue) and proteins (light red). In addition to the core, ribosomes in each domain of life contain their own set of proteins, extensions and insertions in conserved proteins (both in red), and extension segments in ribosomal RNA (blue). 5.8S and 25S rRNA are both homologous to 23S rRNA in bacteria. Dashed lines around the core indicate positions of flexible stalks of the ribosomes that are usually disordered in X-ray structures. For simplicity, these lines are not shown in the other structures. The figure is based on X-ray and Cryo-EM structures from Armache et al., 2010, Ben-Shem et al., 2011, Jenner et al., 2010, Jarasch et al., 2012 (adapted from Melnikov et al., 2012).

## Protein synthesis

Protein synthesis in bacteria can be divided into four main steps: initiation, elongation of the polypeptide chain, termination and recycling of ribosomes (Figure 3). Each of these steps is assisted by protein factors termed initiation factors (IF), elongation factors (EF), release factors (RF) and recycling factors (RRF). Initiation in bacteria involves the accurate positioning of the mRNA start codon (usually AUG), together with the initiator tRNA (fMet-tRNA) at the ribosomal P-site of small (30S) subunit and following binding of large (50S) subunit resulting in formation of 70S ribosome. The efficiency and fidelity of this process is controlled by three specialized translation initiation

factors: IF1, IF2 and IF3. The elongation phase involves a cycle of four major steps. First, an aminoacylated tRNA (aa-tRNA) is delivered to the A-site of the ribosome by elongation factor Tu (EF-Tu) in complex with GTP.

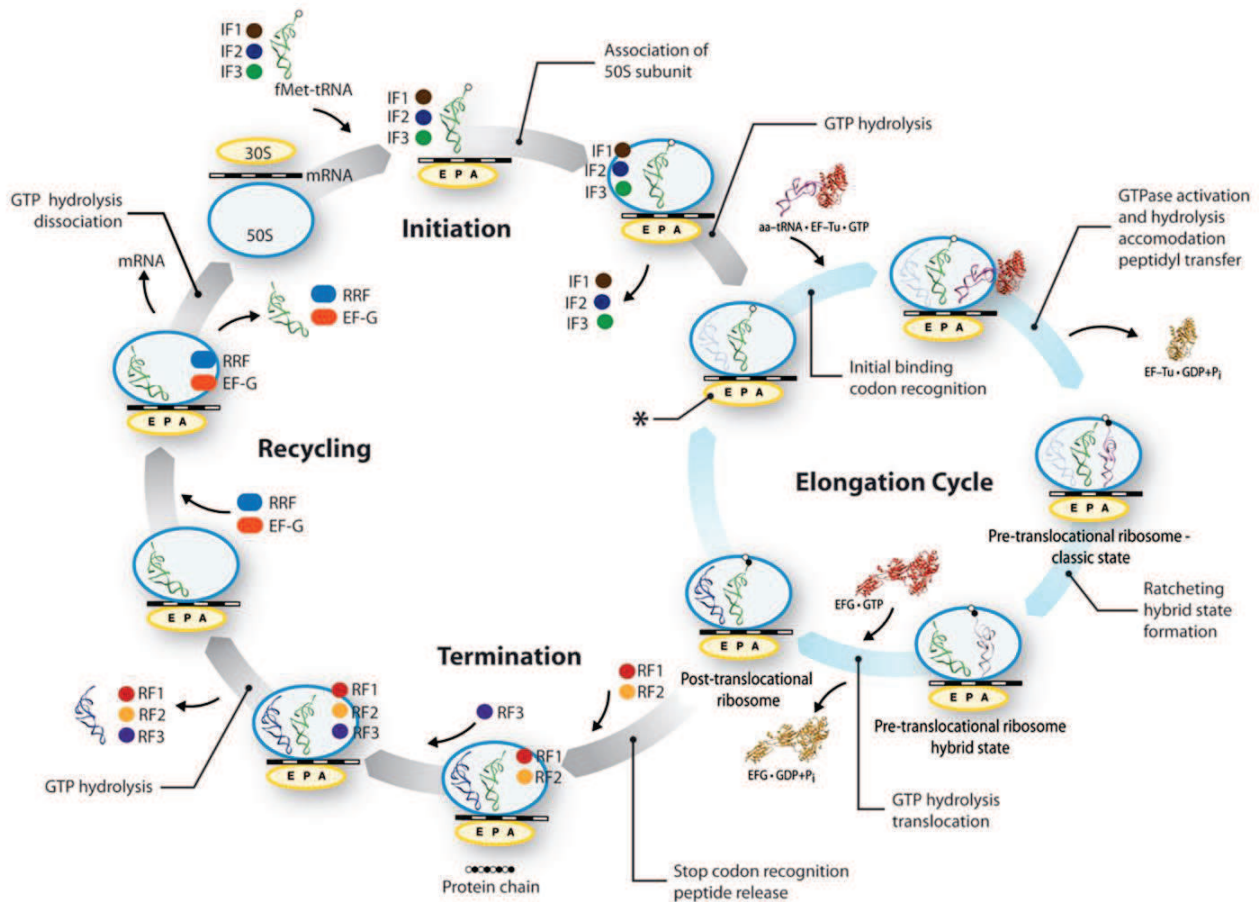


**Figure 3.** Schematic diagram of bacterial protein synthesis. The main steps comprising the translation process are shown. Details regarding each step are provided in the main text. For simplicity, some intermediate stages are omitted. The mRNA is depicted as a strand running horizontally along the small (30S) subunit, with alternating white and black segments, each representing one codon. The tRNAs bind at A-, P- and E-sites. The nascent polypeptide is shown as a string of spheres. The individual structures and cartoons are not drawn to scale (adapted from Agirrezabala and Frank, 2010).

During the process of decoding, the ribosome monitors the base-pairing interaction between the mRNA codon and the tRNA anticodon, ensuring that only tRNAs bearing the correct amino acid are accommodated. Peptide-bond formation occurs between the amino acids attached to the tRNAs in the A- and P-sites, resulting in transfer of the amino acid (or the polypeptide chain in later elongation cycles) from the P-site tRNA to the aa-tRNA in the A-site. In order to accommodate the next incoming aa-tRNA, the tRNAs are moved from the A- and P-sites to the P- and E-sites in a process known as translocation, which is facilitated by EF-G. As the polypeptide chain elongates, it passes through an exit tunnel in the 50S subunit before entering the cytoplasm, where protein folding

occurs. The elongation cycle continues until a stop codon is encountered. The stop codon (UAG, UGA or UAA) recruits release factor instead of tRNA which allows the release of the newly synthesized nascent peptide chain. Finally, the two subunits are dissociated in the recycling step making them available for the next translation cycle. This basic mechanism of the protein synthesis is conserved across species, but there are differences in regulation and certain steps, such as initiation, associated with more complex organisms.

## **Structural studies of the ribosome**

At present the methods of structural biology are at the forefront in the understanding the molecular mechanisms of protein synthesis. Modern structural approaches are bringing fundamental biochemical knowledge about the ribosome accumulated during last century to an atomic level (when visualization of interactions between atoms is available). Pioneering works on structural investigation of biological material (mainly single proteins and nucleic acids) were made in the middle of 20th century using X-ray crystallography: structures of vitamin B12 (Hodgkin et al., 1956), insulin (Blundell et al., 1971), penicillin (Crowfoot et al., 1949) by D. Hodgkin and coworkers; helical structure of the DNA (Watson and Crick, 1953) by R. Franklin, J. Watson, F. Crick, M. Wilkins; structure of protein haemoglobin (Perutz et al., 1960); and many others. Later, in 1984 the laboratory of K. Wüthrich produced the first protein structure determined by NMR (nuclear magnetic resonance), a spectroscopy technique (Williamson et al., 1985). The same year can be considered as an origin of cryo-electron microscopy (cryo-EM) of biological materials, when the first images of adenovirus embedded in a vitrified layer of water were shown (Adrian et al., 1984). The importance of all this discoveries and their colossal impact in biology, chemistry and medicine cannot be overestimated.

Although solving structures of proteins and nucleic acids became possible, structures of big macromolecular complexes such as ribosome remained enigmatic. Massive, asymmetric, highly flexible macromolecular complex composed of two types of molecules (RNA and proteins), the ribosome was always extremely difficult object for structural analysis.

Use of NMR technique is commonly limited by the size of the molecule to analyse, typically 25 – 100 kDa, although sometimes NMR can be used to obtain structural information in large but symmetric systems as big as 900 kDa (Fiaux et al., 2002). At the same time, electron microscopy is limited for working with small objects but suitable for resolving the big ones. Hence, the first 3D reconstructions of the ribosome were obtained using electron microscopy. In 1983 A. Spirin with colleagues modelled the 70S ribosome from *E. coli* showing the main structural features of both

subunits (Vasiliev et al., 1983; see also Vasiliev et al., 1974; Lake 1976 and refs therein; Kastner et al., 1981). During next decades, J. Frank and colleagues worked on ribosome structure determination using cryo-electron microscopy technique. They have achieved significant progress in that area, by reaching 11.5 Å resolution of 70S ribosome in 2000 and contributed to the development of cryo-EM method in general (Wagenknecht et al., 1989; Stark et al., 1995; Gabashvili et al., 2000).

In the middle of 1980s two groups started to work in the direction of X-ray crystallography, the most developed, the most accurate and the most reliable method. However, this method is one of the most challenging one, because the researcher need to produce highly ordered radiation tolerant solid crystals, which requires a lot of stable homogeneous material and specific conditions. Obviously, this becomes excessively difficult task working with the ribosome which is large, asymmetric, flexible, and very dynamic RNA-protein complex. However, years of work and the sharing of experience have enabled researchers to achieve this aim.

### *X-ray crystallography of the ribosome*

X-ray crystallography is the presently the only one technique that conceivably provide the high-resolution structural information of the ribosome.

The first crystals of the large ribosomal subunit were obtained from the thermophilic bacterium *Bacillus stearothermophilus* and extreme halophilic archaeons *Haloarcula marismortui*. in the Max Plank Institute (Berlin) by H. Wittmann and A. Yonath in 1982. Their pioneering work provided the crystals of the large bacterial and archaeal 50S subunits diffracting to 18 Å resolution (Yonath et al., 1984; Yonath et al., 1986; Shoham et al., 1986).

In 1983 new extreme thermophile *Thermus thermophilus* was introduced in the field of ribosome crystallography in the group of Dr. M. Yusupov from the Institute of Protein Research, Academy of Sciences of USSR (Puschino). In this group purification procedures of the ribosomes were developed and reported for the first time crystallization procedures of small ribosomal 30S subunit and full 70S ribosome (Trakhanov et al., 1987; Yusupov et al., 1987). From 1995 to 2000, V. Ramakrishnan from Cambridge University (UK) and A. Yonath groups published the *T. thermophilus* 30S structure at atomic resolution (Schluederger et al. 2000, Wimberly et al. 2000). In 2000, T. Steitz (Yale University, USA) with colleagues produced a 2.4 Å electron density map of the *H. marismortui* 50S subunit (Ban et al., 2000).

The first crystal structure of full 70S ribosome from *T. thermophilus* containing bound functional ligands such as a messenger RNA and three transfer RNAs was solved at 7.8 Å resolution

in 1999 in collaboration between M. Yusupov, G. Yusupova and H. Noller (University of California, Santa Cruz) (Cate et al., 1999). In 2001 the resolution of this crystal form was extended to 5.5 Å, providing for the first time detailed analysis of the interactions between the subunits and their interactions with messenger RNA and tRNAs in the A-, P- and E-sites (Yusupov et al., 2001, Yusupova et al, Cell, 2001). Within the next few years, a similar crystal form pushed their resolution to 3.7 Å (Korostelev et al., 2006). The group of J. Cate (University of California, Berkeley, USA) developed experimental protocol for *E. coli* 70S ribosome and reached 3.5 Å resolution (Schuwirth et al., 2005; Zhang et al., 2009). The resolution limits were soon surpassed again with discovery of a new crystal form of *T. thermophilus* which diffracted to 2.8 Å (Selmer et al., 2006). Once the procedures of ribosome purification and crystallization became well established many of functional complexes have been determined and provided unprecedented insights into process of protein synthesis in bacteria. In 2009 V. Ramakrishnan, T. Steitz and A. Yonath received the Nobel Prize in chemistry for the studies of the structure and function of the ribosome.

However, many questions remained unanswered. Genome analysis, biochemical and biophysical characterization, electron microscopy studies of eukaryotic ribosomes have shown the differences in protein translation between eukaryotes and bacteria, but the atomic structure of eukaryotic ribosome remained elusive. But recently in 2010, the first structure of the full eukaryotic ribosome from *Saccharomyces cerevisiae* was solved at 4.2 Å (Ben-Shem et al., 2010) in the laboratory of M. Yusupov (IGBMC, Strasbourg, France). In 2011 the same group reported the crystal structure of the 80S ribosome from *S. cerevisiae*—including nearly all ribosomal RNA bases and protein side chains as well as an additional protein, Stm1—at a resolution of 3.0 angstroms (Ben-Shem et al., 2011). Structures of the large 60S and small 40S ribosomal subunits of *Tetrahymena thermophila* at 3.5 Å and 3.9 Å respectively were obtained by N. Ban (ETH, Zurich, Switzerland) and his colleagues (Klinge et al., 2011; Rabl et al., 2011). The only crystal structure of mammalian ribosome obtained so far is rabbit 43S initiation complex solved at 11 Å resolution in the laboratory of T. Steitz (Lomakin and Steitz, 2013). Significant advances in deciphering detailed mechanisms, fidelity and stalling of protein synthesis using X-ray analysis were made by the laboratories of H. Noller, M. Yusupov, J. Cate, T. Steitz, V. Ramakrishnan, who carried out many unique studies on crystal structures of different intermediate states of translating or stalled ribosome (references marked by \*).

While X-ray crystallography has been highly informative, one of its limitations is that the result is a static model. The translation process, however, passes through a cycle where major interactions physically change with time. A consequence of the nature of the technique is that only interactions

that minimally alter the ribosome's structure and do not interfere with crystal packing can be observed by modifying any known crystal form. To overcome this problem, the cryo-electron microscopy is employed by researchers.

### *Cryo-electron microscopy of the ribosome*

The relatively "young" but extremely ambitious technique of cryo-electron microscopy (cryo-EM) is currently receiving a lot of attention from structural biologists. Some would even call it "the new era of cryo-EM" where structures at near-atomic resolution are no longer the prerogative of X-ray crystallography or NMR spectroscopy (W. Kühlbrandt, 2014a; W. Kühlbrandt, 2014b). Indeed, cryo-electron microscopy made a huge progress during last several years and due to technological and computational developments is able to reach near atomic and even atomic resolution (Fisher et al., 2015; Khatter et al., 2015; Bartesaghi et al., 2015). Notably, the ribosome played an important role in this development. There are several major reasons why ribosomes are a convenient objects for cryo-EM:

- Size (2.5 – 4.3 MDa): big size and globular shape make it readily visible on cryo-EM micrographs;
- Stability: due to high RNA content it is more stable during the exposure to electrons;
- Availability of crystal structures: fitting already known crystal structure into cryo-EM density facilitates modelling of similar structures.

Cryo-electron microscopy delivers the number of strong methodological advantages to the area of structural investigation of macromolecules. First, molecules in solution can be studied, thus obviating the demanding and limiting step of crystallization. Another advantage is that the amount of material and the concentration required for cryo-EM is considerably lower than that required for crystallography. Third, it provides an opportunity to analyse different populations (even minor ones) of the same sample allowing the trapping of intermediate states of dynamic biological processes.

The advantages outlined above overcame the limitations of X-ray crystallography and have shed light on high resolution structures of the ribosomes from *Trypanosoma brucei* (Hashem et al., 2013), *Plasmodium falciparum* (Wong et al., 2014), humans (Anger et al., 2013, Khatter et al., 2015). Furthermore, it revealed the structures of mitochondrial ribosomal subunits and the full mito-ribosome (Greber et al., 2014 and 2015; Kaushal et al., 2014; Brown et al., 2014; Amunts et al., 2014 and 2015), the chloroplast ribosome (Manuell et al., 2007), the stalled *Bacillus subtilis* ribosome (Sohmen et al., 2015), the membrane bound mammalian ribosomes (Voorhees et al., 2014) and many functional complexes that were difficult to get by X-ray crystallography (see references

marked by \*\*).

Cryo-EM does however suffer from some strong disadvantages. First, the flexibility of the particles on cryo-EM grid is much higher than flexibility of the particles inside the crystal. For example, a distinctive feature of the human ribosome is the presence of human-specific long rRNA expansion segments, which contribute to ~25% of molecular weight of the ribosome. Despite solving structures of human ribosome at 5.0 and 3.6 Å resolution, the structure of these 1 MDa expansion segments remains enigmatic. Another weak point is the problem of resolution. Researchers use different methods to estimate the resolution of their structures due to the absence of a unified approach to calculate it. Moreover, the resolution of the structure is not homogeneous. Due to the movements of the specimen during the exposure with electrons, the resolution on the periphery can be significantly lower than in the centre of the particle. And finally, the field of cryo-EM still lacks the unified tools for validation of the structures. This can cause misinterpretations and errors in the final model.

Summarizing, methods of structure determination are too different to be compared between each other. Every technique has its limitations that must be respected. Especially working with very big asymmetric molecular assemblies like ribosome, we need to be particularly careful with data interpretation, since the resolution is still far below that of the real atomic resolution, which is 1.5 Å and higher (Blow, 2002).

## STAPHYLOCOCCUS AUREUS

The high-resolution structures of ribosomes and ribosomal subunits obtained by crystallography and electron microscopy have revolutionized the field of protein translation. Knowledge of the precise positions of residues in the ribosome in various states has led to a deeper understanding of the complex mechanisms of protein synthesis. Crystal structures of ribosomal complexes with antibiotics and antifungal compounds and other ribosome inhibitors have provided unparalleled insight into their mechanisms of action, and they also facilitate the design of more effective drugs (Garreau de Loubresse et al., 2014; see for review Wilson, 2014). It was discovered that most of translation inhibitors bind to the conserved regions of the ribosomes (PTC, tRNA-binding sites, protein exit tunnel, etc). However, the effects of the same drug on different organism can vary from species to species. An excellent example is provided by the drug-resistant bacteria which are tolerant to many of commonly used antibiotics. Among them is *Staphylococcus aureus* (*S. aureus*), a severe pathogen that causes numerous infections in humans. This bacterium is rather unique and thus, requires individual approach for treatment. Therefore, solving the structure of the ribosome from *S. aureus* will be the first step in understanding precise mechanism of its resistance to antibiotics and will facilitate the design of new antistaphylococcal compounds.

### Main characteristics of *S. aureus*

*Staphylococci* are Gram-positive bacteria, with diameters of 0.5 – 1.5  $\mu\text{m}$  and characterized by individual cocci, which divide in more than one plane to form grape-like clusters (Harris et al., 2002). To date, there are at least 40 species and 11 sub-species in the genus *Staphylococcus*, many of which preferentially colonize the human body. *Staphylococcus aureus* and *Staphylococcus epidermidis* are the two most characterized and studied strains due to their medical importance. *Staphylococci* are non-motile, non-spore forming facultative anaerobes that grow by aerobic respiration or by fermentation. Pathogenic species are commonly identified by their ability to produce coagulase, and thus clot blood. Members of *Staphylococcus* genus are catalase-positive and oxidase-negative, distinguishing them from the genus *streptococci*, which are catalase-negative, and have a different cell wall composition to *staphylococci*.

*S. aureus* is a major pathogen of increasing importance due to high antibiotic resistance (Lowy, 1998). The species name *aureus* refers to the fact that colonies often have a golden colour when grown on solid media. The cell wall of *S. aureus* is a tough protective coat, about 20 – 40 nm thick

(Shockman and Barrett, 1983). About 50% of the cell wall mass is made of peptidoglycan (Waldvogel, 1990). Another cell wall constituent is a group of phosphate-containing polymers called teichoic acids, which contribute about 40% of cell wall mass (Knox and Wicken, 1973). Teichoic acids contribute a negative charge to the staphylococcal cell surface and play a role in the acquisition and localization of metal ions, particularly divalent cations, and the activities of autolytic enzymes (Wilkinson, 1997). Peptidoglycan and teichoic acid together only account for about 90% of the weight of the cell wall, the rest is composed of surface proteins, exoproteins and peptidoglycan hydrolases (autolysins). Some of these components are involved in attaching the bacteria to surfaces and are virulence determinants.

*S. aureus* is responsible for severe nosocomial and community-acquired infections. It can cause a variety of self-limiting to life-threatening diseases in humans. Some skin conditions caused by Staphylococcal exfoliative toxins include blisters, skin loss, pimples, furuncles, impetigo, folliculitis, abscesses, poor temperature control, fluid loss, and secondary infection (Murray et al., 2002; Le Loir et al., 2003; Einstein, 2008; Fridkin et al., 2005). Certain strains of *S. aureus* produce the superantigen TSST-1, which is responsible for toxic shock syndrome (TSS) (Murray et al., 2002), from which mortality is very high; death can occur within 2 hours (Chen et al., 2007). Deeply penetrating *S. aureus* infections can be severe. Such infections include endocarditis, peritonitis, necrotizing pneumonia, bacteremia, meningitis, osteomyelitis, septic arthritis, and infections of bones, joints and organs (Murray et al., 2002; Einstein, 2008; Fridkin et al., 2005).

*S. aureus* is a successful pathogen due to a combination of nasal carriage and bacterial immune-evasive strategies (Kluytmans et al., 1997; Cole et al., 2001). *S. aureus* can grow in a pH range from 4.2 to 9.3 and in salt concentrations of up to 15% (Le Loir et al., 2003). The bacteria can survive for up to 42 days on carcasses and organs, for up to 7 days on floors, for up to 46 hours on glass, after exposure to 17 or 7 hours of sunlight or UV respectively, for 60 days on meat products, for up to 7 days on coins, or from 30 min to 38 days on skin (Cimolai, 2008). It has evolved a number of regulatory mechanisms to control the synthesis of its multiple virulence factors in response to the host, stresses and environmental changes (Lowy, 1998).

## **Virulence determinants**

During bacterial infections, various genes must be expressed in a temporally coordinated manner to allow the bacterium to adapt to the environment in the host and to cause infection. Therefore, the multiplicity of these virulence regulatory factors and the interconnected networks that they form may be required to adapt to most environments (Figure 4). The *S. aureus* genome

encodes more than 100 transcriptional regulators that modulate the production of virulence factors either directly or indirectly (Junecko et al., 2012). The best characterized global regulators are the accessory gene regulator (*agr*), the staphylococcal accessory regulator (*sar*), *S. aureus* exoprotein expression (*sae*), the small regulatory RNAIII and sigma factor B ( $\sigma^B$ ).

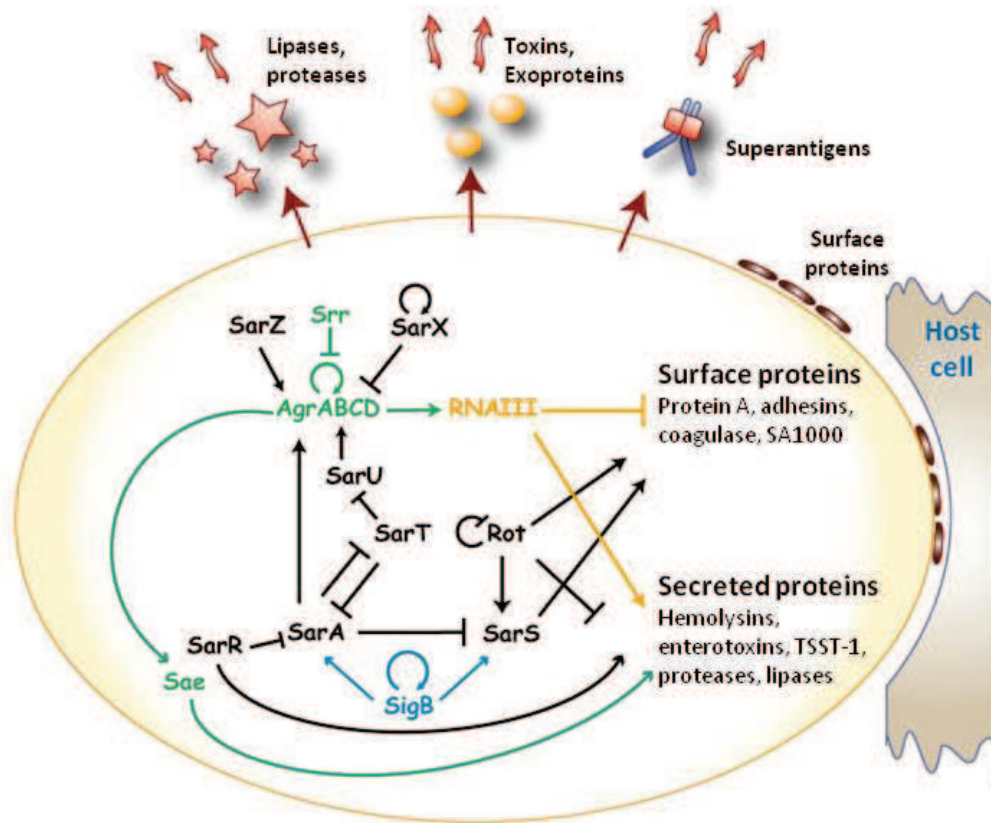


**Figure 4.** Regulation network of production of virulence factors in *S. aureus* (adapted from Chevalier, 2009).

The *agr* up-regulates the production of many exoproteins, including TSST-1, enterotoxin B and C (Recsei et al., 1986; Morfeldt et al., 1988), and V8 protease (*sspA*); Conversely, *agr* down-regulates the synthesis of cell wall associated proteins, including fibronectin-binding proteins, and fibrinogen-binding proteins during the post-exponential and stationary growth phases (Foster et al., 1990; Lindberg et al., 1990). More recent studies identified the *agr*-operon (*agrBCDA*) to be a multicomponent quorum sensing system that regulates production of RNAIII, a global regulator of virulence factors production.

Cheung et al. (1992) identified a second regulatory locus called *sar*, that is distinct from the *agr* locus. The SarA family includes 11 homologs (SarR, SarS, SarT, Rot, etc) that interact with each other forming part of a complex regulatory network controlling virulence factors. A *sarA* mutant decreases the expression of several exoproteins, such as  $\alpha$ -,  $\beta$ -, and  $\delta$ -hemolysin, and increases

others such as proteases (Cheung et al., 1994; Chan and Foster, 1998). Studies have also shown that *sarA* is essential for agr-dependent regulation. A double mutant, *agr sarA* was found to have reduced expression of exoproteins and cell wall-associated proteins compared to single *agr* and *sarA* mutants (Cheung et al., 1992).

A further locus, *sae*, has been identified and shown to have a role in the production of virulence determinants (Giraud et al., 1994). The *sae* locus is essential for the transcription of alpha-toxin,  $\beta$ -hemolysin and coagulase coding genes, but does not affect the expression of *agr* or *sarA*. Several studies have demonstrated that *sae* also modulates the production of virulence factors other than toxins including surface proteins and capsule biosynthesis components (Novick and Jiang, 2003; Voyich et al., 2009; Mainiero et al., 2010; Sun et al., 2010; Luong et al., 2011).

The regulation of virulence determinants may also involve **sigma factors** ( $\sigma$ ), which are proteins that bind to the core RNA polymerase to form the holoenzyme that binds to specific promoters (Moran, 1993; Deora and Misra, 1996). In *S. aureus* there are two sigma factors:  $\sigma^A$ , the primary sigma factor responsible for the expression of housekeeping genes, whose products are necessary for growth (Deora et al., 1997); and  $\sigma^B$ , the alternative sigma factor, that regulates the expression of many genes involved in cellular functions (Deora and Misra, 1996).  $\sigma^B$  has a role in virulence determinant production, and the stress response. At least 30 genes in *S. aureus*, most of which are involved in stress responses, have been shown to be controlled by  $\sigma^B$ . Amongst them, SigB is involved in bacterial aggregation by modulating the expression of the genes encoding clumping factor or other adhesins (Gertz et al., 2000; Horsburgh et al., 2002).

Another important virulence regulator I would like to mention is RNAIII. It is a highly abundant and stable regulatory RNA, with a complex secondary structure (Figure 5). Some of the structural motifs allow RNAIII to interact with Shine-Dalgarno (SD) sequence of some coding RNAs, such as *rot* mRNA. RNAIII directly upregulates translation of  $\alpha$ -hemolysin and carries the coding sequence of  $\delta$ -hemolysin. It also known to downregulate translation of protein A and fibrinogen-binding protein encoded by gene SA1000 (Novick et al., 1993).

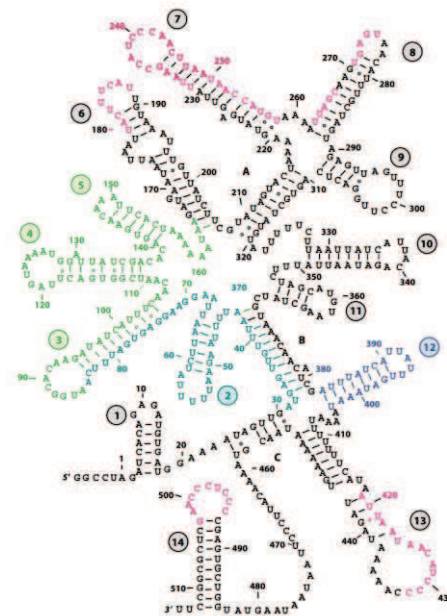


**Figure 5.** RNAIII secondary structure (adapted from Benito et al., 2000). Numbers refer to individual stem-loops; pink nucleotides are complementary to *rot* mRNA or other SD sequences; blue nucleotides delineate the terminator stem loop; aqua, pre-delta coding region; green,  $\delta$ -hemolysin coding region.

### ***S. aureus* - superbug**

Although *S. aureus* carries powerful arsenal of virulence determinants, its presence does not always indicate infection. Bacteria can be found as part of the normal skin flora and in anterior nares of the nasal passages as a commensal (Kluytmans et al., 1997; Cole et al., 2001). It is estimated that around 20% of individuals are long-term carriers of *Staphylococcus aureus* (often colonized by a single strain of *S. aureus* over long time periods), about 60% are intermittent carriers (may carry different strains over time), and approximately 20% rarely carry it (Kluytmans et.al., 1997; VandenBergh et.al., 1999). These numbers attributed to the ability of *S. aureus* to evade the host immune response including immunoglobulin A and G, lysozyme, lactoferrin and antimicrobial peptides (Kaliner, 1991). A variety of escape mechanisms can be used: staphylokinase (Jin et al., 2004) and membrane lipid modification (Peschel et al., 2001) against cationic antimicrobial peptides; production of protein A that binds Fc region of immunoglobulins, thereby inactivating them (Crossley and Archer, 1997). Furthermore, all *S. aureus* strains are lysozyme resistant because they possess the peptidoglycan-specific O-acetyltransferase (Bera et al., 2005).

Besides protection from mammalian defensins, *S. aureus* shows extremely high level of resistance to antibiotics and antimicrobial compounds in general. Since the time antibiotics were introduced to masses, *S. aureus* has developed resistance to most of them and now *staphylococcal* infections have become very difficult to treat. Antimicrobial resistance of pathogenic bacteria is a

genuine problem of the modern medicine. The therapeutic outcome of infections that result from antibiotic resistant strains is worse than the outcome of those that result from sensitive strains (Cosgrove et al., 2003). Once identified in a new setting, unique resistant clones rapidly spread. Moreover, they frequently carry resistance genes to other antimicrobial agents (Lyon et al., 1984).

A 2014 report by World Health Organization (WHO) reveals that antimicrobial resistance, including antibiotic resistance is no longer a prediction for the future, it is happening right now in every region of the world and has the potential to affect anyone, of any age, in any country. Antibiotic resistance is now a major threat to public health. According to the report, as many as 60% of *Staphylococcus aureus* infections are determined to be methicillin-resistant (MRSA) in Europe. This value was 90% in the WHO Region of Americas, 80% in African Region, 80% in Western Pacific Region. 50% of *S. aureus* infections in Eastern Mediterranean Region and more than 25% in some parts of South-East Asia Region were reported to be methicillin-resistant. Despite of recent progress in suppressing the emergency of multiresistance bacteria, antimicrobial resistance is still one of the hottest topic at the Health Assembly 2015 (World Health Organization, 2015).

### **Antibiotic resistance of *S. aureus***

The development of antibiotics enormously improved our survival from infectious diseases, yet the rise of antimicrobial resistance is threatening to make them ineffective in the future. The World Health Organization (WHO) estimates that antibiotics have added an average of 20 years to the average human lifespan. But in the almost 90 years since the discovery of penicillin, many pathogenic species have developed resistance to the most of commonly used antimicrobials. Among them *Escherichia coli*, *Mycobacterium tuberculosis*, *Neisseria gonorrhoeae*, *Streptococcus pneumoniae*, *Staphylococcus aureus*.

Notably, the Alexander Fleming observed the first antimicrobial activity of the *Penicillium* fungus on the culture of *S. aureus* in 1928 (Fleming, 1928). After several years, in the early 1940s, mass production of penicillin using the method devised by Howard Florey dramatically improved the prognosis of patients with staphylococcal infection. However, as early as 1942, penicillin-resistant staphylococci were recognized, first in hospitals and subsequently in the community (Rammelkamp, 1942). By the late 1960s, more than 80% of both community- and hospital-acquired staphylococcal isolates were resistant to penicillin. To date, penicillin-resistant isolates of *S. aureus* have reached as much as 98% in some regions. The resistance was attributed to the activity of  $\beta$ -lactamase enzyme, penicillinase. Modifications of the penicillin molecule were supposed to overcome bacterial resistance. The first semi-synthetic penicillinase-resistant penicillin was

methicillin, which is no longer in use. Introduced in 1961 it became known as antistaphylococcal penicillin, however, the reports of methicillin-resistant isolates appeared shortly (Jevons, 1961).

To date, methicillin-resistant *Staphylococcus aureus* (or MRSA) is one of the most frequent causes of antibiotic-resistant healthcare-associated infections worldwide. The emergence of antibiotic-resistant forms of pathogenic *S. aureus* (e.g. MRSA) is a worldwide problem in clinical medicine. Disease prevention and treatment strategies must be adapted to reflect infection risk factors and available treatment options.

## **Mechanisms of antibiotics action and bacterial resistance.**

To overcome the problem of antimicrobial resistance both, the mechanism of drug action and strategies of bacterial defence should be elucidated on molecular level. Most of known antibiotics act on following major targets in bacterial cells: cell wall and components of cell wall synthesis process; protein synthesis and nucleic acids synthesis machineries. In turn, bacterial resistance can be mediated by a range of mechanisms: from preventing the compound to pass the cell wall barrier to the drug degradation inside the cell (Figure 6). Different antibiotics aiming different targets, mechanisms of their action and respectively the manner of resistance to them will be discussed below. Particular regards will be given to compounds that interfere with bacterial protein synthesis apparatus, more precisely the ribosome. Taking in account the vast number of antibiotics and even countless number of their derivatives, the overview will include only some of them, most studied and most frequently used in medicine.

### *Overview of antibiotic resistance mechanisms*

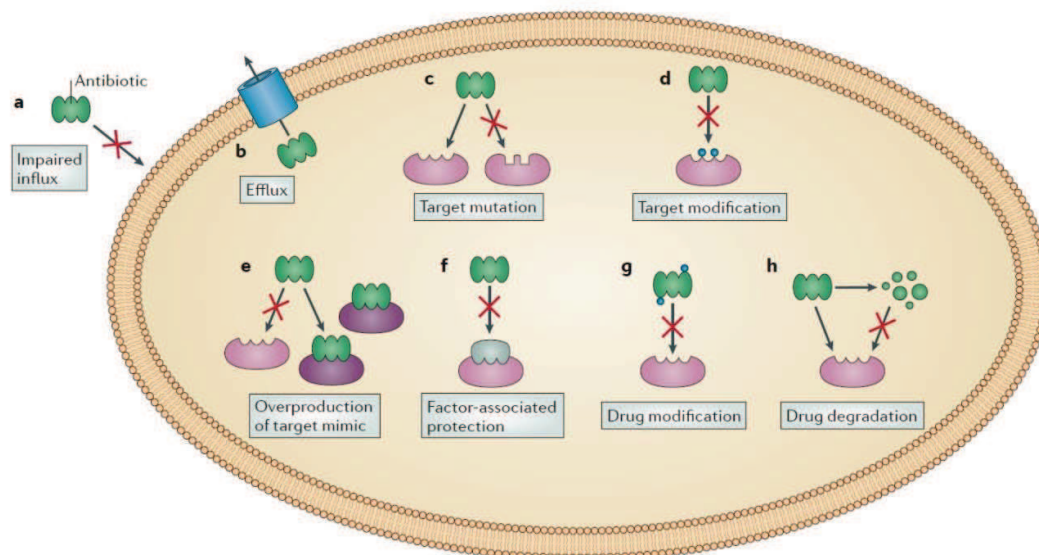


**Figure 6.** Antibacterial resistance mechanisms (adapted from Wilson, 2014):

- a. impaired influx owing to low membrane permeability;
- b. active efflux of the drug from the cell;
- c. target modification;
- d. target alteration, which lowers the affinity of the drug for the target;
- e. overproduction of a molecule that mimics the target, which lowers the effective drug concentration so that the target remains unbound;
- f. the recruitment of a specialized protein factor to actively remove the drug from the target;
- g. modification of the drug;
- h. degradation of the drug.

### *Antibiotics interfering with cell wall synthesis*

Antibacterial drugs that work by inhibiting bacterial cell wall synthesis were historically first antibiotics introduced to masses to treat bacterial infections. They have made the major contribution in treatment of many severe diseases caused by pathogenic bacteria and gave rise of antibiotic era in medicine. This class of antibiotics includes  $\beta$ -lactams, such as the penicillins, cephalosporins, carbapenems, and monobactams, and the glycopeptides, including vancomycin and teicoplanin (Neu, 1992; McManus, 1997).  $\beta$ -lactam agents inhibit synthesis of the bacterial cell wall by interfering with the enzymes required for the synthesis of the peptidoglycan layer. Due to the ability to bind penicillin these enzymes were called penicillin-binding proteins (PBPs).

Predominantly, resistance to these antibiotics is driven by the activity of  $\beta$ -lactamase enzymes that cleave  $\beta$ -lactam ring of drug molecule turning it ineffective (Bondi and Dietz, 1945). Modification of existing drugs and development of new generation of  $\beta$ -lactam antibiotics led to the evolution of a new generation of  $\beta$ -lactamases, which have an extended substrate spectrum.

A widely used mechanism against second-generation  $\beta$ -lactams (methicillin, carbapenems, etc) depends on the changes in PBPs. Mutational changes in the original enzymes, or the acquisition

of different ones, leads to inability of antibiotic to bind its target and to interfere with cell wall synthesis.

Analogously to methicillin, resistance to glycopeptide antibiotics (vancomycin, teicoplanin) has manifested itself largely through the expression of genes that encode proteins that reprogram cell wall biosynthesis and thus evade the action of antibiotic (Pootoolal et al., 2002). The genes conferring antibiotic resistance are usually part of a transposable element located on a large plasmid, often with additional antimicrobial resistance genes (e.g., gentamicin and erythromycin) (Poole, 2004; Jacoby and Munoz-Price, 2005).

### *Antibiotics interfering with nucleic acid synthesis*

Antibiotics interfering with synthesis of nucleic acids are the most commonly prescribed antibacterials in the world. However, the resistance to these antibiotics can rise extremely rapidly (Aldred et al., 2014). The main antibiotics in this class are quinolones and fluoroquinolones, which experienced several modifications resulting in four generation with different spectrum of antimicrobial activity. Quinolones interfere with bacterial DNA replication process by converting their targets, gyrase and topoisomerase IV, into toxic enzymes that fragment the bacterial chromosome (Andriole, 2000). Another important representative of this class is rifampycin (or rifampin), the antibiotic binds to bacterial RNA polymerase and inhibits its activity (Hartmann, 1967; Calvori et al., 1965; McClure et al., 1978).

Bacteria can use several resistance pathways to discriminate the action of quinolons: 1) efflux pumps (Morita et al., 1998), 2) production of gyrase binding proteins, which either decrease the affinity of enzyme to DNA or competing for the binding site with antibiotic (Tran et al., 2005a; Tran et al., 2005b), 3) mutations of enzyme residues critical for antibiotic binding (Hooper, 1999). The resistance to rifampicin is mainly mediated by mutation of the antibiotic binding site on the RNA polymerase (Goldstein, 2014).

### *Antibiotics interfering with protein synthesis*

The majority of antibiotic classes that are used in the clinical setting and target the ribosome have been marketed in the twenty-first century. Ribosome-binding antibiotics differ from compounds used in many other therapeutic areas as their mechanism of action is dominated by interactions with RNA rather than with target proteins. Therefore, ribosome-targeting antibiotics provide an important paradigm for the study of RNA molecular recognition by small molecules.

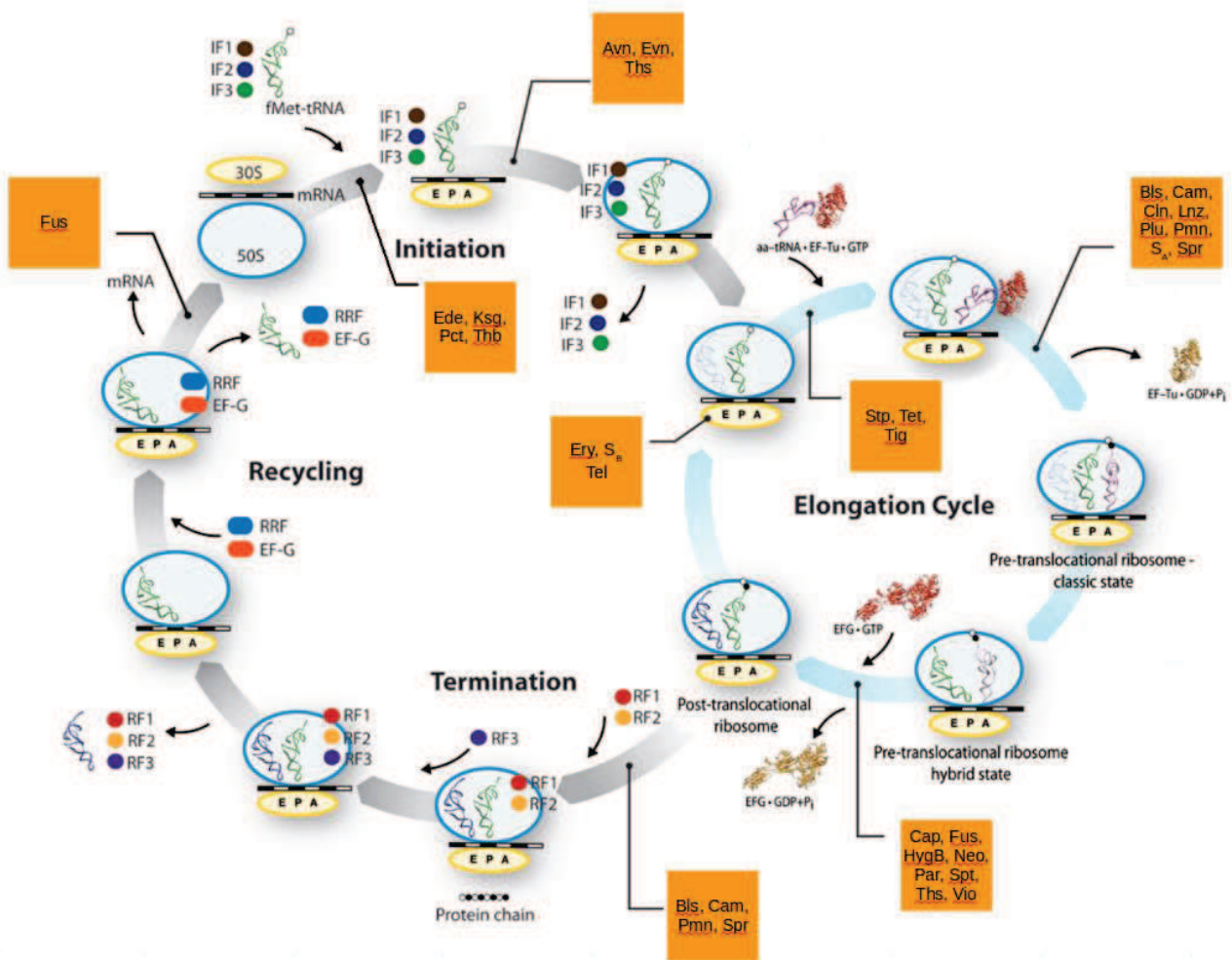


**Figure 7.** Antibiotics targeting sites during protein synthesis (adapted from Agirrezabala and Frank, 2010; Wilson, 2014). *Fus* - fusidic acid; *Ede* - edeine; *Ksg* - kasugamycin; *Pct* - pactamycin; *Thb* - thermorubin; *Avn* - avilamycin; *Evn* - evernimycin; *Ths* - thiostrepton; *Bls* - blasticidine S; *Cam* - chloramphenicol; *Cln* - clindamycin; *Lnz* - linezolid; *Plu* - pleuromutilins; *Pmn* - puromycin; *S<sub>A</sub>* - streptogramin A; *Spr* - sparsomycin; *Cap* - capreomycin; *HygB* - hygromycin B; *Neo* - neomycin; *Par* - paromomycin; *Spt* - spectinomycin; *Vio* - viomycin.

Bacterial ribosome is the target of a chemically diverse group of natural secondary metabolites that bind to specific sites within the ribonucleoprotein complex, where they interfere with protein synthesis and ultimately inhibit microbial growth. Interest in the ribosome as a target for the discovery of new antibacterials has been spurred over the past few years by the structure determination of whole bacterial ribosomes, subunits, domains and antibiotic complexes thereof (see for review Hermann, 2005; Tenson and Mankin, 2006). Three-dimensional structures of ribosome–antibiotic complexes have confirmed earlier biochemical work, revealing that the natural products interact predominantly with the RNA components in the functional sites of the ribosome such as tRNAs binding sites, PTC, decoding centre, peptide exit tunnel (see for review Blaha et al., 2012; Sohmen et al., 2009; Wilson 2011). Table 1 presents an overview on the antibiotics that target

the ribosome, their binding sites and mechanism of bacterial resistance.

**Table 1.** Mechanisms of action and resistance mechanisms of selected ribosome-targeting antibiotics (adapted from Wilson, 2014).

DM - drug modification/degradation; E - efflux/membrane permeability; EF - elongation factor; FP - factor-assisted protection; ND - not determined; PTC - peptidyl-transferase center;  $S_A$  - Streptogramin A;  $S_B$  - streptogramin B; TA - target alteration via modification (or lack thereof); TM - target mutation.

Antibiotic	Molecular target	Inhibition mechanism	Resistance mechanisms
Edeine	30S	Initiation	DM, TM
Kasugamycin	30S	Initiation	DM, TA, TM
Paromomycin, neomycin	30S	Translocation, tRNA delivery	DM, E, TA, TM
Spectinomycin	30S	Translocation, tRNA delivery	DM, E, TA, TM
Streptomycin	30S	Translocation, tRNA delivery	DM, E, TA, TM
Doxycycline, tigecycline	30S	tRNA delivery	DM, E, FP, TM
Chloramphenicol	50S	PTC	DM, E, TA, TM
Clindamycin, lincomycin	50S	PTC	DM, E, TA, TM
Streptogramins A, B	50S	PTC	E, TA, TM
Linezolid	50S	PTC	E, TA, TM
Puromycin	50S	PTC	DM
Sparsomycin	50S	PTC	E, TM
Tiamulin	50S	PTC	E, TA, TM
Blasticidin S	50S	PTC, termination	DM, TM
Evernimicin, avilamycin	50S	Initiation	TA, TM
Erythromycin, telithromycin	50S	Nascent chain elongation	DM, E, TA, TM
Thiostrepton	50S	Factor binding	TA, TM
Thermorubin	70S	Initiation	ND
Viomycin, capreomycin	70S	Translocation	DM, TA, TM
Kirromycin	EF-Tu	Elongation	TM
Fusidic acid	EF-G	Elongation, recycling	E, FP, TM

### Current drugs used in treatment of *S. aureus* diseases

Despite the fact that in general *S. aureus* shows high level of resistance to many commonly used antibiotics, different strains display different antibiotics susceptibility profiles (Figure 8). Fine diagnostics, right antibiotic selection and correct medical prescriptions may help to fight this pathogen more effectively. Factors to consider may include the efficacy of the drug, incidence of toxicity, potential for resistance development, penetration of the antibiotic into certain tissues (e.g.

bone, cerebrospinal fluid), cost, stability, and dosing convenience for home intravenous use.

Today,  $\beta$ -lactamase-resistant penicillins (methicillin, oxacillin, cloxacillin, and flucloxacillin) are used as first-line treatment of MSSA. MRSA infections are commonly treated with non- $\beta$ -lactam antibiotics, such as clindamycin (a lincosamine) and co-trimoxazole (also commonly known as trimethoprim/sulfamethoxazole). Resistance to these antibiotics has also led to the use of new, broad-spectrum anti-gram-positive antibiotics, such as linezolid, because of its availability as an oral drug. First-line treatment for serious invasive infections due to MRSA is currently glycopeptide antibiotics (vancomycin and teicoplanin). There are number of problems with these antibiotics, such as the need for intravenous administration (there is no oral preparation available), toxicity, and the need to monitor drug levels regularly by blood tests. Based on the information described in several comprehensive reviews (Rayner and Munckhof, 2005; Johnson and Decker, 2008; Morgan, 2011), the main antimicrobial agents and their therapeutic use are summarized in Table 2. Several antimicrobial agents and their therapeutic use are summarized in Table 2.

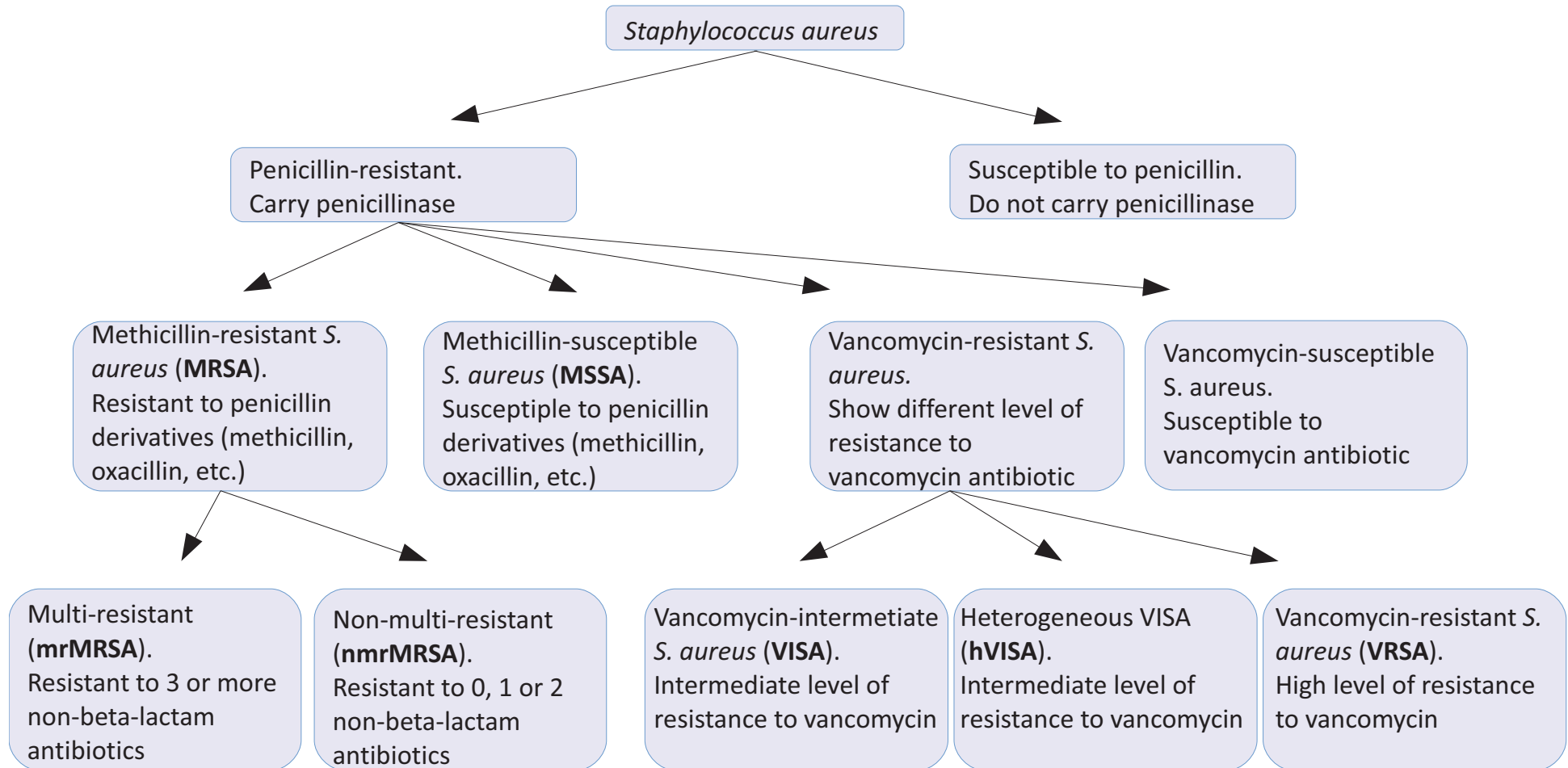


**Figure 8.** Antibiotics susceptibility profiles of *S. aureus*. (Vancomycin resistant strains highlighted separately here. Though, they can be allocated in almost all classes presented in the scheme.)

**Table 2.** Several antimicrobial agents and their therapeutic utilization

Antibiotic	Mechanism of action	Infections to treat	Used against
<b>ANTIBIOTICS USED PRIMARILY TO TREAT METHICILLIN-SUSCEPTIBLE <i>S. AUREUS</i> (MSSA)</b>			
<b>B-lactam antibiotics not resistant to <math>\beta</math>-lactamase</b>			
Penicillin, benzpenicillin	Inhibiting the synthesis of bacterial cell wall	Broad spectrum but active only against a very small part of <i>S. aureus</i> species	Only against strains without $\beta$ -lactamase enzyme
Cephalosporins (cephazolin, cephalothin, cephalexin)	Inhibiting the synthesis of bacterial cell wall	Skin and soft tissue infections	Against some strains which don't hydrolyze antibiotic by lactmase
<b>B-lactam antibiotics resistant to <math>\beta</math>-lactamase</b>			
Methicillin	Inhibiting the synthesis of bacterial cell wall	Broad spectrum, but has side effects.	MSSA
Flucloxacillin	Inhibiting the synthesis of bacterial cell wall	Rather bactericidal. Used for serious infections	nmrMRSA
Dicloxacillin	Inhibiting the synthesis of bacterial cell wall	Not very bactericidal. Used for minor infections	nmrMRSA
Carbapenems (imipenem, meropenem)		Broad spectrum. Agents to be held in reserve for treatment of <i>S. aureus</i> infections	MSSA
<b>Non-<math>\beta</math>-lactam</b>			
Macrolides (erythromycin, clarithromycin, roxithromycin)	Binding 50S ribosomal subunit. Inhibiting protein synthesis	Bacteriostatic. Used for minor infections	MSSA and some nmrMRSA
Azalides	Binding 50S ribosomal subunit. Inhibiting protein synthesis	Bacteriostatic. Used for minor infections	MSSA and some nmrMRSA
Lincosamides (lincomycin, clindamycin)	Binding 50S ribosomal subunit. Inhibiting protein synthesis	Bacteriostatic. Skin soft tissues infections	MSSA and most nmrMRSA

Antibiotic	Mechanism of action	Infections to treat	Used against
Tetracyclines (tetracycline, minocycline)	Binding 30S ribosomal subunit. Inhibiting protein synthesis	Not very efficient but cheap. Used in developing countries	Some mrMRSA are susceptible to minocycline but not tetracycline
Aminoglycosides (gentamicin, kanamycin, streptomycin)	Binding 30S ribosomal subunit. Inhibiting protein synthesis	Used for synergy in the treatment of <i>S. aureus</i> endocarditis	Most strains of MSSA and nmrMRSA
<b>ANTIBIOTICS USED PRIMARILY TO TREAT METHICILLIN-RESISTANT <i>S. AUREUS</i> (MRSA)</b>			
Vancomycin	Inhibiting proper cell wall synthesis	Broad effect against Gram+ bacteria. Used to treat serious <i>S. aureus</i> infections. Has some side effects.	Efficient against MRSA, but against MSSA shows less efficiency compared to $\beta$ -lactam antibiotics
Teicoplanin	Inhibiting proper cell wall synthesis	Broad effect against Gram+ bacteria. Very similar to vancomycin	Very similar to vancomycin
Rifampicin	Inhibiting DNA-dependent RNA polymerase	Broad spectrum. Usually used in combination with other antibiotics since the resistance to rifampicin appears fast	Active against many pathogens including mrMRSA.
Fusidic acid	Binding translation elongation factor G (EF-G). Inhibiting protein synthesis	Broad effect against staphylococci. Usually used when more simple antibiotics are ineffective	Active against staphylococci, including mrMRSA
Fluoroquinolones (cyprofloxacin, gatifloxacin, moxifloxacin)		Broad spectrum. Used rarely cause rapid emergency of resistance. Usually not used alone	MSSA, some mrMRSA
<b>LAST RESORT ANTIBIOTICS</b>			
Streptogramins (quinupristin / dalfopristin)	Binding 50S ribosomal subunit	Complicated skin and skin structure infections	Suspected or proven MRSA
Streptogramins (pristinamycin)	Binding 50S ribosomal subunit	Used in combination with doxycycline if possible	mrMRSA when other antibiotics are inefficient or cause an allergy
Oxazolidinones (linezolid)	Binding to the ribosome, prevents initiation complex formation	Broad spectrum. From Skin infections to pneumonia	Against many pathogenic Gram+ bacteria including MRSA

## ***S. aureus* Ribosome as a target for new antibiotics**

A rise in the antimicrobial resistance of *S. aureus* has forced researchers to modify existing or find/synthesize new drugs to overcome resistance. The ribosome looks very attractive target for new drugs. *A fortiori* there are already some examples of successfully introduced synthetic antibiotics, linezolid and tedizolid, that were developed for treatment of serious infections caused by Gram-positive bacteria that are resistant to several other antibiotics. As already mentioned, unrevealing the structure of ribosomes from Gram-negative bacteria has led to significant progress in understanding antibiotics' action. However, this knowledge cannot be always expanded to Gram-positive bacteria that have differences in translation apparatus. Thus, solving the structure of *S. aureus* ribosome will lead us to better understanding of the regulation of protein synthesis in Gram-positive bacteria, their mechanisms of antibiotics resistance. Structure of *S. aureus* ribosome will provide insights for design of new drugs against this pathogen.

## TRANSLATION ELONGATION FACTORS

Ribosomal peptidyl transferase centre (PTC) and translation elongation cycle are one of the most preferred targets of naturally produced inhibitors of protein synthesis (see Figure 7 and Table 1). The elongation cycle is the most conserved step of protein synthesis among all organisms. It is the most energy-consuming step of translation (incorporation of 1 amino acid requires hydrolysis of 4 high energy bonds). PTC and translation elongation factors are highly homologous between pro- and eukaryotes. Finally, elongation factors are the targets for the protein synthesis inhibitors. Remarkably, translational elongation factors carry unique modifications that influence protein synthesis by direct or indirect effect. In this chapter I will discuss some unique properties of elongation factors (mainly translocases) of bacteria and eukaryotes, as well as their interactions with the ribosome and with inhibitors of translation.

### Translation elongation cycle

As it was mentioned above, translation elongation factors are very conserved proteins that facilitate the elongation cycle of protein synthesis, which is a multi-step process that has a very complex regulation and is aimed at specific incorporation of amino acids into the growing peptide chain. The main steps of elongation process are described in Figure 9. During each cycle of elongation, correct aminoacyl tRNA (aa-tRNA) is delivered to the A-site on the ribosome by EF-Tu (eEF1A in eukaryotes) protein in complex with GTP. Upon hydrolysis of GTP, EF-Tu-GDP leaves the ribosome and with help of EF-Ts nucleotide exchange factor transforms to GTP form, and is ready to deliver new aa-tRNA when the A-site will be rescued. A peptide bond is formed between the peptidyl-tRNA in the ribosomal P-site and aa-tRNA in the A-site. It is suggested that protein EF-P (eIF5A) stimulates the formation of peptide bond, especially "difficult" ones such as proline-proline. To free the A-site for next aa-tRNA, the A-site and P-site tRNAs are moved to P- and E-sites respectively and mRNA advances by one codon. This reaction called translocation and provided by EF-G (eEF2) in GTP-dependent manner. It's been shown that translocation can be reversible - bacterial-specific factor EF4 (Qin et al., 2006) may push tRNAs and mRNA back to P- and A-sites (reaction of back translocation is coloured in pink in the Figure 9). When the A-site is free, the ribosome continues elongation of nascent peptide until stop codon is encountered.

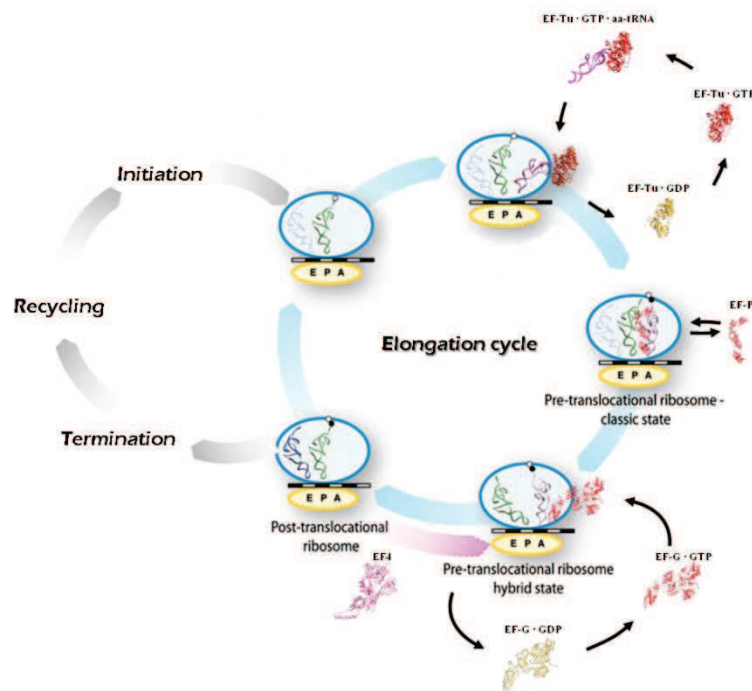


**Figure 9.** Main steps of elongation cycle of translation (adapted from Agirrezabala and Frank, 2010).

#### *Elongation factor EF-Tu (eEF1A)*

Eukaryotic factor eEF1A carries ethanolamine and phosphoglycerol (EPG) modification on the conserved Glu62 residue. It has been found in mammals, plants and protozoan parasites, but not in archaea, bacteria or lower eukaryotes. Direct role of EPG modification in translation has not yet been discovered. Since eEF1A is involved in various other functions in the cell, such as organization of cytoskeleton, regulation of protein degradation and viral propagation (Mateyak and Kinzy, 2010), modification might be required there. No EPG-like modification was found in its ortholog, bacterial EF-Tu protein, but it can be deactivated by phosphorylation of conserved threonine Thr-382 (Lippman et al., 1993) by P1 Doc toxin from bacteriophage harboured in the genome of pathogens (Cruz et al., 2014). In addition, bacterial translation inhibition via interference with EF-Tu can be caused by antibiotic kirromycin. The crystal structure of the complex EF-Tu\*GDP and kirromycin demonstrated that upon binding of antibiotic the protein stays locked in the ribosome in GDP-bound conformation (Vogelely et al., 2001). Utilization of EF-Tu as a model for developing new drugs led to a successful developing of semisynthetic thiopeptide inhibitors that are active against Gram-positive pathogens including MRSA and VRSA (Leeds, 2011).

#### *Elongation factor EF-P (eIF5A)*

eIF5A in eukaryotes and EF-P in bacteria are homologous elongation factors that carry unique

modifications. eIF5A has hypusine modification located on a conserved lysine, Lys51 amino acid residue whereas EF-P has an unusual lysinylation of Lys34 (Yanagisawa et al., 2010; Roy et al., 2011). Lysinylation of EF-P suggested to enhance the ability of this protein to stimulate peptide bond formation (Park et al., 2012), especially for polyproline synthesis (Doerfel et al., 2013; Ude et al., 2013). Crystal structures of eIF5A and EF-P from a variety of eukaryotes, archaea and bacteria have been solved and the proteins show significant structural similarity (Yao et al., 2003; Tong et al., 2009; pdb code 3ER0). Structural analysis of eIF5A bound to the 80S ribosome (Melnikov et al., 2015) showed the significance of hypusine modification in elongation of nascent peptide chain. In the structure of bacterial ribosome with initiator tRNA and EF-P protein (Blaha et al., 2009), the authors did not see lysinyl modification but the data suggested that its presence may facilitate the peptide bond formation in prokaryotes.

### *Elongation factor EF-G (eEF2)*

eEF2 is one of the main regulator of protein synthesis in eukaryotes. It serves as a mediator of global physiologic processes and metabolic pathways of eukaryotic cells such as mTOR, cell cycle, stress response and cancer (reviewed in Proud, 2002; White-Gilbertson et al., 2009). Under particular conditions induction of eEF2-specific kinase (eEF2K) leads to phosphorylation of threonine, Thr56 of eEF2 protein, and in this way a cell can instantly alter protein synthesis (Ovchinnikov et al., 1990; Price et al., 1991).

Apart several phosphorylation sites eEF2 protein carries a unique modification called diphthamide on conserved histidine residue (His699 in yeast, His715 in human) on the tip of domain IV. Diphthamide modification of eEF2 is well conserved in archaea and eukaryotes but not eubacteria. Its biosynthesis involves 6 enzymes (Chen and Bodley, 1988) and its absence is lethal for eukaryotic cell (Chen and Behringer, 2004; Liu et al., 2006). On the other hand, diphtheria toxin from *Corynebacterium diphtheriae* and *Pseudomonas* exotoxin A transfer ADP-ribose from NAD<sup>+</sup> to the diphthamide residue, thus blocking the activity of eEF2 and inhibiting protein synthesis (Honjo et al., 1968; Sitikov et al., 1984; Liu et al., 2004). The exact role of diphthamide in translocation reaction remains unknown. It was demonstrated that its deficiency leads to diminishment of translation fidelity in yeast (Ortiz et al., 2006) and in mice (Liu et al., 2012). Using cryo-EM analysis of 80S\*eEF2 complex C. Spahn and his colleagues confirmed that diphthamide might be close enough to interact with decoding center (Spahn et al., 2004). In addition to phosphorylation and ADP-ribosylation, binding of a small antifungal molecule called sordarin may inhibit yeast eEF2 activity. It significantly alters the conformation of eEF2 and prevents its dissociation from the ribosome (Figure 10 C).

Recently new antimalarial compound DDD107498 was shown to inhibit eEF2 from the *Plasmodium* parasite (Baragaña et al., 2015).

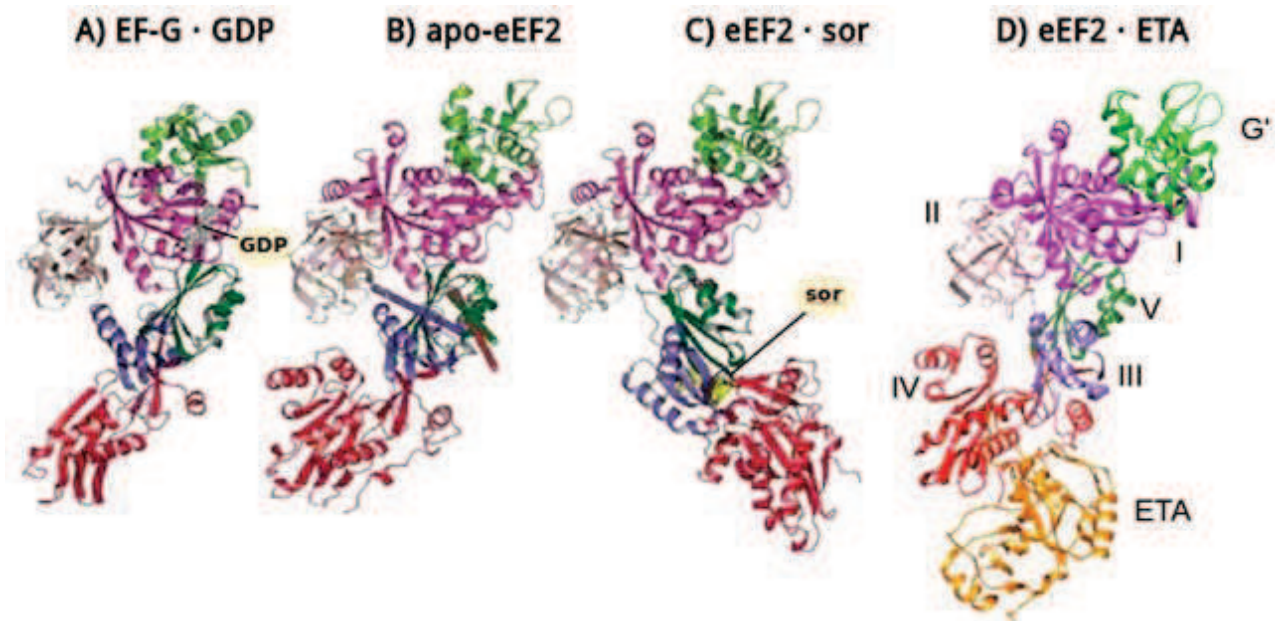


**Figure 10.** The structures of EF-G in complex with GDP (A), apo eEF2 (B), eEF2 in complex with sordarin (sor) (C), eEF2 in complex with enterotoxin A (ETA) (D). The domains are labelled by roman numerals I–V except for the G' domain. The location of the screw axes describing the motion of domains III, IV and V relative to the three N-terminal domains are shown on apo eEF2 as rods colored similarly to the domain (adapted from Jørgensen et al., 2003).

Bacterial protein, EF-G, also has conserved histidine residue His583 on the tip of domain IV. Replacement of this histidine with lysine or arginine decreases the rate of tRNA translocation at least 100-fold (Savelsbergh et al., 2000). No specific modifications have been detected on His583, but EF-G factor is known to be phosphorylated by the kinase from bacteriophage T7 (Robertson et al., 1994). Phosphorylation was suggested to promote bacteriophage specific mRNA. EF-G protein is also a well-known target for fusidic acid, antibiotic against Gram-positive bacteria that inhibits EF-G turnover, in either GTP hydrolysis or translocation (Bodley et al., 1969; Lee-Huang et al., 1974; Johanson et al., 1996). Fusidic acid, as kirromycin, belongs to the least antibiotics that inhibit protein synthesis via interaction with protein rather than rRNA.

X-Ray analysis of translocases derived from bacteria (Czworkowski et al., 1994) and yeast (Jørgensen et al., 2003) revealed relatively high homology of these two proteins. They are composed of 5 or 6 domains where the crucial role in translation is assigned to domain G (nucleotide binding) and domain IV (responsible for translocation reaction). The X-ray structures of EF-G in complex with fusidic acid and dityromycin (Lin et al, 2015), eEF2 in complex with sordarin (Jørgensen et al., 2003)

and bacterial toxin (Jørgensen et al., 2005) uncovered the mechanism of protein deactivation. Recently several delicate crystallographic experiments led us to better understanding of translocation reaction in bacteria in atomic level (Pulk and Cate, 2013; Tourigny et al., 2013; Zhou et al., 2013; Chen et al., 2013, Lin et al., 2015). Unfortunately, to date, the only well developed experimental model for crystallographic studies of eukaryotic translation system (*S. cerevisiae* 80S ribosome, Ben-Shem et al., 2011) cannot be used to study translocation reaction since stress protein Stm1 occupies the binding site of eEF2 protein.

## **eEF2 is a potential target for drug development**

Elongation factors have high homology between the domains of life and very high homology within one domain. So, the eEF2 from lower eukaryotes as yeast and higher organisms such as human are believed to be very similar. Indeed, they have high similarity in amino acid sequence, identical modification sites, including phosphorylation of conserved triptophane 56 (57 in human) and diphthamidation of conserved histidine 699 (715 in human). However, they differ in ability of binding the ligands, especially small molecules that block the activity of elongation factor. Notably, fusidic acid binds preferably Gram-positive EF-G, sordarin affects solely eEF2 of fungi, but not higher eukaryotes. So far, no archaea- or mammalian-specific inhibitor of elongation factor 2 has discovered. The recent discovery of a *Plasmodium* specific inhibitor of eEF2 shows the need for a more thorough investigation of this protein, including structural analysis. From practical point of view the crystal structure of human eEF2 will clarify the reasons for selectivity of binding small molecules. Fundamentally it may provide us new insights about the mechanism of translocation in higher eukaryotic organisms. Structural information will be helpful for understanding more thoroughly the role of eEF2 as a unique target for bacterial toxins and, more generally, it can provide new hints about how translocation might take place in humans. Finally, obtaining an atomic model of eEF2 will facilitate interpretation of cryo-EM experiments on human translocation reaction. So far, cryo-EM is the only structural method to use, due to absence of crystallographic experimental model for mammalian ribosome.

## PROJECT OUTLINE

The project of present PhD thesis is dedicated to solving *S. aureus* ribosome structure and was initiated in 2011. By that time the structures of *Thermus thermophilus* and *Escherichia coli* ribosomes had already been solved by X-ray crystallography. However, the structure of any Gram-positive or any pathogenic bacteria ribosome was missing. It is known that some aspects of protein synthesis differ between Gram-negative and Gram-positive bacteria. Additionally, pathogenic bacteria have evolved complex mechanisms of translation regulation, that provides high efficiency of pathogenesis and facilitate survival under stressful conditions. Moreover, many pathogenic bacteria (including Staph) show extremely high resistance to ribosome-targeting antibiotics, which is often mediated by modifications of the ribosome. The structure of the ribosome from Gram-positive multi-resistant pathogenic bacteria *Staphylococcus aureus* would reveal peculiar structural features of translation machinery, thus will lead us to better understanding the specifications of regulation of its protein synthesis, and pathogen survival. Most importantly, it will serve as a model system for developing new anti-staphylococcal drugs.

Initially, the main goal of this project was to elucidate the structure of full 70S ribosome from *S. aureus* using X-ray analysis as a main tool. Thus the project consisted of next tasks:

- preparing the cells: growing, harvesting, breaking
- developing a purification protocol that will provide pure and stable ribosomes, suitable for crystallization
- crystallization and post-crystallization treatment: searching for crystallization conditions, growing big crystals and preparation for diffraction analysis;
- developing the strategy of data collection at the synchrotron;
- solving the structure: processing the data and building the model.

As a result we developed the protocols of purification of 70S ribosome from *S. aureus* in amount sufficient for the search of crystallization conditions. Consequently, the crystals of 70S ribosome from *S. aureus* were obtained. But as we experienced specific difficulties with the diffraction of these crystals and because of limit of time, we used cryo-EM technique to determine the structure of the *S. aureus* ribosome. The purity of the sample and serious progress in cryo-EM field during last several years gave a hope to obtain high-resolution structure. The data were collected using the latest generation of microscope (Titan Krios, installed at the Centre de Biologie

Intégrative (CBI, Illkirch, France)). Then, processing electron microscopy data and obtaining high resolution cryo-EM structure took up my attention. At the same time my colleagues are continuing crystallographic studies of 70S ribosome from *S. aureus* in the laboratory.

Results of my work on the determination of high resolution structure of the ribosome from *S. aureus* will be discussed in next the chapters.

Another part of my work was devoted to determination of the crystal structure of human elongation factor 2. This protein was found to be rather tightly bound to the human 80S ribosomes during purification using protocol developed in our lab. It is well known that eEF2 is one of the major regulator of translation in eukaryotes and is often involved in cell stress response and cancer. Determination of structure of human eEF2 would clarify some aspects of regulation and repression of protein synthesis in humans. eEF2 protein is known to be a target of specific protein synthesis inhibitors, so the structure of human eEF2 could also help to discover potential anti-cancer compounds.

Initially, the project on eEF2 started with developing the protocol of purification of native eEF2 protein using as a source the ribosome-free cytosolic fraction of HeLa cells. When protocol was developed and first crystals were obtained, we switched to the recombinant production of the protein in bacteria.

---

RESEARCH PROJECT 1:

**STRUCTURE DETERMINATION OF *S. AUREUS* RIBOSOME**

---

## **S. AUREUS CELL GROWTH**

### ***S. aureus* strain**

*Staphylococcus aureus* strain RN6390 was used in the study. It derives from clinical strain NCTC8325 and carries mutation in the gene *rbsU*, the activator of sigma B factor. Thus the production of RNAIII is increased and the ability to form biofilms is decreased in this strain (see Figure 4). Avoiding biofilm formation is important for cells growth and harvesting.

### **Cells preparation**

All manipulations with *S. aureus* cells were performed in special laboratory with safety level 2. Two litres of *S. aureus* culture was grown at 37 °C / 180 rpm in Brain Heart Infusion broth (BHI) and harvested in early logarithmic phase ( $OD^{600} = 1.0$ ), when the ribosomes are found in the highest concentration and are generally considered to be the most active (Gourse et al., 1996). Cells were washed two times with 10 mM Tris-HCl pH 7.5 and kept frozen at -80 °C. Freezing the material could not be avoided due to time constrains.

## RIBOSOMES PURIFICATION

In actively growing cells, ribosomes are relatively heterogeneous and have different conformational states, activity levels and are bound to a variety of ligands. Certainly, most ribosomes actively participate in the elongation step of translation, so they have minor conformational divergence and bind similar ligands involved in translation. However, there are other populations of non-translating ribosomes, which can be present as dissociated particles, stalled or inactive ribosomes.

When the cells are transferred to unfavourable conditions, all translating ribosomes continue the synthesis until they reach the stop codon and release newly synthesized protein. These ribosomes do not prepare for the next cycle and keep associated as 70S particles called run-off ribosomes. They are relatively homogeneous, although, some still have residual tRNAs, mRNA and translation factors bound.

Due to their mass, the total ribosome pool is rather easy to separate from other cellular components simply by several high-speed centrifugation steps. However, a sample for X-ray studies requires very high level of purity, homogeneity and stability. Therefore, purification of a unique population of ribosomes, capable of being crystallized, is a delicate procedure that requires a lot of effort, care and patience.

Two crucial parameters that have to be thoroughly controlled during purification are the concentrations of  $Mg^{2+}$  ions and monovalent salts. Magnesium stabilizes the ribosome and is particularly important for the association of small and large ribosomal subunits of bacterial ribosome. Monovalent salts at concentrations below 200 mM also contribute to the stability of bacterial ribosome, but at concentrations above 200 mM these salts can have an opposite effect (Spirin et al., 1971c; Stahli and Noll, 1977). Variations in the balance between magnesium and monovalent salts often help to ameliorate the selection of ribosomal populations.

Purification of *S. aureus* ribosomes was based on the protocols used for bacteria *Thermus thermophilus* (Gogia et al., 1986; Yusupov et al., 2001) and yeast *Saccharomyces cerevisiae* (Ben-Shem et al., 2011). Lysis procedure, ionic conditions, magnesium and polyethylene glycol (PEG) concentrations, sucrose gradients etc. were optimized during development of purification protocol.

Chemicals, plastic and kits were purchased from Sigma-Aldrich, Fluka, Merck Millipore, Hampton Research, Macherey Nagel, Qiagen. Ultrapure Milli Q water was used to prepare all buffers. All solutions were filtered using 0.22  $\mu$ m filters or autoclaved.

## Buffers

Numbers above the name indicate Mg<sup>2+</sup>/salt concentrations, mM.

Buffer A<sup>20/100</sup>:

20 mM HEPES-KOH pH 7.5  
100 mM NH<sub>4</sub>Cl  
21 mM MgOAc<sub>2</sub>  
1 mM DTT

Buffer B<sup>25/500</sup>:

10 mM HEPES-KOH pH 7.5  
500 mM KCl  
25 mM MgOAc<sub>2</sub>  
1.1 M Sucrose  
0.5 mM EDTA  
1 mM DTT

Buffer E<sup>10/100</sup>:

10 mM HEPES-KOH pH 7.5  
100 mM KCl  
10.5 mM MgOAc<sub>2</sub>  
0.5 mM EDTA  
1 mM DTT

Buffer G<sup>10/60</sup>:

5 mM HEPES-KOH pH 7.5  
50 mM KCl  
10 mM NH<sub>4</sub>Cl  
10 mM MgOAc<sub>2</sub>  
1 mM DTT

## Lysis

*Work with Staphylococcus cells have special safety requirements and should be done in a special laboratory with safety level 2. Usually these type laboratories are limited in space, and therefore they can accommodate only middle-sized incubators, shakers and centrifuges. This necessitated the adaption of purification procedure to use smaller amounts of cells initially, but nevertheless to obtain reasonable yields of ribosomes for crystallization. In the end, replacing mechanical lysis (French press, microfluidizer) with enzymatic lysis resulted in a very high efficiency of cell disruption. We used lysostaphin, a specific enzyme that cleaves cross-linking pentaglycin bridges in the cell wall of Staphylococci.*

Frozen cells (5 g) were re-suspended in 30 ml of buffer A<sup>20/100</sup> containing 1 mM EDTA, 30  $\mu$ l DNase I, 3.5 mg lysostaphin and protein inhibitors cocktail (Roche) according to recommendations of manufacturer. After incubation at 37 °C for 45 min, suspension was transferred on ice and all following step were performed either at +4 °C or on ice. Cell debris was removed by centrifugation at 30000 $\times$ g for 90 min.

## PEG precipitation and sucrose cushion

*PEG precipitation step was adapted from purification of yeast ribosomes and used to fractionate the lysate quickly and gently in order to recover the fraction containing ribosomes. Pelleting through the sucrose cushion containing 0.5 – 1 M salt is classical procedure for purification of vacant bacterial ribosomes. High concentration of KCl is compensated with increased concentration of  $Mg^{2+}$  ions. It allows the washing out remaining ligands (tRNAs, mRNA, translation factors) and some other proteins bound to the ribosome but keep 70S particle stable. At the same time the treatment should not be too harsh, so that the ribosomal proteins will not dissociate.*

The resulting supernatant (often called S30 for supernatant after centrifugation at 30000×g) was further subjected to a differential precipitation by PEG. PEG 20000 was added from a 30% w/v stock (Hampton Research) to a final concentration of 2.8% w/v for the first fractionation. The solution was centrifuged at 20000×g for 5 min. The ribosomes and light cellular components remained in soluble fraction, while components that are heavier than the ribosome such as residual polysomes, remaining cell debris, were precipitated. The supernatant was recovered and PEG 20000 was increased to 4.2% for the second fractionation. Under these conditions the ribosomes become insoluble while the smaller components (small complexes, individual proteins) remain soluble. The solution was centrifuged at 20000×g for 10 min, the ribosome pellet re-suspended to 30 – 35 ml in buffer A<sup>20/100</sup> containing 1 mM EDTA, layered on 25 ml of buffer B<sup>25/500</sup> and then centrifuged at 45000 rpm / 15 hours using Beckman Type 45 Ti rotor.

## Sucrose density gradient centrifugation

*This step is typical for purification of ribosomes of any kind (full ribosomes or individual subunits), any origin (cytoplasmic, mitochondrial or chloroplast) and any organism (bacteria, archaea or eukaryotes). The idea is to separate full ribosomes from ribosomal subunits. Due to the different size, weight and density, 70S, 50S and 30S particles sediment with different speed through the gradient of viscous solution such as sucrose. It is important to select the right concentration of sucrose and maximum amount of ribosomes for good resolutions of the particles along the gradient. It is also important to find the proper speed/time balance of centrifugation. Fractionation of gradients further allows selective collection of only the particles of interest.*

Ribosome pellet after sucrose cushion was re-suspended in buffer E<sup>10/100</sup> till 7 mg/ml and loaded on the sucrose density gradients. During development of the protocol, using sucrose gradients 10 – 30% (w/v) we found that our sample contains some particles, bigger than 70S, that were not detectable on 5 – 20% sucrose gradients usually used for purification of bacterial ribosome. Later we proved that these are ribosomal particles that sediment faster than monosomes. Later we proved that these particles are ribosomes that sediment faster than monosomes and called this fraction 100S. The presence of 100S and 50S fractions together with 70S ribosomes made sucrose

gradient step difficult to set up. To purify only 70S ribosomes, the gradient was modified to 7 – 30% (w/v) and the amount of material loaded on one gradient was decreased to 3.5 mg. Sucrose gradients 7 – 30% were cast in 36 ml Beckman SW28 tubes using the Gradient Master machine (BioComp). Ribosomal sample (0.5 ml) was layered on each gradient and centrifuged at 17100 rpm / 15.5 hours in swinging rotor Beckman SW28.

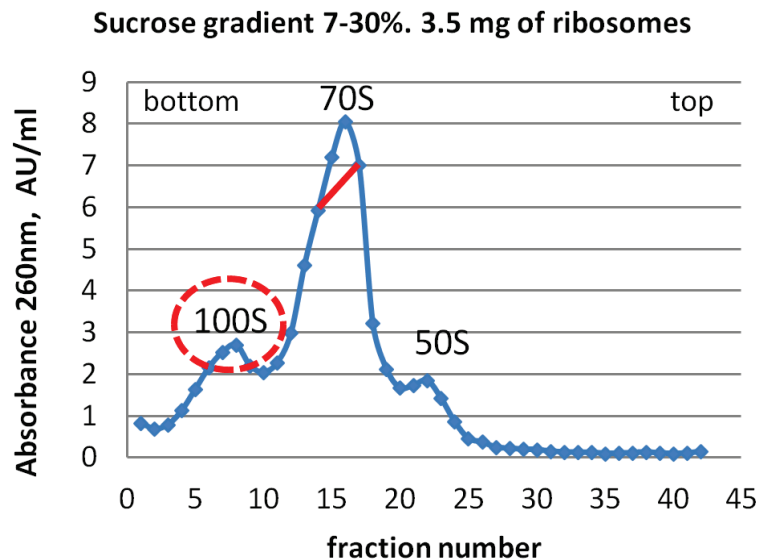


**Figure 11.** Sucrose gradient profile. Fractions (1 ml) were collected and absorbance was measured by Nanodrop 2000c (Thermo Scientific). The solid red line indicates pooled 70S fractions and red dashed circle indicates the peak of 100S ribosomes. One of the unique features of translational control in *S. aureus* is the presence of so-called 100S ribosomes in actively growing cultures (Ueta, 2009). Ribosomal dimers are referred to as 100S, and do not participate in translation. The phenomenon of ribosomal dimerization has been observed in many bacteria; however disomes were usually found during transition of cells to the stationary growth phase when the substrate is limited and the cells have to alter metabolism. The role of ribosomal dimers in actively growing cells of *S. aureus* remains unclear.

## Ribosome concentration and storage

The appropriate fractions were pooled and  $\text{MgOAc}_2$  concentration was adjusted to 25 mM. In order to precipitate ribosomes, PEG 20000 was added to a final concentration of 4.5% w/v. Ribosomes were pelleted by centrifugation (20000 $\times$ g / 12 min). The white pellet was gently dissolved in buffer G to a final concentration of 20 – 25 mg/ml; 30  $\mu$ l aliquots were flash frozen in liquid nitrogen and stored at -80 °C. Typically 10 – 12 mg of pure ribosomes were obtained from 5 grams of cells.

## RIBOSOMES CHARACTERIZATION

### One- and two-dimensional polyacrylamide gel electrophoresis (PAGE)

#### *Sample preparation for PAGE*

Sample preparation for both analyses was performed according to method described by Hardy and co-workers (Hardy et al., 1969). Ribosomes were digested for 30 min / 0 °C with 66% acetic acid in presence of 33 mM MgOAc<sub>2</sub>. rRNA was precipitated by centrifugation at 15000×g / 30 min. The soluble protein fraction was treated with by 80% acetone for at least 3 hours at -80 °C. Proteins were precipitated at 15000×g / 60 min, pellet was dried by speed-vac for 30 min and dissolved in buffer G. This preparation allowed the removal of PEG that caused diffusion of bands on 1D-PAGE and to eliminate rRNA that would occupy all positively charged ampholytes and block any movement of ribosomal proteins (RP) along the gel in the capillary.

#### *One-dimensional PAGE*

*One-dimensional PAGE separates proteins in denaturing conditions according their molecular weight but not charge.*

There are no specifications for ribosomal proteins to run this type of gel. Therefore, the standard Laemmli method (Laemmli, 1970) with slight modifications was used. The gel was stained in Coomassie Brilliant Blue R-250 according to standard protocols.

The gel demonstrated the purity of the ribosomal sample and did not reveal contamination by high molecular weight proteins such as components of the pyruvate dehydrogenase complex, which sometimes co-purify with bacterial ribosomes.

#### *Two-dimensional PAGE*

*Two-dimensional PAGE is dedicated to separation proteins by charge first with further separation by molecular weight. Running ribosomal proteins on 2D-PAGE has several challenges. First, the ribosome has to be denatured and any rRNA has to be removed. Second, most of RPs are highly positively charged with isoelectric points of 9 and higher, which makes using standard protocols unsuitable. Therefore two dimensional gel was performed using combination of protocols described (Kaltschmidt and Wittmann, 1970; O'Farrell, 1975).*

Gel for isoelectric focusing (9.2 M Urea, 2% Nonidet P-40, 4% acrylamide (28.4:1.6), 2% ampholytes (pH range 3-10), 0.01% ammonium persulfate, 0.1% TEMED) was casted in 1 mm

capillaries. Sample was mixed with 2X loading buffer (9 M urea, 2% Nonidet P-40, 10 mM DTT, 1% ampholytes) loaded on the top of vertically positioned capillary and covered with cover buffer (9 M urea, 1% ampholytes, 0.0025% bromophenol blue). Anode buffer (0.1 M H<sub>3</sub>PO<sub>4</sub>) was loaded on the bottom of electrophoretic chamber, cathode buffer (0.02 M NaOH) on the top, and isoelectric focusing launched at 500 V / 15 min then 750 V / 190 min with inverted electrodes (under these settings ribosomal proteins will not be fixed in the gel, but can be resolved relatively well). When finished, gels were removed from capillaries, soaked in solubilisation buffer (6 M urea, 0.05 M Tris-HCl pH 7.5, 30% glycerol, 2 mM DTT, 2% SDS, 0.0025% bromophenol blue) for 15 min and loaded on one-dimensional SDS polyacrylamide gel described above.

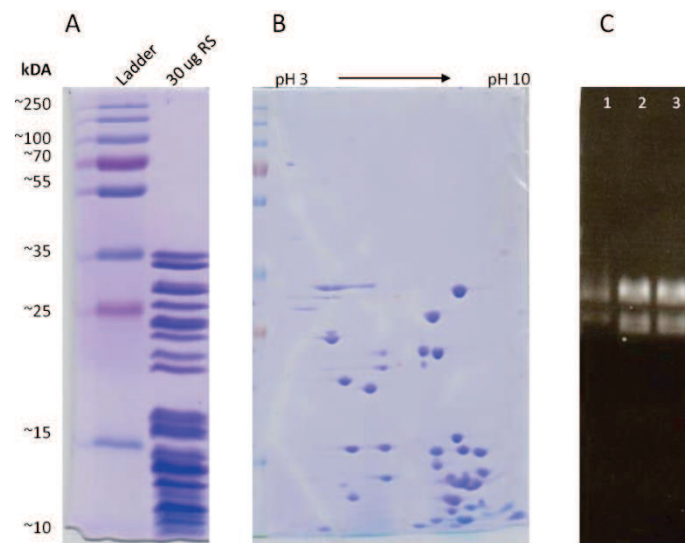


**Figure 12.** One-dimensional (A) and two-dimensional (B) PAGE of *S. aureus* ribosome sample. C. Agarose gel electrophoresis of the ribosomes: 1 – *T. thermophilus* 70S (5 µg), 2 and 3 – *S. aureus* 70S (15 µg). The upper and lower bands correspond to 23S and 16S rRNA respectively.

## Agarose gel electrophoresis

Agarose gel electrophoresis was performed according to the standard protocol (Sambrook et al., 1989). The gel was prepared in buffer TAE (40 mM Tris, 1 mM EDTA pH 8.0, 5.7% acetic acid) and contained 1% agarose. Ribosome samples were loaded directly on the gel. The gel has demonstrated the intactness of the rRNA in this condition (Figure 14 C), and the size of *S. aureus* rRNA is comparable to the size of rRNA of *T. thermophilus*.

## Analytical sucrose density gradient centrifugation

*Sucrose gradient centrifugation is very simple and powerful method to analyse stability of ribosomes under different conditions. It also allows examining the presence of different populations of ribosomes which are barely detectable during purification. In early seventies it was discovered*

that empty (or vacant) 70S ribosome can exist in two forms – tightly associated subunit couples and loosely associated subunit couples. Sucrose gradients at specific speeds and  $Mg^{2+}$ /salt concentrations revealed that tight couples stayed as 70S particles while loose couples dissociated during centrifugation forming so-called 60S peak on the gradients (Infante and Bairlein, 1971; Spirin et al., 1972; Hapke and Noll, 1976; Noll and Noll, 1976). The presence of loose couples may affect crystallization of purified sample; if they appear during analytical ultracentrifugation it is recommended to use more mild conditions during purification or to perform specific purification of tight couples using Toyopearl-Butyl hydrophobic chromatography.

Analytical gradients have exactly the same principal as preparative ones with only difference that they require much less material. Sucrose concentration of, time and speed of centrifugation were optimized for analysis of purified *S. aureus* ribosome sample.

The stability of the ribosomes was analysed under different conditions. The following conditions were tested: concentration of  $MgOAc_2$  (1 – 25 mM), concentration of KCl (60 – 200 mM), stability at 4 °C during several weeks (Figure 13 A). Before loading on gradients samples were dialysed in appropriate buffer with respective concentrations of interests; same concentrations were kept in the gradients. Additionally, preparative sucrose gradients were optimized for purification of ribosomal dimers (100S particles) and ribosomal subunits (50S and 30S particles). Results and conditions are indicated on Figure 13 B and C respectively. Analytical sucrose gradients were performed in the following buffers: 10 mM Hepes pH 7.5, 60 – 200 mM KCl, 1 mM DTT, 2-25 mM  $MgOAc_2$  using Beckman rotor SW41 and centrifugation parameters of 17000 rpm / 13 h.

As a stability test we thawed the sample and kept it at 4 °C for 2 weeks in buffer G at its original concentration (20 mg/ml). The control sample was thawed immediately before the experiment. Ribosomes (0.3 mg) from each variant were dialysed in buffer with appropriate concentration of  $MgOAc_2$  and KCl. Two samples had almost identical profiles on the gradients, and showed negligible differences only at low  $Mg^{2+}$  concentrations. Usually in the presence of 2 mM  $Mg^{2+}$  *S. aureus* ribosomes dissociated to individual 50S and 30S subunits; 6 mM  $Mg^{2+}$  prevents dissociation of 70S particles; and in the presence of 3-4 mM  $Mg^{2+}$  *S. aureus* ribosomes were found to be in transient form between 70S and 50S+30S state (Figure 13 A).

As a part of sample characterization, we also purified 100S fraction. Fractions 5 – 9 from preparative gradients (Figure 11) were pooled together, dialysed in buffer E<sup>15/100</sup>, concentrated using Centricon MWCO100 till 3.5 mg/ml and loaded on preparative sucrose gradients 7-30%. The majority of 100S peak remained intact on the gradient (Figure 13 B).

Optimization of subunits purification using sucrose gradient centrifugation was performed in preparative Beckman SW28 tubes. The aim of this purification was to obtain pure 30S particles. All the crucial conditions and profile of the gradient presented in Figure 13 C. The following agarose gel electrophoresis was used to discriminate the fractions containing only 30S particles. Fractions 14 –

16 were pooled and prepared for functional studies (data not shown).

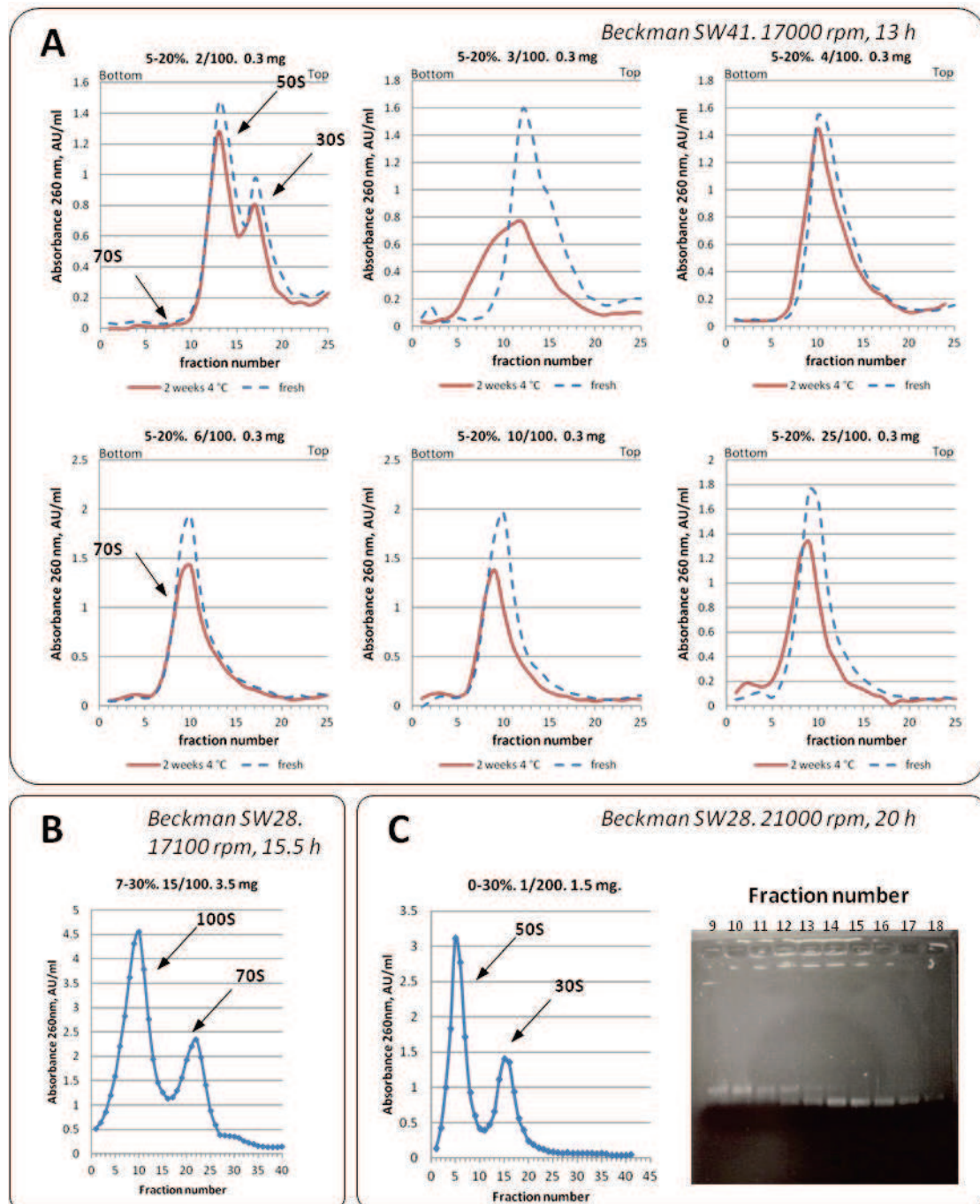


**Figure 13.** Characterization of *S. aureus* ribosomes sample by sucrose density gradient centrifugation. **A.** Analytical sucrose gradients performed in different concentration of  $MgOAc_2$ . Blue dashed curves correspond to freshly thawed sample, red curves to thawed sample that was further incubated on ice for two wk. Positions corresponding to the full 70S ribosome and large (50S) and small (30S) subunits are indicated on the top left curve. Conditions of centrifugation are indicated in the top right corner of the images. **B.** Centrifugation conditions and sucrose gradient profile of purification of 100S particles found during 70S ribosomes preparation. **C.** Centrifugation conditions and sucrose gradient profile (left) of purification of ribosomal subunits. Positions of 50S and 30S particles are indicated. Agarose gel (right) of the fractions 9-18 of the gradient: upper and

lower bands correspond to 23S and 16S rRNA respectively.

## Analytical ultracentrifugation

Analytical ultracentrifugation allows quantitative analysis of macromolecules in solution. As the sample is centrifuged, the components separated out into layers forming boundaries due to movement of particles. Sedimentation is observed (measuring absorbance/fluorescence) in real time, used to calculate the Svedberg's coefficient ( $S$ ) for the molecule. Sedimentation coefficient values, in turn, depend on the size, shape and interactions of macromolecules in solution.

Experiments were conducted using Beckman Coulter Proteome Lab XL-I analytical ultracentrifuge with the 8-hole Beckman An-50Ti rotor at 4 °C. Ribosomes were thawed and diluted to 1.0 OD<sup>260</sup>/ml in buffer G<sup>10/50</sup>. The sample (400 µl) was loaded into one of the two quartz cuvettes of the centrifuge tube. The other cuvette was filled with 410 µl of buffer G. Sedimentation at 16000 rpm was monitored by absorbance at 280 nm and 260 nm with scans made at 4 min intervals. The solution density and viscosity for re-suspension buffer were calculated using SEDNTERP software. Data were analysed using a c(s) model in SEDFIT. The results showed that the major part of material after freezing stays in the 70S form and only a few part is dissociated to subunits (Figure 14 A).

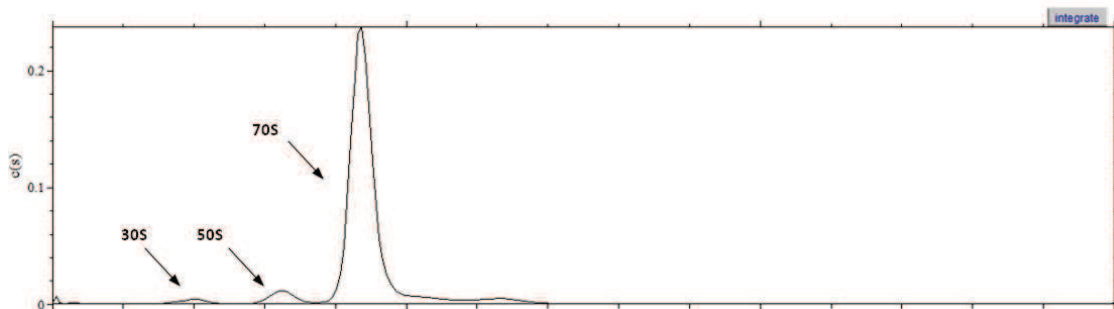


**Figure 14. A.** Sedimentation profile of *S. aureus* ribosome sample.

## Mass spectrometry

We performed a mass spectrometry analysis known as MudPit for multidimensional protein identification technology, a combination of liquid chromatography separation and mass spectrometry measurements (Washburn et al., 2001). First, the sample to be analysed is denatured and digested by the endoproteases LysC and trypsin. The digested mixture is loaded on chromatography system for a two steps separation using a strong ion exchange followed by reversed phase in a micro capillary column. Elution is performed gradually and iteratively to generate bundles of peptides which are immediately ionized and enter the tandem mass-spectrometer (MS/MS). Spectra are generated and queried against a protein database to determine

their protein origin.

The MudPit experiment was performed by Virginie Chavant at the IGBMC proteomics facility. The protein search was performed using the Sprot\_Staphylococcus-aureus\_2014205.fasta protein database. All identified proteins are indicated in the tables below. Diversity in scores for each protein may indicate some inhomogeneity of the sample.

**Table 3.** List of ribosomal proteins found in *S. aureus* ribosome sample by LC-MS/MS analysis, where b – bacterial specific proteins, u – universal proteins.

Small subunit proteins					Large subunit proteins				
Protein	Score	Coverage	MW [kDa]	calc. pI	Protein	Score	Coverage, %	MW [kDa]	calc. pI
bS1	6.75	5.37	43.3	4.60	uL1	3083.59	68.56	24.5	8.85
uS2	845.85	65.88	29.1	5.52	uL2	827.54	49.46	30.1	10.77
uS3	308.55	60.83	24.1	9.76	uL3	1717.26	61.82	23.7	9.80
uS4	364.81	63.50	23.0	10.02	uL4	1357.71	56.52	22.5	9.91
uS5	190.76	52.41	17.7	9.88	uL5	837.22	81.01	20.3	9.32
bS6	337.69	69.39	11.6	5.19	uL6	463.40	64.61	19.8	9.54
uS7	470.91	60.90	17.8	9.98	bL7/L12	951.30	76.23	12.7	4.65
uS8	170.56	47.73	14.8	9.33	bL9	6.65	16.89	16.4	9.38
uS9	251.62	58.46	14.6	10.56	uL10	504.23	74.10	17.7	4.83
uS10	150.94	46.08	11.6	9.74	uL11	275.97	45.00	14.9	8.98
uS11	313.99	58.91	13.9	11.21	uL13	748.02	64.14	16.3	9.31
uS12	76.38	46.72	15.3	11.25	uL14	253.70	31.97	13.1	9.99
uS13	348.91	55.37	13.7	10.42	uL15	573.66	61.64	15.6	10.29
uS15	105.90	40.45	10.6	10.51	uL16	292.34	46.53	16.2	10.64
bS16	206.64	49.45	10.2	9.92	bL17	345.14	47.54	13.7	9.85
uS17	43.83	43.68	10.2	9.76	uL18	155.11	43.70	13.1	9.95
bS18	70.75	42.50	9.3	11.00	bL19	107.02	28.45	13.4	11.50
uS19	267.08	68.48	10.6	9.99	bL20	111.81	27.97	13.7	11.25
bS20	47.24	36.14	9.0	10.51	bL21	524.56	67.65	11.3	9.85
bS21	38.99	18.97	7.0	11.11	uL22	409.14	60.68	12.8	9.92
					uL23	163.22	51.65	10.6	9.85
					uL24	208.20	41.90	11.5	9.82
					bL25	432.73	55.76	23.8	4.42
					bL27	295.54	45.74	10.3	10.17
					bL28	10.98	41.94	7.0	12.23
					uL29	163.47	66.67	8.1	9.60
					uL30	100.87	54.24	6.5	10.11
					bL31	356.15	54.76	9.7	8.44
					bL32	125.17	50.88	6.5	10.01
					bL33	137.39	42.86	5.9	9.73

Although LC-MS/MS analysis is semi quantitative technique, it can help to observe presence or absence of protein in extreme cases. In many cases very low score values mean only traces of the protein and *vice versa*. Thus, analysis of the sample of *S. aureus* ribosome shows that there are only traces of ribosomal proteins bS1 and bL9 and bL28.

Protein S1 is the biggest ribosomal protein that facilitates bacterial translation initiation by proper positioning of mRNA molecule on the 30S subunit. Positioning is provided by the interaction

between the Shine-Dalgarno (SD) sequence of mRNA and the anti-SD sequence on the ribosome. In the cells, one copy of S1 protein corresponds to 10 copies of ribosomes. It is very weakly associated with the ribosome and can be easily dissociated. In *S. aureus* S1 protein does not bind to the ribosome.

Protein L9 is structural constituent of ribosome. It is well known among bacterial ribosomal crystallographers. L9 is located on the periphery and protrudes at the side of bacterial ribosome. During crystallization of vacant ribosome L9 protein of one ribosome occupied tRNA-binding sites of another ribosome, thus providing compact crystal packing (Yusupov et al., 2001). On the one hand, it has provided additional stabilization of the structure; on the other hand, it has obstructed structural studies of functional complexes of bacterial ribosome. Nowadays L9 deficient strains are often used for crystallographic studies.

**Table 4.** List of non-ribosomal proteins found in *S. aureus* ribosome sample by LC-MS/MS analysis.

<b>Non-ribosomal proteins</b>				
Protein	Score	Coverage, %	MW [kDa]	calc. pI
Pyruvate dehydrogenase E1 component subunit	154.95	55.14	41.4	5.00
Pyruvate dehydrogenase E1 component subunit beta	133.76	52.62	35.2	4.73
Dihydrolipoyllysine-residue acetyltransferase component of pyruvate dehydrogenase complex	124.17	45.12	46.3	5.00
Trigger factor	66.96	36.49	48.6	4.42
DNA-directed RNA polymerase subunit beta'	46.21	13.09	135.3	6.89
Formate acetyltransferase	43.08	15.22	84.8	5.48
DNA-directed RNA polymerase subunit beta	34.42	8.79	133.2	5.03
DNA-directed RNA polymerase subunit alpha	32.65	35.35	35.0	4.75
Uncharacterized protein SAB0704	31.97	30.53	22.2	5.29
Elongation factor Tu	28.89	24.37	43.1	4.86
SsrA-binding protein	15.82	32.47	17.8	10.02
L-lactate dehydrogenase 1	14.06	18.93	34.5	5.07
Pyruvate kinase	10.54	5.13	63.1	5.35
Glyceraldehyde-3-phosphate dehydrogenase 1	10.22	11.90	36.3	5.05
Translation initiation factor IF-3	9.38	21.14	20.2	9.70
Cell division protein FtsZ	8.04	10.00	41.0	4.98
Uncharacterized RNA methyltransferase SACOL1957	7.80	7.06	51.6	6.74
Peptide chain release factor 2	6.78	7.59	42.3	4.94
Elongation factor G	6.41	4.04	76.6	4.91
Putative septation protein SpoVG	6.36	23.00	11.3	4.81
Dihydrolipoyl dehydrogenase	6.28	6.84	49.4	5.02
Extracellular matrix-binding protein EhbB	5.42	0.67	752.1	7.64
Triosephosphate isomerase	5.29	11.46	27.3	4.87
Staphopain A	4.75	6.96	44.2	9.64
N-acetylneuraminase lyase	4.67	5.46	33.1	5.02

## CRYSTALLOGRAPHIC STUDIES OF *S. AUREUS* RIBOSOME

### Why x-rays and why crystals?

Information about three-dimensional atomic structures of biological molecules help us to understand the mechanism of their action and regulation, to visualize intermolecular interactions, and even to design new molecules with altered activity. Atomic structure can tell you almost everything you want to know about your material: its bond length and angles, torsion angles, non-bonded distances.

There are several reasons why we cannot simply use powerful optical microscope and visible light but we need x-rays to determine the atomic structure of the molecules. First, atoms are too small to interact with visible light (390 – 700 nm wavelength) whereas the wavelength of x-rays is close to 1 Å (0.1 nm). Second, in contrast to visible light that can give us information about the surface only, x-rays can penetrate the matter (inorganic or organic). This property of X-rays is extensively used in radiology, whereas structural scientists use another property – the ability of matter (more precisely the electrons of the atoms) to scatter X-rays. These scattered rays contain all information about the position of each atom of the molecule. However, if molecules are randomly spread in solution, they scatter randomly, in all possible directions. If we detect these randomly distributed signals, we will not be able to get any information from it. In order to make the information understandable, we need to force all x-rays to scatter in the same directions. That is why crystallographers cannot use sample in solution but rather have to crystallize it. Crystals are essentially a solid comprised of highly ordered identical units. When passing through such an ordered structure, photons are scattered in particular directions and registered on the detector forming a diffraction pattern. Diffraction pattern is representation of a structure in reciprocal space that contains the information about the directions of scattering and the intensity, but the information about the phase is missing. The phase information can be recovered using different methods such as anomalous scattering, isomorphous replacement, molecular replacement etc. Diffraction pattern with exact positions of diffraction spots, their intensities and phases then can be converted to the electron density (real space representation of protein structure) using Fourier transform method.

Thus, obtaining crystals of the object of interest is crucial in X-ray crystallography and is always challenging with biological molecules that are asymmetric and dynamic.

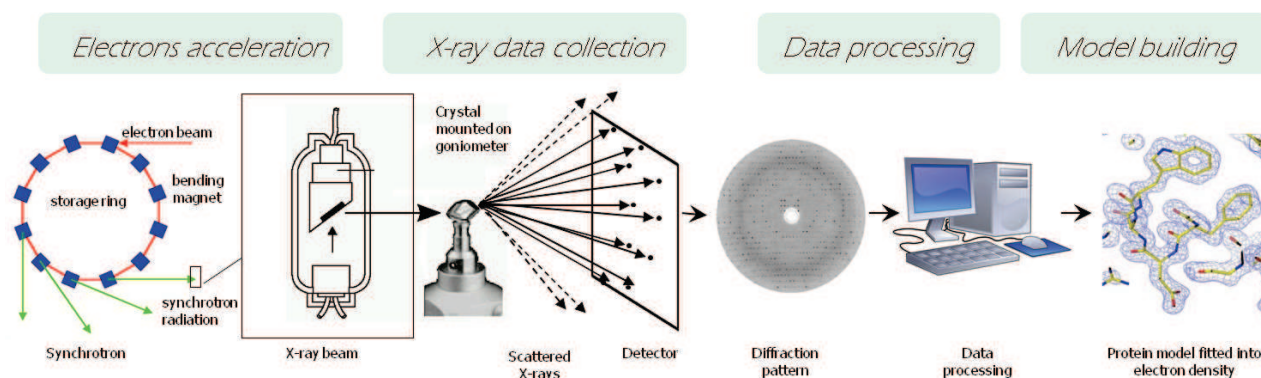


**Figure 15.** Schematic representation of diffraction experiment. Electrons accelerated in the synchrotron ring can be partially transferred to experimental beamlines where the X-ray beam bombards the crystal that is mounted on goniometer. The most of the x-rays passing directly through the crystal and absorbed by the beam stop (these signals are not registered). Only scattered photons are captured on the detector forming a diffraction pattern (representation of crystal structure in reciprocal space). The data collected at the synchrotron are then processed at powerful computers and transformed into electron density (representation of crystal structure in real space) and 3D model of macromolecule is build according to the density thereafter.

## Macromolecular crystallization in theory

The laws of physical chemistry and thermodynamics control the process of crystallization. Thermodynamically, crystallization of macromolecules (proteins, nucleic acids, macromolecular complexes, etc.) is not very different from the crystallization of salt. In both cases, we need to bring the solution into a supersaturated state after which the salt or the protein will start to crystallize. However, protein crystallization methods are very different and not as simple. Protein solubility depends on many factors: temperature, pressure, pH, concentration of protein, type and concentration of precipitant agent, type and concentration of salts, metal ions, co-factors and ligands interacting with the protein, etc.

Different crystallization methods may be used to bring the solution into supersaturation, normally through a gradual decrease of the solubility of the protein. Protein crystallization is generally a matter of searching, as systematically as possible, the ranges of the individual parameters that influence crystal formation, finding a set, or multiple sets of factors that yield some kind of crystals, and then optimizing the individual variables to obtain the best possible crystals. This is usually achieved by carrying out an extensive series of experiments, or establishing a vast matrix of crystallization trials, evaluating the results, and using the information obtained to improve conditions in successive rounds of trials. Because the number of variables is so large, and the ranges so broad, experience and insight into designing and evaluating the individual and collective trials

becomes an important consideration (McPherson, 2004).

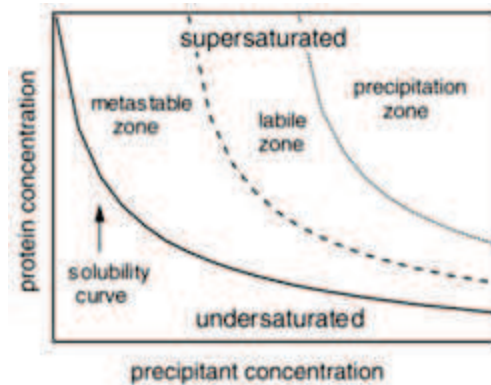


**Figure 16.** Schematic phase diagram of protein crystallization.

### *Phase diagram*

A schematic diagram of a solubility curve, illustrating how the solubility varies with the concentration of a precipitant (e.g., polyethylene glycol (PEG) or a salt), is shown in Figure 16. When a protein crystal is placed in a solvent which is free of protein, the crystals will begin to dissolve. If the volume of solvent is small enough, the crystal will not dissolve completely; it will stop dissolving when the concentration of protein in solution reaches a specific value. At this concentration, the crystal loses protein molecules at the same rate at which protein molecules rejoin the crystal – the system is said to be at equilibrium. The concentration of proteins in the solution at equilibrium is the solubility. The solubility of a protein varies with the solution conditions. Crystals dissolve in the undersaturated region – where the concentration is below the protein solubility – and grow in the supersaturated region (Asherie, 2004).

### *Crystals growth*

In principle, crystals will form in any protein solution that is supersaturated i.e., when the protein concentration exceeds the solubility. In practice, considerable supersaturation is required to overcome the activation energy barrier which exists when forming the crystal. This barrier represents the free energy required to create the small microscopic cluster of proteins – known as a nucleus – from which the crystal will eventually grow (Kashchiev, 2000).

Since there is an energy barrier, nucleation (the process of forming a nucleus) takes time. If the supersaturation is too small, the nucleation rate will be so slow that no crystals form in a reasonable period of time. The corresponding area of the phase diagram is known as the "metastable zone" (Figure 16). In the "labile" or "crystallization" zone, the supersaturation is large

enough that spontaneous nucleation is observable. If the supersaturation is too large, then disordered structures, such as aggregates or precipitates, may form. The "precipitation zone" is unfavorable for crystal formation, because the aggregates and precipitates form faster than the crystals. Because these zones are related to kinetic phenomena, the boundaries between the zones are not well defined (this in contrast to the solubility line which is an unambiguous delimitation of the equilibrium between solution and crystal). Even though the division in zones is qualitative, the different behaviors serve as guide when searching for the appropriate conditions to produce crystals (Mikol et al., 1990; Saridakis et al., 2003).

## **Macromolecular crystallization in practice**

The kinetics of equilibration, through dehydration of the protein-containing experiment drop or through liquid diffusion, will determine the rate at which supersaturation is obtained as well as the trajectory through the phase diagram and can often be passively controlled (Luft and DeTitta, 1997). There are three main categories of crystallization methods: vapour-diffusion, batch and liquid-diffusion.

### *Vapour diffusion*

Vapour diffusion crystallization techniques such as hanging drop and sitting drop methods are the most commonly used techniques for crystallization. A small droplet containing both protein and precipitant is dispensed onto a surface. The experiment droplet is then sealed in an airtight chamber with a reservoir solution. The drop undergoes a dynamic equilibration with the reservoir solution until the vapour pressure of any volatile species, typically water, over the experiment drop and the reservoir reach a state of equilibrium. The purpose of the reservoir solution is to dehydrate the experiment drop and to set the endpoint for the dehydration.

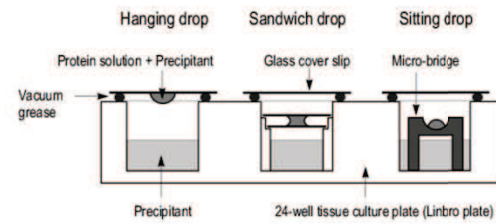
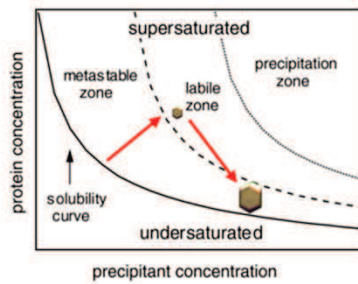
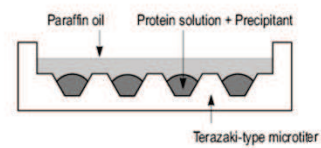
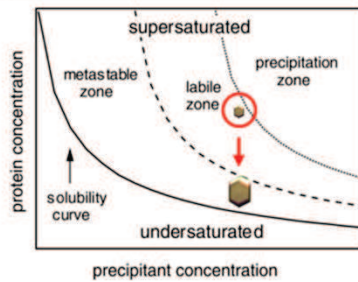
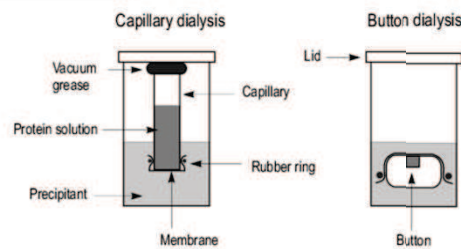
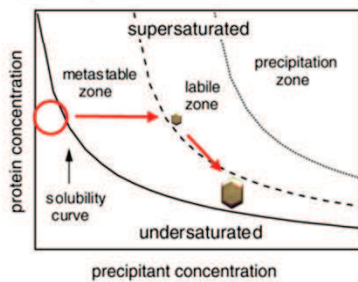
### *Microbatch*

Batch experiments, in particular microbatch under oil (Chayen et al., 1992) experiments, are conceptually simple: a protein solution is combined with a crystallization cocktail under oil; the oil is a barrier to dehydration of the experiment drop, but also acts as an interface that can affect crystallization. The dehydration rate can be controlled by making the oil barrier more or less water-permeable, for example by combining paraffin (less water-permeable) and silicone-based (more water-permeable) oils (D'Arcy et al., 1996). Microbatch experiments can be especially useful if the

temperature is not stable, as they do not suffer from the condensation in the experiment well that can occur during vapour diffusion experiments.

### *Liquid diffusion*

These techniques are not as widely used as the batch or vapour diffusion techniques but have their own advantages and disadvantages. Liquid-diffusion techniques include microdialysis (Zeppezauer et al., 1968; Lagerkvist et al., 1972; Lee & Cudney, 2004), counter-diffusion (García-Ruiz, 2003) and free-interface diffusion (Salemme, 1972). Free-interface diffusion is generally based on a single precipitation event, whereas counter-diffusion exploits the difference in the speed of diffusion between protein molecules and small molecules, and is designed to generate multiple precipitation events at different levels of supersaturation. Dialysis crystallization is another type of liquid diffusion: protein solution is placed within a container, sealed with a semi-porous dialysis membrane which has a molecular-weight cutoff (MWCO) that is small enough to prevent the protein molecules from escaping but big enough for the free diffusion of the reservoir solution.

**A** Vapour diffusion**B** Batch**C** Dialysis

**Figure 17.** Idealized phase diagrams showing the trajectories of three different crystallization methods, vapour-diffusion, batch and liquid-diffusion (dialysis) on the left side and their experimental setups on the right side. The open red circle is the starting point of the experiment, the small crystal is the point of spontaneous homogeneous nucleation and the big crystal is the equilibrium point of the crystal. The dynamic of each process described below (adapted from Luft et al. (2014) and Chirgadze (2001)).

In the vapour-diffusion method, the initial drop conditions are undersaturated (Figure 17 A). As the drop dehydrates, typically through a dynamic equilibrium with the reservoir solution, the relative concentration of the protein and precipitant will steadily increase until the drop reaches a metastable state that will kinetically and thermodynamically support spontaneous homogeneous nucleation. The drop will typically further dehydrate as it equilibrates with the reservoir solution and the crystal will pass through the metastable zone; here it will grow to a larger size, but the solution will not be sufficiently supersaturated to support nucleation events. The drop reaches a saturation point when the drop and reservoir have equilibrated with respect to the vapour pressure of water, and the protein in the drop is in a dynamic equilibrium between the liquid and solid

(crystalline) phase. For batch method (Figure 17 B), a successful experiment involves setting up at labile supersaturation. A nucleation event takes place and protein in solution undergoes a phase change to the solid (crystalline) form. Equilibrium is reached when the protein in the surrounding solution reaches a state of saturation with the solid (crystal) phase. The final example shows the dialysis method (Figure 17 C). The protein solution is held at a fixed volume. As precipitant passes through the semi-permeable dialysis membrane, the concentration of the precipitant will continue to increase while the protein concentration remains constant. When the solution reaches a metastable state then the protein will form a solid phase (crystalline). At this point, the concentration of the protein in the solution will decrease as protein transitions from a liquid to a solid phase. Saturation is reached when the solid and liquid phases have reached a state of dynamic equilibrium.

## **Crystallization of *S. aureus* ribosome**

### *Challenges in crystallization of the ribosome*

The main challenge in crystallographic studies of any biological molecule is finding well-diffracting crystals. And it was obvious that macromolecular complex such as ribosome, with molecular weight 2 300 000 Da, is much more challenging to crystallize than single proteins. For today the ribosome is the largest asymmetric molecular assembly that have been solved crystallographically, and the complexity of ribosome crystallography continues to increase with the addition of translation factors and other accessory proteins. The challenge to crystallize the ribosome consist not only in its huge molecular weight, but also in the fact that the ribosome is an asymmetric complex, thus ordering and packing into the crystal can be very sophisticated. Moreover, ribosomes are very dynamic in the solution meaning that they can have high conformational heterogeneity within one crystallization drop. Heterogeneity may disturb some crystal contacts. Ribosome is composed of two different types of molecules, RNA and proteins, therefore it is rather tricky to find the conditions where ribosome would tend to crystallize rather than form an amorphous precipitate. The phase diagram for the ribosome is far more complex than for individual protein. Basically it is the result of convolution of phase diagrams of each individual molecule comprising the full ribosome and their intermolecular interactions. Hence, ribosomes from different organisms require unique new searches of correct crystallization conditions. Nowadays, there are several tens of commercially available crystallization screens developed to facilitate a comprehensive search of crystallization conditions for proteins. These screens are based on the

knowledge of thousands of successful crystallization experiments, but unfortunately are suitable mostly for individual proteins rather than macromolecular complexes (because the better part of solved structures belongs to individual proteins). However, even if there are no commercial screens designed for the ribosomes, the compilation and analysis of crystallization conditions published for bacterial 70S ribosome revealed only a limited amount of variation summarized in Table 5.

**Table 5.** Published crystal conditions for 70S ribosomes (adapted from Pearson, 2011). Summary of the concentration and identity of salts, precipitants, and critical additives from multiple 70S ribosome crystallization conditions (Trakhanov et al. 1987, Yusupov et al. 1987, Yusupov et al. 2001, Korostelev et al. 2006, Korostelev et al. 2008, Petry et al. 2005, Selmer et al. 2006, Gao et al. 2009, Schuwirth et al. 2005, Vila-Sanjurjo et al. 2003, Zhang et al. 2009, Blaha et al. 2009).

Component	Concentration	Types			
Buffers, pH 6.5 – 7.5	0 – 100 mM	Tris	MES	Hepes	
Cations	0 – 380 mM	K <sup>+</sup>	NH <sub>4</sub> <sup>+</sup>	Arginine	
Anions	0 – 380 mM	Cl <sup>-</sup>	SCN <sup>-</sup>	Acetate <sup>-</sup>	
Magnesium	0 – 35 mM	MgCl <sub>2</sub>	MgOAc <sub>2</sub>		
Precipitant	3.5 – 4.5%	PEG 400			
	3.5 – 4.5%	PEG 550 mme			
	2 – 4.5%	PEG 8000			
	2.5 – 4.5%	PEG 20000			
	11 – 26%	MPD			
Polyamines	0.5 – 5 mM	Spermine	Spermidine	Thermine	Putrescine
Additives	0.25 mM	ETDA			
	0.5 – 6 mM	2-mercaptoethanol			
Detergent	2.8 mM	Deoxy Big Chap			

### *Crystallization*

Initial crystal-like particles of 70S ribosome from *S. aureus* were obtained using robotic screening of variety of combination of conditions listed in Table 5. Ribosome sample (100 nl of at 8 mg/ml containing 2.8 mM Deoxy Big Chap) was mixed with 100 nl of reservoir solution (100 mM bis Tris-propane pH 7.0, 400 mM NH<sub>4</sub>SCN, 10 mM MgOAc<sub>2</sub>, 6% PEG 8000) in MRC 2drop plates by the Mosquito robot. Plates were stored at 20 °C, and crystalline particles appeared after 3 – 5 days (Figure 18 A).

### *Crystallization optimization*

Optimization of *S. aureus* ribosome crystallization was carried out at 24 °C and included several global steps:

1. **Variation of salt and precipitant concentrations.** As the first step, fine titration of  $\text{NH}_4\text{SCN}$  and PEG 8000 concentrations gave better-shaped crystals (Figure 18 B).
2. **Scale up.** To grow bigger crystals we switched to larger scale crystallization, making drops 2 + 2  $\mu\text{l}$  in 24 - well sitting drops in CrysChem plates (Hampton Research). This led to shift of PEG 8000 concentration down to 4.8%.  $\text{NH}_4\text{SCN}$  remained 325 mM. As a result crystals grew to approximately 100 × 40 × 10  $\mu\text{m}$  big on average (Figure 18 C).
3. **Variation of  $\text{Mg}^{2+}$  and introduction of polyamines** increased the size of the crystals to approximately 200 × 80 × 20  $\mu\text{m}$ . Variation of drop to reservoir ratio produced sometimes crystals as large as 400 × 120 × 40  $\mu\text{m}$  (Figure 18 D and E).
4. In the next step of optimization we wanted to introduce into the crystallization conditions some **cryo-protective compounds** such as glycerol, EG (ethylene glycol), small PEGs (PEG 400, PEG 550 mme), and MPD. This would be very helpful for further post-crystallization treatment (this subject will be discussed in the next sub-chapter). However, the idea was unsuccessful – increasing the concentration of cryo-protectant led to the deterioration of the quality of crystals. The only positive result was observed after introduction of 2% glycerol, which improved the sharpness of the crystals. However the size of obtained crystals was smaller than previously, 35 × 35 × 15  $\mu\text{m}$  (Figure 18 F).
5. **Volume of reservoir.** Changing volume of reservoir solution (400, 500, 600, 700 or 800  $\mu\text{l}$ ) didn't affect crystallization significantly. Thus, 500  $\mu\text{l}$  was used in all further experiments.

The following crystallization protocol was obtained after optimization. The ribosome sample was prepared as follows. The frozen sample of 70S ribosome was thawed at room temperature for 10 min, filtered through 0.22  $\mu\text{m}$  filters (Merck, Millipore), diluted to 8 mg/ml ribosome solution in buffer G containing 2.8 mM Deoxy Big Chap, incubated at 30 °C for 30 min and then left to cool down to room temperature before crystallization. Crystallization was performed at 24 °C using CrysChem sitting drop (Hampton Research) plates by mixing 2 – 2.4  $\mu\text{l}$  of ribosome solution with 1.6 – 2  $\mu\text{l}$  of 500  $\mu\text{l}$  reservoir solution (100 mM bis-Tris propane pH 7.0, 325 mM  $\text{NH}_4\text{SCN}$ , 15 mM  $\text{MgOAc}_2$ , 4.8 – 5.0% w/v PEG 8000, 10 mM spermidine). Typically, crystals appeared reproducibly within 7 – 10 days and reached their full size after two additional weeks. Unfortunately, almost all these crystals were attached to the plastic of crystallization plate, preventing any manipulations

with them. In order to overcome this problem, several more optimization steps were performed, but unfortunately without any improvement. The details of this optimization are discussed below.

6. **Replacing salts and precipitants.** To improve the crystal quality we have decided to replace  $\text{NH}_4\text{SCN}$  in crystallization trials to more commonly used salts, but keeping either the  $\text{SCN}^-$  anion or the  $\text{NH}_4^+$  cation. We therefore tried to introduce  $\text{KSCN}$ ,  $\text{NH}_4\text{Cl}$  and  $\text{NH}_4$ -acetate in combination with  $\text{NH}_4\text{SCN}$  or each of these salts individually. We observed no changes in the kinetics of crystals growth, most of them were still attached to the plastic. Moreover, when we shifted away from using the  $\text{NH}_4\text{SCN} \bullet \text{PEG 8000}$  pair the shape and the size of the crystals became worse.
7. **Changing geometry and plastic.** Another possible way to solve the problem was to change geometry of the crystallization plates and the surface where crystallization drop was mixed. To do this, we used a hanging drop setup in VDX plates (Hampton Research). In this setup the drop is mixed on the glass cover slide and kept upside down during equilibration (Figure 17 A). Crystals were attached to the glass cover slide, although they were big enough to use in diffraction experiments (Figure 18 G). The second type of setup used was a sitting drop in the CombiClover plate (Rigaku Reagents) that is made from another type of plastic. Crystals were too small for any further analysis, as the nucleation rate was very high at this setup (Figure 18 G).
8. **Changing the temperature.** Crystallization at 4 °C did not results in crystals at the conditions used. Crystals appeared at 16 °C, but they were less sharp and were also attached to the plastic.
9. **Growing in batch.** Batch crystallization under the oil prevents the contact of the crystallization drop with the surface of the plate. However, it had another negative consequence – the crystals of *S. aureus* ribosome appeared in the phase boundary between the oil and the drop. Moreover, they were small and not suitable for diffraction experiments.
10. **Growing in agarose.** Another technique we try to use was crystallization in agarose. The principal is to add certain amount of agarose into the drop and keep it at an appropriate temperature (usually 12 – 16 °C), so that agarose will not be completely soluble already but also will not polymerise yet. Introduction of agarose into crystallization conditions never produced satisfactory crystals.
11. **Seeding** was used as a last resort to change the kinetics of crystals growth. Seeding is a very powerful crystallization technique that can in some cases drastically improve

the quality of crystals. We start the process of drop equilibration from metastable zone in the phase diagram (see Figure 16). Together with our ribosome in solution we put the seeds of crystals (usually smashed by mechanical force) of our crystallized ribosome sample. These seeds serve as nuclei for the formation of new crystals. Since we unaware of the exact phase diagram for *S. aureus* ribosome in particular crystallization conditions, we used different initial concentrations of every compound as initial point. Seeds were prepared by vortexing or using a seed-bead kit (Hampton Research) or by smashing the crystal with glass bead (all done in reservoir solution where crystal doesn't dissolve). Seeds were diluted up to 10000 times in reservoir solution. Crystallization drops were set up in CrysChem sitting drop at 24 °C: 1.8  $\mu$ l of ribosomes were mixed with 2  $\mu$ l of reservoir and 0.2  $\mu$ l of seeds.

Under these conditions, seeding did not improve crystallization. All crystals were exactly as before (Figure 18 I). Possibly, the treatment of the crystals was too harsh, and all the nuclei were destroyed during the preparation of the seeds. Although the technique is simple in theory, realization is always challenging. Much care, patience, material and optimization are required to perform seeding properly. For the moment, we have not succeeding in seeding *S. aureus* ribosome, although in future further optimization may yet be successful.

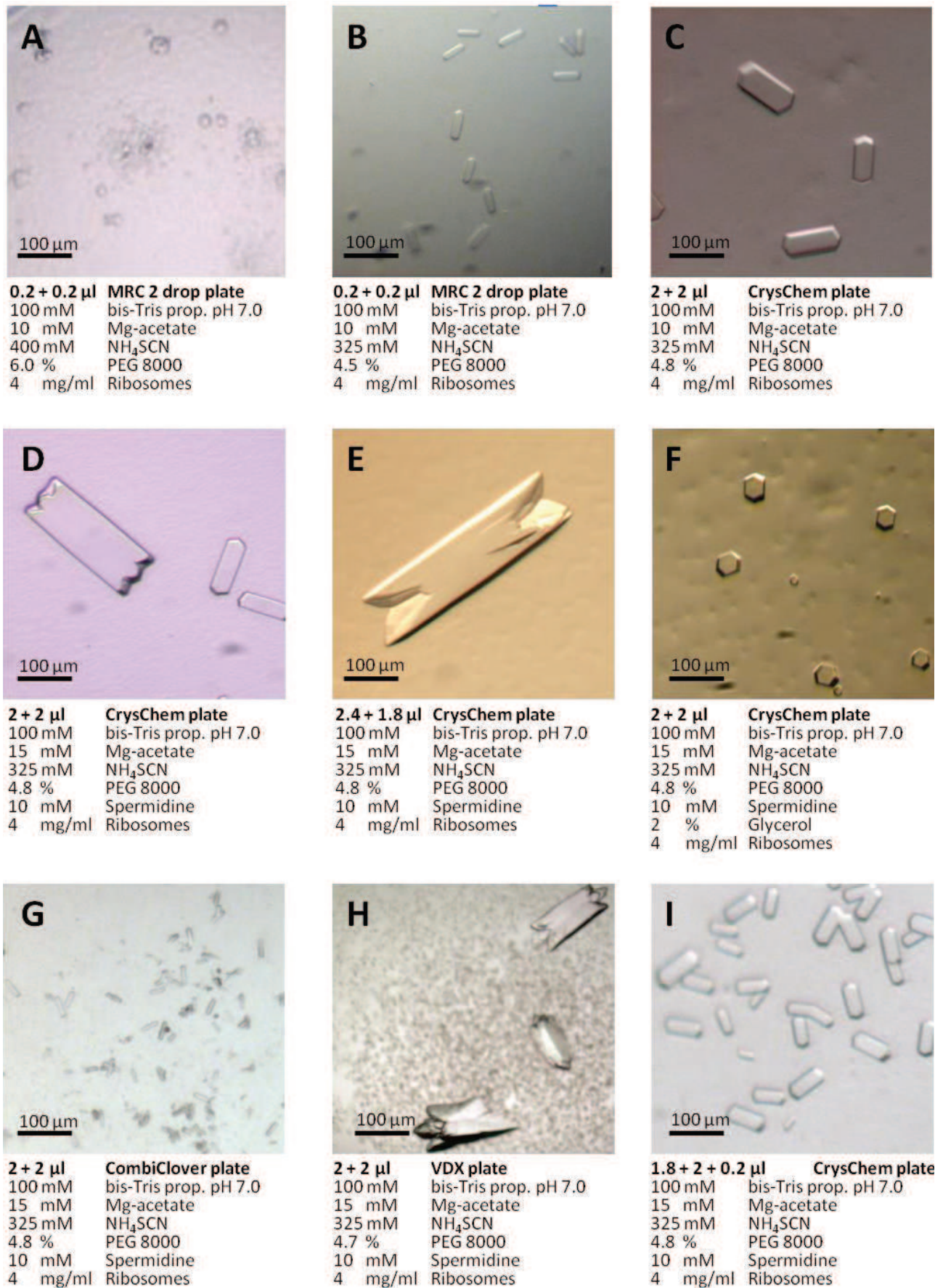


Figure 18. Crystals of *S. aureus* 70S ribosome.

## Post-crystallization treatment

### *Dehydration*

Crystals of macromolecules and macromolecular complexes are usually composed of approximately 50% solvent on average, so that in many ways it represents an ordered gel with a very few intermolecular contacts. Since these contacts provide the lattice interactions essential for crystal maintenance, it is absolutely necessary to decrease the water content by dehydration procedure. Usually alcohols like EG, PEG, MPD or salts like  $(\text{NH}_4)_2\text{SO}_4$  are used as dehydration agents.

Several classic methods exist for protein crystal dehydration which include: simple air drying, vapour diffusion using salts, and soaking with dehydrating compounds (Heras & Martin, 2005, Newman, 2006). The advantages of these methods are that the experiment can be performed with very small humidity steps over long periods of time, and that the number of crystals can be modified at the same time. Unfortunately, the outcome of the dehydration is unknown until the experiment is finished, and there is no direct way of assessing the progress of the experiment. Although, it is the most popular method, it is crystal- and time-consuming and can be difficult to reproduce.

To standardize the process of dehydration and increase its reproducibility, the European Molecular Biology Laboratory (EMBL) and European Synchrotron Radiation Facility (ESRF) in Grenoble (France) have developed a humidity control device (HC1) coupled with a synchrotron beamline. Based on a modified cryo-stream nozzle, it produces an air stream at the sample position and allows precise control of the relative humidity between 50 and 99% (Sanchez-Weatherby et al., 2009).

### *Cryo-protection*

Special care has to be taken during post-crystallization treatment to avoid damaging the crystals (i.e., when transferring cryo-protection) and even for the freezing process itself we only use the most robust methods of freezing directly in the gaseous  $\text{N}_2$  stream at 100 K rather than plunging into liquid  $\text{N}_2$ , ethane, or propane as is common practice in X-ray structural projects. A combination of severe radiation decay and generally weak diffracting power limits the amount of data that can be collected from each crystal making it necessary to merge data collected on different crystals to obtain complete datasets which invariably degrades the data quality.

. Several different methods for cooling macromolecular crystals have been developed. An excellent overview is given in the review by Garman and Schneider (1997). Currently the most

common method is to fish the crystal with a polyethylene loop via surface tension and cool the crystal either by submerging it in a liquid cryogen or placing it directly into a cold gas stream (Teng, 1990). This usually vitrifies the bulk solvent, slowing diffusion of damaging free radicals produced by the ionizing radiation.

Another relatively recent development in cryo-cooling techniques is recovery of "lost" diffraction by cycling crystals between a low temperature and some higher temperature.

## **Post-crystallization treatment of *S. aureus* ribosome crystals**

Several strategies were used to dehydrate crystals (Figure 19).

### *Strategy 1*

This involved soaking in a reservoir solution with increasing concentrations of dehydration agents (in future called dehydration solutions) for different periods of time. The dehydration solution was introduced into the drop stepwise by sequential transfer or directly into the crystallization drop. As dehydration agents we used different PEGs (PEG 400, PEG 500 mme, PEG 6000, PEG 8000, PEG 20000), EG, glycerol, or MPD.

Scheme 1. Crystals were sequentially treated by reservoir solution containing increasing concentrations of cryo-protectants. After different periods of time, crystals were fished using nylon cryo loops (Hampton Research) and immediately cryo-cooled in a stream of liquid nitrogen.

Scheme 2. Crystals were sequentially treated by reservoir solution containing 5.3 – 10% of PEG 8000. After different periods of time, crystals were cryo-protected by increasing the glycerol concentration up to 30% and were subsequently fished using nylon cryo loops and immediately cryo-cooled in a stream of liquid nitrogen.

Scheme 3. Crystals were sequentially treated by reservoir solution containing 5.3 – 30% of PEG 8000. After different periods of time, crystals were fished using nylon cryo loops and immediately cryo-cooled in a stream of liquid nitrogen.

### *Strategy 2*

This involved dehydration under vapour pressure of the reservoir (Scheme 4). The crystallization drop was diluted with 10 ul of reservoir solution. Then reservoir solution was replaced by 600 ul of dehydration agent: EG or MPD 50 – 80%; reservoir solution containing 120 mM MgOAc<sub>2</sub> or 2 M NH<sub>4</sub>SCN or 30% PEG 8000. After a certain time (4 – 28 h) the drop was treated by reservoir

solution containing 30% cryo-protectant. After different periods of time, crystals were fished using nylon cryo loops (Hampton Research) and immediately were cryo-cooled in a stream of liquid nitrogen.

### *Strategy 3*

This involved dehydration by decreasing humidity with HC1 (ESRF, Grenoble, France). First, to manipulate with the crystals, they were soaked in reservoir solution containing 7.5% PEG 8000 for the least possible time (20 – 30 min). When crystals became accessible, they were fished from crystallization drop using MicroMesh (MiTeGen) and immediately mounted on the goniometer where HC1 device was installed. Humidity of 99.5% was chosen as the value. Every 3 – 5 min humidity was decreased by 0.5 – 1% and two images were collected. At the certain humidity value the diffraction pattern started to change suggesting some changes in crystal order. A new crystal was mounted, humidity was slowly decreased to estimated value but without shooting x-rays to avoid radiation damage. When the desired humidity (new initial humidity point) was reached, the data collection continued.

The result of dehydration procedure is often an internal rearrangement of the molecules that form this crystal. Notably, after dehydration and cryo-protection, *S. aureus* ribosome crystals detached from the surface (plastic or glass). It means that some changes in the internal organization of the crystals took place. However, since we could not analyse crystals before any treatment it is difficult to estimate whether these changes improved the diffraction limit or the contrary. Sometimes the crystal packing changed so dramatically that it completely broke the order inside the crystal. If it happens, we could observe some cracks or other defects on the crystal (Figure 20). Usually, cracked crystals diffract very poor.

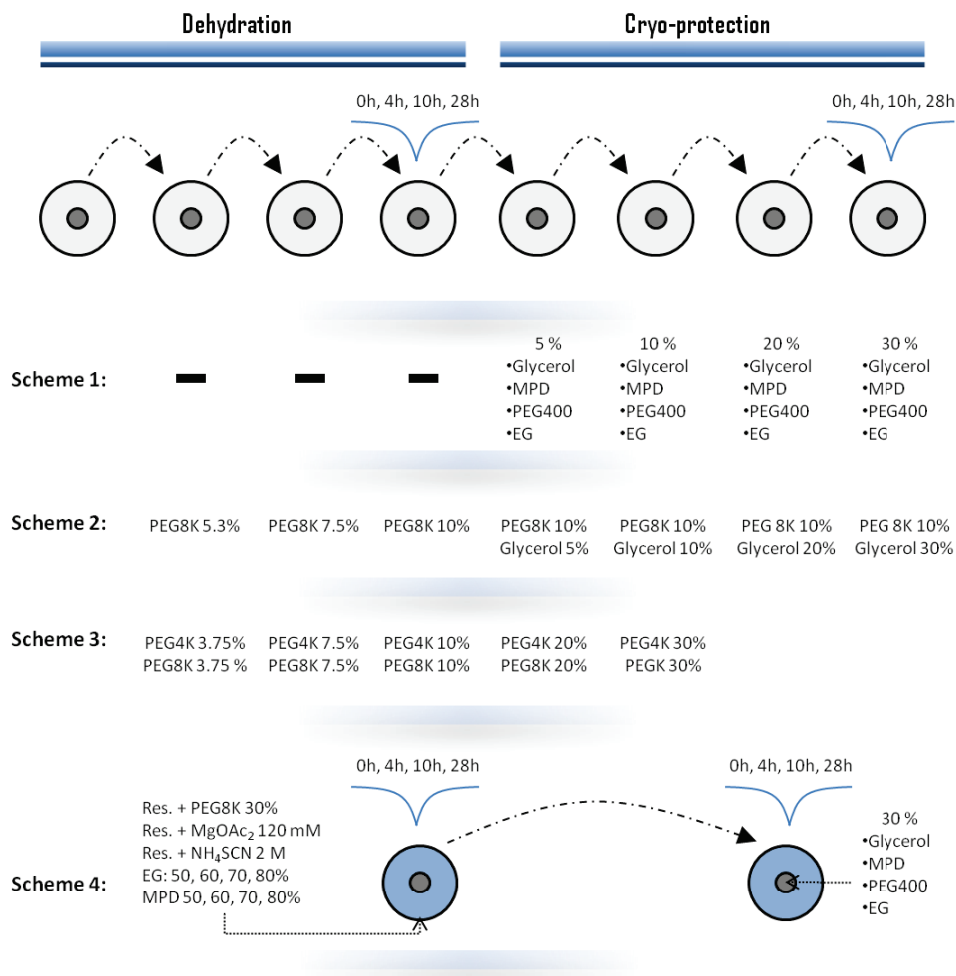


**Figure 19.** Scheme of post-crystallization treatment. Dehydration and cryo-protection of *S. aureus* ribosome crystals was performed according to the scheme. Treated crystals were further fished into crystallization loop and cryo-cooled at nitrogen stream at 100K and tested at the synchrotron.

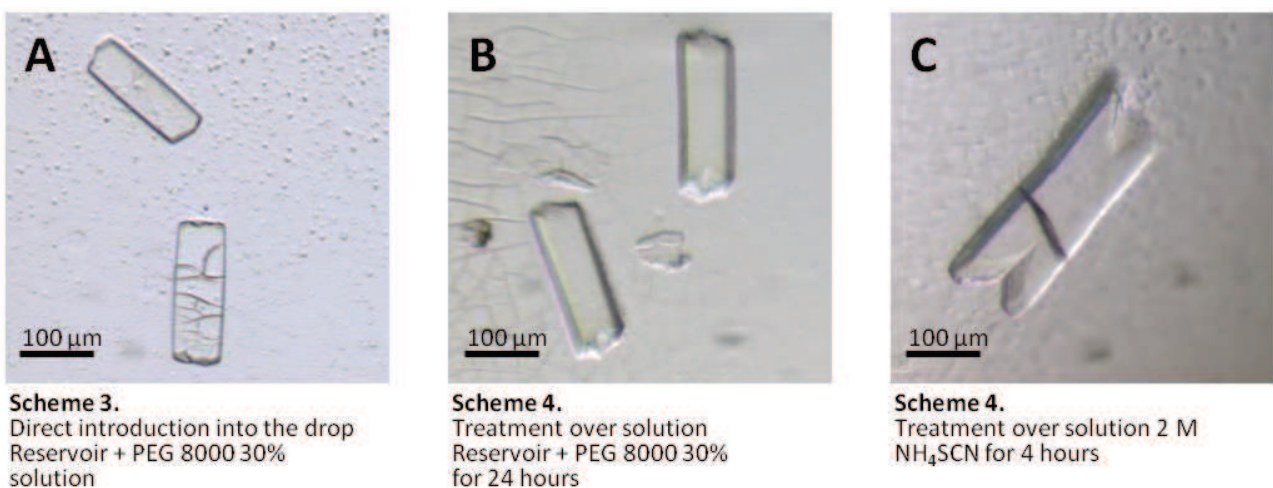


**Figure 20.** Crystals cracked during post crystallization treatment.

## X-ray data collection

Crystals of *S. aureus* 70S ribosome were tested at different synchrotrons and beamlines including Swiss Light Source (SLS), Villigen, Switzerland (PXI beamline); Soliel, Massy, France (Proxima2 beamline), European Synchrotron Radiation Facility (ESRF), Grenoble, France (ID 29 beamline).

Proper data collection from each individual crystal is one of the important parameter to obtain high quality data and get as much information from the crystal as possible. Different synchrotrons and beamlines require different conditions for data collection. Detector distance, beamstop distance, beam size and intensity, exposure time, oscillation angle and other parameters were optimized empirically according to the properties of crystals and specifications of the beamlines.

### *SLS*

X-ray data collection at SLS synchrotron was performed at the the beamline PX1 - X06SA. All data was collected using single-photon-counting detector PILATUS 6M (Dectris). In average crystals diffracted around 30 Å resolution, reaching 20 Å in some cases. Depending on post-crystallization treatment crystals showed different resolution and mosaicity, although, such evaluation is quite subjective. Nevertheless, the "best" crystals were chosen to collect a full dataset. Dataset was collected at 100K and processed using XDS. The resolution limit was shown to be 17.5 - 18 Å. However the space group was impossible to estimate due to deficiency of the number of reflections. Diffraction pattern of one of the shots is shown in Figure 21 B.

### *ESRF*

Data collection at ESRF synchrotron was performed at ID29 beamline. A Humidity Control device (HC1) installed at the beamline was used to dehydrate crystals that were immediately shot at 295K. All data was collected using single-photon-counting detector PILATUS 6M (Dectris). Dehydration by stepwise decreasing humidity did not improve diffraction. Moreover, the resolution limit was extremely low and crystals were strongly affected by radiation damage (Figure 21 C). This could have been caused either by the inefficiency of the dehydration technique or by shooting crystals at room temperature. Diffraction at the initial value of humidity (99.5%) can be considered as diffraction of crystal without dehydration. The poor level of this diffraction confirms the necessity of post-crystallization treatment.

## Soleil

Data collection at Soleil synchrotron was performed at Proxima2 beamline. All data were collected at 100K under micro-focused X-ray beam using ADSC Q315r detector (Area Detector System Corporation). Only dehydrated and cryo-cooled crystals were tested. Crystals were treated according to the scheme 2 (Figure 19) with the only difference that two temperatures were used (4 and 24 °C) and 1% glycerol was introduced during all steps. In general all crystals diffracted as usual around 30 Å reaching 20 Å in some cases. Four datasets from the best crystal were collected. Diffraction pattern of one of the shot is shown in Figure 21 D. Data was processed by XDS and scaled by XSCALE. Crystal belonged to the space group  $P4_22_12$  and contained 1 ribosome per asymmetric unit with dimensions  $450 \times 450 \times 280$  Å. Maximum resolution reached was 21.7 Å.

From the crystallographic studies of *S. aureus* ribosome, we can conclude that the purified sample was good enough to be crystallized. All but one of the compounds used ( $\text{NH}_4\text{SCN}$ ) are very well known for ribosome crystallization. Crystals of *S. aureus* ribosome can be grown reproducibly until they reach a reasonable size ( $200 \times 80 \times 20$  µm in average) at 24 °C. They appear in 7 - 10 days and grow till maximum size during next 2 weeks. The space group was determined as  $P4_22_12$  and contained 1 ribosome per asymmetric unit with dimensions  $450 \times 450 \times 280$  Å. Crystals survived relatively well under radiation beam, but the resolution limit was always around 25 – 30 Å reaching 18 – 20 Å in rare cases. There are several possible explanations of bad diffraction of the crystals. The first could be the impurity of the sample. Purified sample may have some inhomogeneity that could not be detected by biophysical methods. Ribosomes could have some conformational differences that did not influence crystal contacts. They could therefore be freely incorporated into the crystal without affecting crystal packing but may strongly diminish the diffraction. A second reason could be the post-crystallization treatment. These crystals may require unique and specific dehydration and cryo-cooling procedures that were not identified yet. In addition, crystallization conditions themselves, particularly high temperature, may be the reason of poor diffraction. Keeping ribosomes of mesophilic bacteria at 24 °C during 2 – 3 weeks may cause some structural alterations in the molecule. All these explanations, however, are quite speculative and there may be any other reasons for the weak diffraction that we are unaware of.

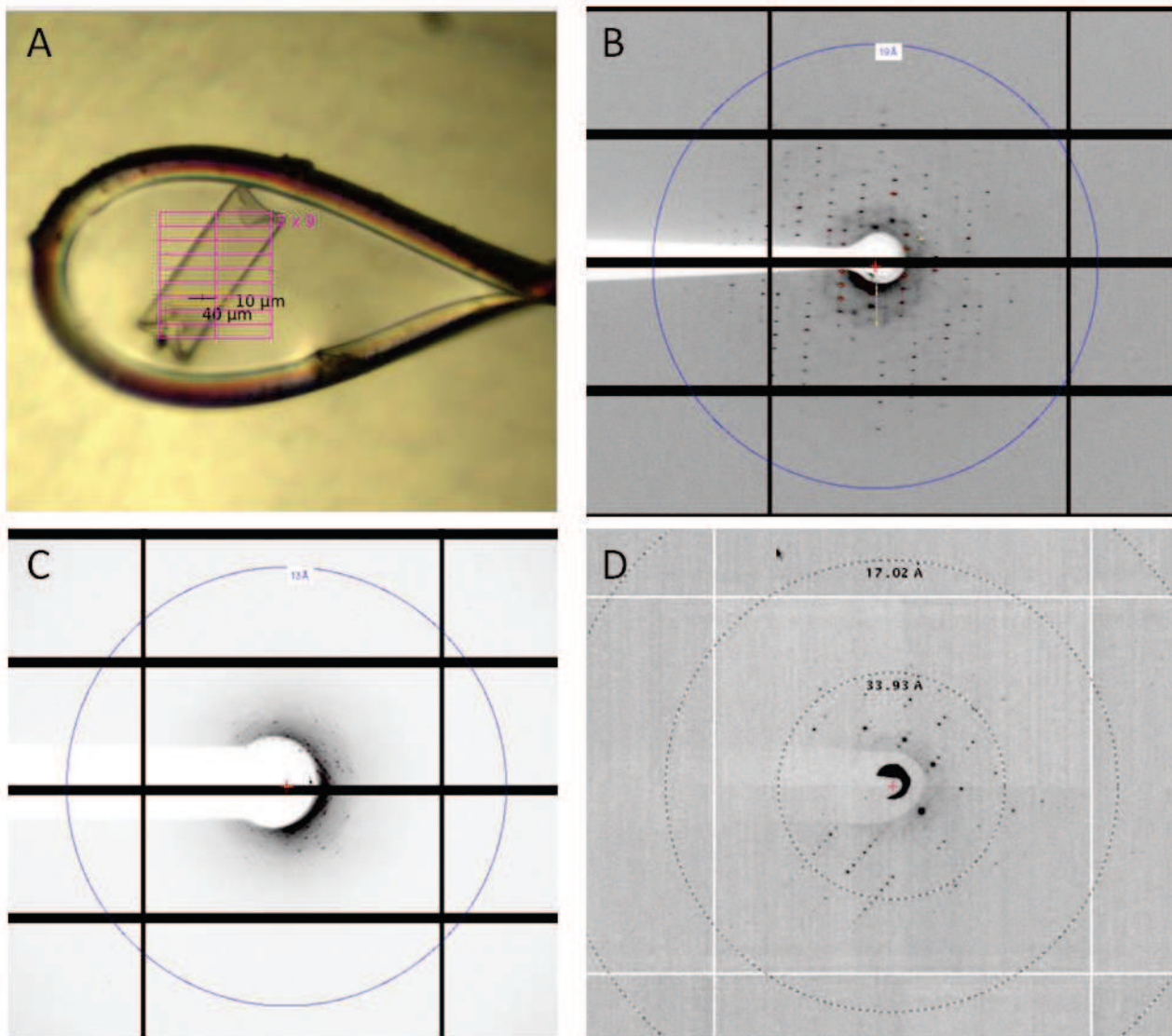


**Figure 21.** Diffraction patterns of different crystals. **A.** Cryo-cooled crystal in the loop. **B.** Diffraction pattern of the crystal reached 17.5 Å resolution limit (Pilatus 6M detector). **C.** Diffraction pattern of the crystal shot at room temperature using HC1 device (Pilatus 6M detector). **D.** Diffraction pattern of the crystal reached 21.7 Å resolution limit analysed at micro focused beam (ADSC Q315r detector).

## CRYO-EM STRUCTURE DETERMINATION OF *S. AUREUS* RIBOSOME

Cryo-electron microscopy, the structural analysis of samples embedded in vitreous ice, is a powerful approach for determining three-dimensional (3D) structures of biological specimens. Over the past two decades, this technique has been successfully used to calculate subnanometer ( $<10 \text{ \AA}$ ) resolution and, in some cases,  $<5 \text{ \AA}$  resolution structures of big objects such as icosahedral viruses or ribosomes. The recent development of electron microscopes with automated data collection capabilities and robust direct electron detection cameras, as well as new powerful image processing algorithms, has dramatically expanded the number of biological macromolecules amenable for study using cryo-EM. In addition, these new technological and computational developments have been successfully used to determine relatively high resolution 3D structures of proteins and protein complexes with either low or no symmetry, that before were not considered promising candidates for high-resolution cryo-EM. With these exciting new advances, cryo-EM will soon be able to determine near-atomic resolution 3D structures (Binstein and Ohi, 2015).

### Latest improvements in cryo-EM

The acceleration of the use of cryo-EM can be attributed to improvements in microscopes, imaging technologies, and computational approaches.

#### *Field emission gun (FEG)*

Some of the greatest advances for microscopes have come from the use of higher acceleration voltages (200 – 300 kV) and a FEG electron source. This increase both the temporal and spatial coherence of the electron beam, making it possible to collect high-resolution images at the defocus values required to visualize unstained particles in vitrified ice. Other advances in electron microscopes include stable lens systems (Glaeser et al., 2011), improved vacuums and stable cryo-stages that minimize sample drift.

#### *Detectors*

The remarkable progress in single-particle cryo-EM has been enabled by the development of direct electron detector device (DDD) cameras (Faruqi and McMullan, 2011; Li et al., 2013a; Milazzo et al., 2011). DDD cameras have a superior detective quantum efficiency (DQE), a measure of the

combined effects of the signal and noise performance of an imaging system (McMullan et al., 2009). Underlying complementary metal-oxide semiconductor (CMOS) technology makes it possible to collect dose-fractionated image stacks, referred to as *movies*, that allow computational correction of specimen movements (Bai et al., 2013; Campbell et al., 2012; Li et al., 2013a). Together, these features produce images of unprecedented quality, which, in turn, improves the results of digital image processing.

### *Software and Computing*

Along with technological developments and improved cryo-EM data collection, the need of software development to process these data was strongly required. Conveniently for cryo-EM, large computer clusters have become more readily available, and more powerful, over the past decade. Thus, many sophisticated and computationally demanding algorithms for alignment and classification of hundreds of thousands of noisy 2D projections have been developed, resulting in greatly improved and more reliable 3D density maps (Cheng, 2015).

Much effort has been invested in simplifying and automating the collection of EM images and the use of image processing software (reviewed in Lyumkis et al., 2010). The problematic issue with single-particle EM, however, is that there is still no objective quality criterion that is simple and easy to use, that would allow one to assess whether the determined density map is accurate or not. Even the resolution of a density map remains controversial.

## **Electron microscope organization**

Transmission electron microscopy (TEM) operates on the same principles as light microscopy, but uses electromagnetic lenses instead of glass lenses and electrons instead of light. Electrons as light are characterized by wave-particle duality. As particles, they interact with other particles such as atoms and can be scattered; as a wave, they can be diffracted by atoms. The wavelength of electrons is much shorter than the wavelength of visible light, and even shorter than the wavelength of X-rays; that brings the promise of extremely high resolution of electron microscopy. For example, according to the de Broglie wavelength, the wavelength of the electron accelerated to 100 kV is 0.037 Å. However, because of lens aberration, the highest resolution of modern microscopes falls to 1 – 2 Å.

Electrons are also scattered by the molecules of the air, and therefore the electron microscope column needs to be permanently kept at high vacuum. The need to maintain a vacuum makes it

necessary to introduce specimens through special airlock mechanisms. The problem posed by the basic incompatibility between the vacuum requirements and the naturally hydrated state of biological specimens has only recently been solved by cryo-EM. techniques (Dubochet et al., 1982): the specimen is kept frozen, hydrated throughout the experiment, at a temperature of liquid nitrogen or helium at which the vapour pressure of water is negligible.

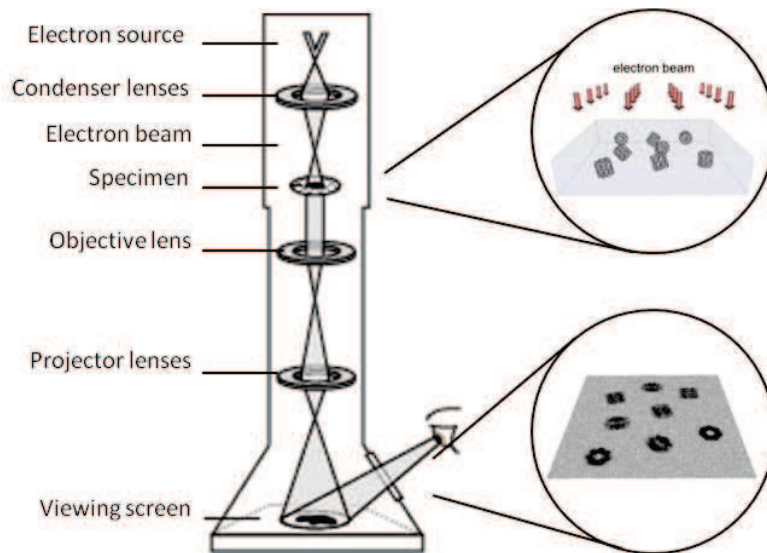


**Figure 22.** Schematic representation of basic composition of an electron microscope.

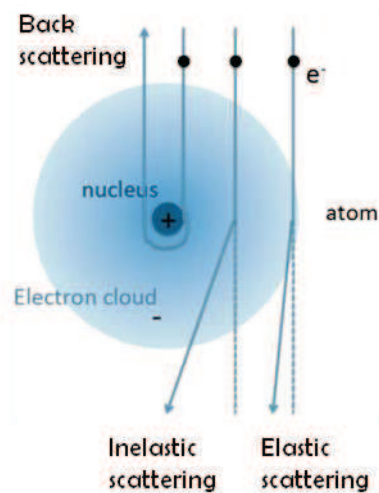


**Figure 23.** Scattering of the electrons by atom. Electron as a particle can interact with other particles, such as atoms. Each atom consists of a positively charged nucleus and a negatively charged electron cloud. When the incoming electron passes close to the atom in the sample, it is influenced by the electromagnetic field of the atom and changes its direction, in other words electrons are scattered by the atom. There are two types of scattering in EM: elastic scattering and inelastic scattering. Elastically scattered electron maintains its energy and gives rise to high resolution information. Inelastic scattering involves transfer of energy to the atom, thus first damaging the sample, and second producing an undesired background term of the image. In some cases even back scattering might happen, but back-scattered electrons do not contribute to the image formation.

An electron source at the top of the microscope emits the electrons that travel through vacuum in the column of the microscope where electromagnetic condenser lenses focus them into a very thin beam aimed at the specimen. Electrons are scattered by atoms as illustrated in Figure 23. The electron beam then travels through the objective lens, which is the first image-forming lens of electron microscope that gives us the information about amplitude contrast. Further, along the column several intermediate lenses produce magnification of the image, and the projector lens projects the image on the viewing screen or the detector/camera.

## Sample preparation and data collection

Sample preparation for cryo-EM experiment includes purification of the sample, preparation of the grids, vitrification of the sample. Appropriate sample concentration and choice of buffer for the sample provide enough freedom for particles to be evenly distributed on the grid and to avoid preferred orientations. Cryo-EM grid is a metallic mesh (usually copper or nickel) covered by thick layer perforated carbon, sometimes coated with a slightly charged layer of thin carbon (recently gold grids have been developed and shown to improve the quality of cryo-EM data (see Russo & Passmore, 2014b)). A drop of sample is usually applied on the grid under high humidity and low temperature conditions, blotted to remove the excess of liquid to get monolayer of sample and immediately plunged into liquid ethane cooled down to the temperature of liquid nitrogen. Liquid ethane has high heat capacity and, in contrast to liquid nitrogen, does not boil upon the contact with the grid. Vitrified sample is then transferred to liquid nitrogen.

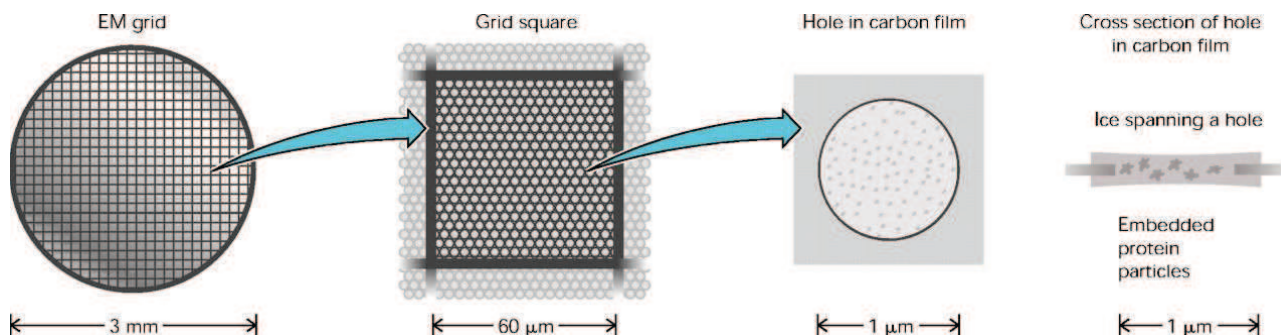


**Figure 24.** Representation of the cryo-EM grid at different scales (adapted from Wang and Sigworth, 2006).

During data collection and irradiating a sample with electrons, the protein being denser than ice, appears as a dark area on the image. Contrast generated by interference between unscattered and scattered electrons and, to a lesser extent, by aberrations of the electromagnetic lenses called phase contrast. It is generated by the differences in the phase shifts of electrons when they traverse different parts of the sample. Obtaining high contrast between the object (signal) and the background (noise) is a crucial criterion for cryo-EM imaging. Several adjustable parameters can increase the contrast level during data collection. However, all of them have a side effect on the final image. For example:

- Increasing the dose of electrons during exposure improves the contrast, but causes stronger radiation damage to the sample;

- Taking underfocused (or defocused) images provides better visibility of the particles on the micrograph, but decreases the resolution limit of these particles;
- Decreasing the electron acceleration voltage provides more interaction of the electrons with the sample, thus increases the contrast but also decreases the resolution limit.

Therefore it is necessary to find a delicate balance between these parameters to get maximum signal while not destroying the structural integrity of the sample.

Purification of *S. aureus* ribosomes for cryo-EM experiment was performed using the same protocol as for crystallization (see page 59). The ribosome solution was clarified by centrifugation at 10000×g / 10 min, and then diluted in buffer G<sup>10/60</sup> to 40 – 60 nM. The sample (4 µl) was loaded on the 300 carbon mesh 2 × 4 µm grid and blotted using FEI Vitrobot Mark IV operated at following settings: 95% humidity, 4 °C, blotting time 4 sec, blotting force 5 and immediately vitrified in liquid ethane. The quality of sample preparation was analysed using the in-house FEI Tecnai F30 (Polaris) cryo electron microscope (Figure 25). The grids were clean and almost did not contain thick ice or broken regions, and ribosomes were equally distributed over the grid, indicating that the concentration of sample and choice of buffer were selected properly.

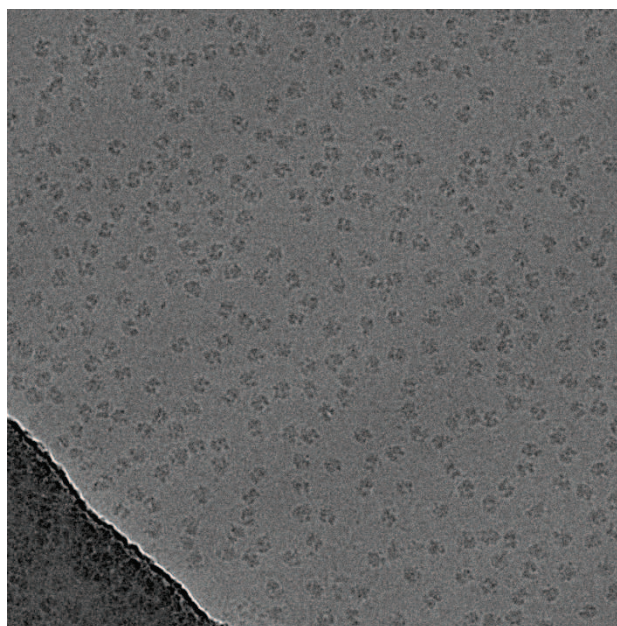


**Figure 25.** Electron micrograph of the vitrified *S. aureus* 70S ribosome sample taken on the F-30 Polaris microscope. Magnification 59000, Voltage 300kV, Detector CCD eagle 4Kx4K.

To get the highest Signal-to-Noise Ratio (SNR) and retrieve high resolution details, several approaches are used during data collection. First, appropriate energy level is selected according to the sample. Small objects such as single proteins or small complexes can be better visualized at low voltage due to less inherent contrast, while big complexes are usually imaged at high voltages (Reviewed in van Heel et al., 2000). Second, images are taken at different defocus values. By

changing the current of the magnetic lenses, the electron beam is focused at different positions, allowing a set of images with different contrast and resolution to be obtained.

Recently, the quality of cryo-EM imaging has been greatly improved by the ability of new CMOS detectors to make several read-outs during an exposure. (our version). Thus, instead of taking one image of fully irradiated sample, it is possible to get a stack of intermediate frames ("movies") with different levels of irradiation. Intermediate frames revealed that the sample is not static and may slightly drift and turn because of heating during the exposure. This beam-induced drift can be compensated during image processing using specific algorithms implemented into several recently developed cryo-EM software programs.

Data for the *S. aureus* ribosome were collected using the in-house spherical aberration (Cs) corrected Titan Krios S-FEG instrument (FEI, Eindhoven, Netherlands) operated at 300 kV acceleration voltage, at a magnification 59000X and an underfocus of  $\Delta z$  from 0.4 to 4.0  $\mu\text{m}$ . The data were recorded using the second-generation back-thinned direct electron detector CMOS (Falcon II) during automated data collection with EPU software (FEI, Eindhoven, Netherlands). The camera was set up to collect 7 frames out of 17 possible, with pixel size of 1.1  $\text{\AA}$  and total exposure dose of 60  $\text{e}^-/\text{\AA}^2$  (or approximately 3.5  $\text{e}^-/\text{\AA}^2$  per frame).

## Image processing for single particle cryo-EM

### *Frame re-alignment*

*The collection of cryo-EM images in "movie" mode allows for the tracking of beam-induced movement of both the vitrified ice layer and the embedded particles (Brilot et al., 2012; Campbell et al., 2012). This movement causes blurring of the final image, limiting the ability to generate high-resolution structures. A number of algorithms that correct for this beam-induced motion have now been developed. These approaches align the individual dose fractionated images, either using the entire image or the individually windowed particles, before summing the frames into a final image (Li et al., 2013; Shigematsu and Sigworth, 2013; Rubinstein and Brubaker 2014; Sheres, 2014). This procedure significantly improves the quality of the final data for two reasons. First, the alignment algorithms correct the beam-induced motion, and second, the effects of radiation damage can be reduced by carefully choosing which dose-fractionated images are included in the final summed image (Baker, 2010; Sheres, 2014).*

As the first step of image processing, the stack of 7 frames collected for each image was aligned, beam-induced local (movement of individual particle) and global (movement of the whole frame) drifts were compensated and frames were averaged into one micrograph. The frame re-alignment was performed using optical flow algorithms integrated in Scipion workflow. All subsequent image processing was performed in Scipion workflow using algorithms integrated there.

### *Contrast transfer function*

*For weakly scattering samples, the image formation process in the electron microscope is linear, i.e., the densities in collected image are linearly proportional to the densities in the imaged object, and this is described by the Contrast Transfer Function (CTF) (Frank, 2006; Wade, 1992). CTF mathematically describes how aberrations in the electron microscope modify the image. To compensate imperfections of the image, CTF of each micrograph has to be estimated.*

*There are several parameters required for CTF estimation. Some of them, such as wavelength and spherical aberration coefficient are given by the settings of the microscope, whereas the others (defocus and astigmatism) are established experimentally. Once the mathematical form of the CTF is calculated, it is used to correct the image for the CTF effects. CTF is an oscillating function which crosses zero several times; every zero-cross means the loss of information therefore a single image cannot be fully corrected. Therefore, it is necessary to collect many images at different defocus settings, as these give rise to CTFs with zeros at different spatial frequencies, and averaging them with appropriate weights (Penczek, 2010) will result in a CTF-corrected average.*

To estimate the CTF, Fourier transform of the image is calculated. Fourier transform is a sum of all sine waves with the amplitudes and frequencies that compose that image. The sine waves with a big wavelength (in other words low frequency waves) have large amplitude and describe low-resolution components of the image. They contribute to the image contrast. The sine waves with high frequencies usually have small amplitude and do not contribute to the contrast, but carry high-resolution components of the image. Fourier transform (as a function of frequency vs amplitude) corresponds to the amplitude spectrum of the image, as the phase components are omitted. It is common to plot Fourier transform as a function of intensity vs frequency (intensity = amplitude<sup>2</sup>). Such plot is known as a power spectrum, where approximated by computed CTF, amplitude oscillations are shown as Thon rings (Mindell and Grigorieff, 2003).

Estimation and correction of CTF was performed using `ctffind4` (Rohou and Grigorieff, 2015). Characteristic parameters and some more explanations are given in Figure 26. The micrographs where the CTF parameter was difficult to estimate were excluded from further processing (usually these micrographs contained either crystallized ice particles or the edge of the carbon hole). The micrographs with estimated resolution lower than 10 Å were also excluded.

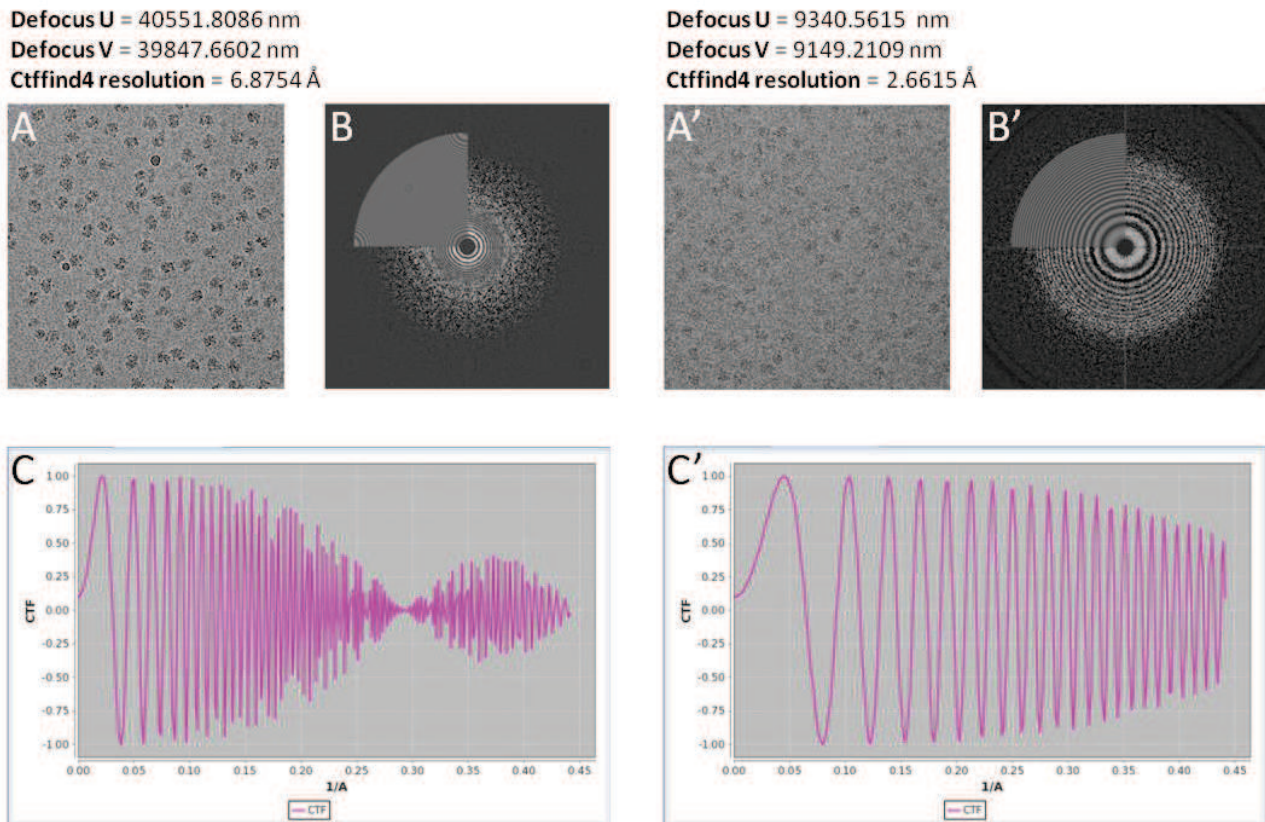


**Figure 26.** Processing of *S. aureus* ribosome cryo-EM images taken at different defocus (high defocus on the left side and low defocus on the right side). Defocus values and calculated resolution limits are indicated above the image. Electron micrographs after frame re-alignment are shown in figures **A** and **A'**. The image taken far from the focus (**A**) has very high contrast, that makes particles very visible. However, according to the CTF estimation, most of the high-resolution information is lost in this image, but can be recovered from image taken closer to focus. Power spectra are shown in the figures **B** and **B'**. Contrary to the far-from-focus image, calculated Thon rings of close-to-focus image (**B'**) have big radii and are a good match with the theoretically predicted ones. This means that the image contains sine waves with high spatial frequencies, in other words carries high-resolution information. Another representation of CTF estimation is shown on plots **C** and **C'**. Plot **C** is a frequently oscillating curve, which fades out at high spatial frequencies, where high-resolution information is located. Thus, this image contains very few signals at high resolution, moreover, any information is lost at the points where the CTF curve crosses the zero value. In turn, the CTF curve of the close-to-focus image (**C'**) oscillates much less, has a high signal at the high spatial frequency, and therefore carries high-resolution information.

### *Particle picking and extraction*

Once a dataset has been collected, movies have been aligned and averaged (if applicable), and good micrographs have been selected (e.g., based on Thon rings being visible to high resolution in all directions), a project continues with the labour-intensive process of particle picking. Particles can be selected in a manual, semi-automated, and fully automated manner (Figure 27).

Picking of the particles of *S. aureus* ribosome was performed in semi-automated mode using XMIPP (Sorzano et al., 2004) software. Around 1000 particles were picked manually and used as a reference for automated picking. During particle extraction the particles were normalized and the

contrast was inverted, so that particles became white and the background became dark.

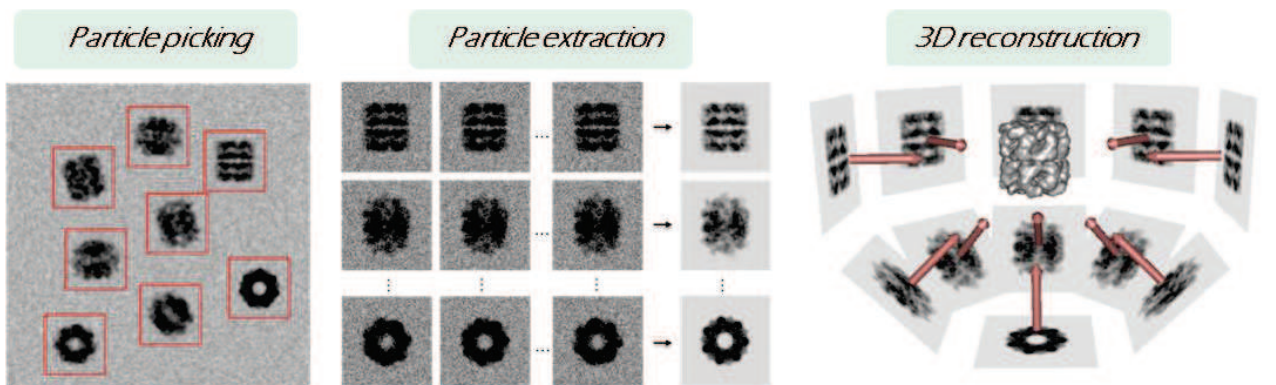


**Figure 27.** Schematic and idealized representation of particle extraction and 3D reconstruction. An example of the GroEL complex is presented. For the reason of proper visualization, the contrast is not inverted, therefore particles are dark and the background is less dark.

### *Particles classification*

*To determine a high-resolution 3D structure, only images of structurally identical molecules should be included in the reconstruction. Numerous image processing approaches have been developed to precisely assign orientation parameters to 2D projections and ensure projections of only structurally homogeneous particles are included in a 3D reconstruction. The ability of cryo-EM to classify structurally diverse datasets, sometimes termed in silico purification, makes single-particle EM a powerful method for determining structures of many biologically essential complexes that are difficult to crystallize because of their inherent conformational heterogeneity. However, at this time, the image processing algorithms are still limited by the amount of structural heterogeneity that can be tolerated. Classifying small, asymmetric, and/or extremely dynamic samples remains a significant challenge.*

A cryo-EM image is a 2D projection of a 3D object. An object, sampled from a range of angles is then reconstructed by reprojecting these projections at the original sampling angle into the object space (Figure 27). To provide maximum 3D information as many projections as possible should be acquired over as wide range of angles as possible. However, sometimes molecules, especially elongated ones, take a preferable orientation on the grid, that limits the angular coverage of the projections. During classification 3D models are reconstructed for each class in iterative manner and each particle is assigned to one or another class based on cross-correlation or maximum likelihood approach.

Extracted particles of *S. aureus* ribosome were classified into 10 classes using Relion 1.3 (Scheres, 2012), which is based on a maximum likelihood algorithm, and require the initial (reference) model. As a reference model we used the crystal structure of the *E. coli* ribosome (Schuwirth et al., 2005, PDB code 4V4Q) low-pass filtered to 40 Å. Two stages of the 3D classification were performed

using stepwise sampling, starting from 30° angular sampling interval, 10 pix offset search range and 2 pix offset search step. Each subsequent round of classification was performed with finer sampling and was started from the iteration of the previous step, when P-max value reached the plateau. As the last step the following sampling was used: 1.8° angular sampling interval, 4 pix offset search range and 1 pix offset search step. The result of the first stage of 3D classification allowed sorting out rough heterogeneity of the sample e.g. free 50S subunits, ribosome particles containing E-site tRNA, 70S particles with SSU in different conformations and other impurities. Classes of interest were further re-classified using the same sampling as that used for the first stage of classification. The final result revealed two identical classes of non-rotated ribosome with very residual P-site tRNA (see Figure 28). These two classes together contained 109580 particles (26.6% of the full dataset). They were subsequently merged together and subjected to further refinement.

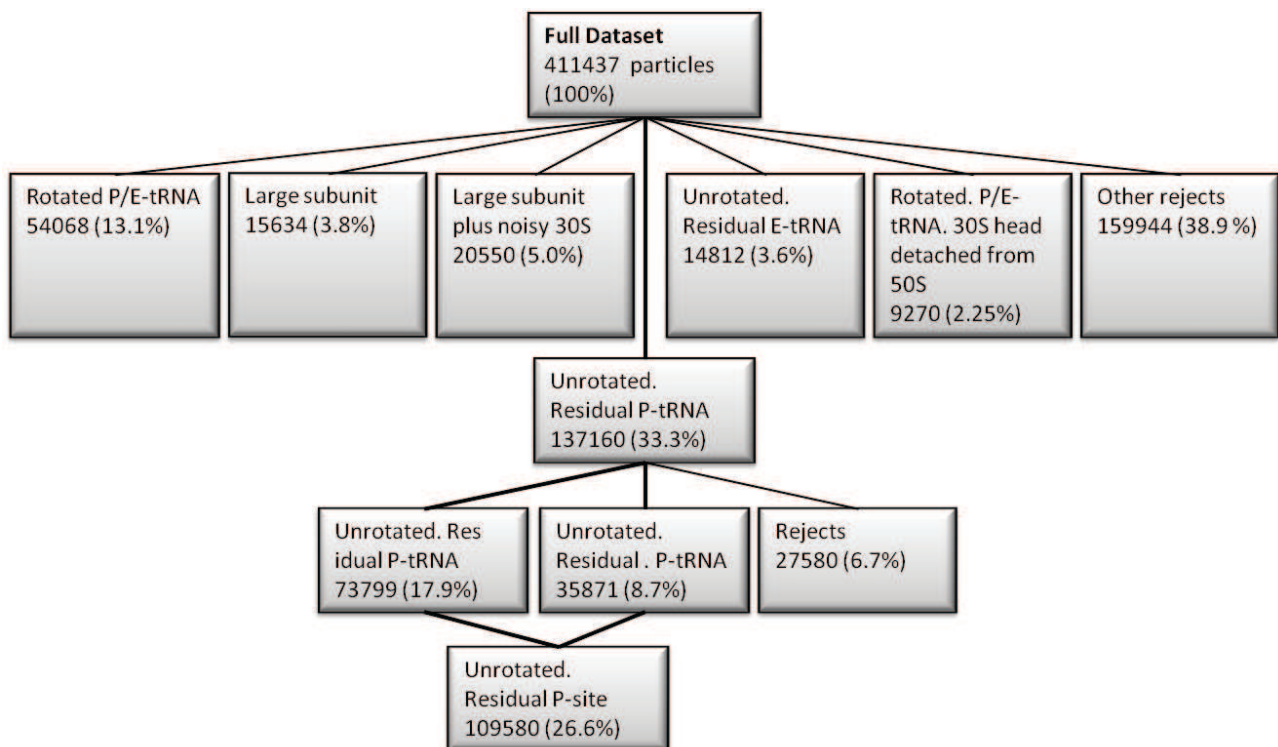


**Figure 28.** Schematic representation of 3D classification of *S. aureus* ribosome dataset.

### Refinement

After successful 3D classification, the particles from the classes of interest are subjected to structure refinement. All single-particle EM packages use a more or less elaborate version of the iterative 3D projection matching procedure for structure refinement. At the end of every iteration, Fourier Shell Correlation (FSC) curve is computed using half-subsets of the projection data and the current resolution is derived from it. FSC provides information on the level of SNR as a function of a spatial frequency. Based on the FSC, the structure is low-pass filtered and passed to the next iteration of the procedure as the new template. "Resolution" in single-particle EM is a somewhat arbitrarily chosen cut-

off level of the SNR or FSC curve. For example, the resolution can be defined as the spatial frequency at which the FSC curve is 0.5 or as the spatial frequency at which the SNR is 1.0 (corresponding to an FSC of 0.33), the level at which the power of the signal is equal to the power of the noise (Rosenthal and Henderson, 2003). Another common choice of threshold is 0.143 (often called gold-standard FSC), the value selected based on relating EM results to those in X-ray crystallography (Sheres & Chen, 2012).

Refinement of the selected classes was performed using the Relion 3D auto-refine protocol. This procedure employs gold-standard FSC calculations to estimate resolution, so that overfitting may be avoided. Combined with a procedure to estimate the accuracy of the angular assignments, it automatically determines when a refinement has converged. The refinement was performed under following conditions: 15° angular sampling interval, 30 pix offset search range and 6 pix offset search step, 3.7 pix local search from auto-sampling.

The gold-standard FSC curves inside the auto-refine procedures only use unmasked maps to strictly prevent overfitting. However, this also means that the actual resolution is under-estimated somewhat because a noisy solvent area. Therefore, after performing a 3D auto-refinement, the map was sharpened, using a soft mask with 4 pix mask extensions and 4 pix soft-edge width. The resolution of the final sharpened structure was estimated to be 3.9 Å at FSC=0.143 and 4.7 Å at FSC = 0.5 (Figure 29).

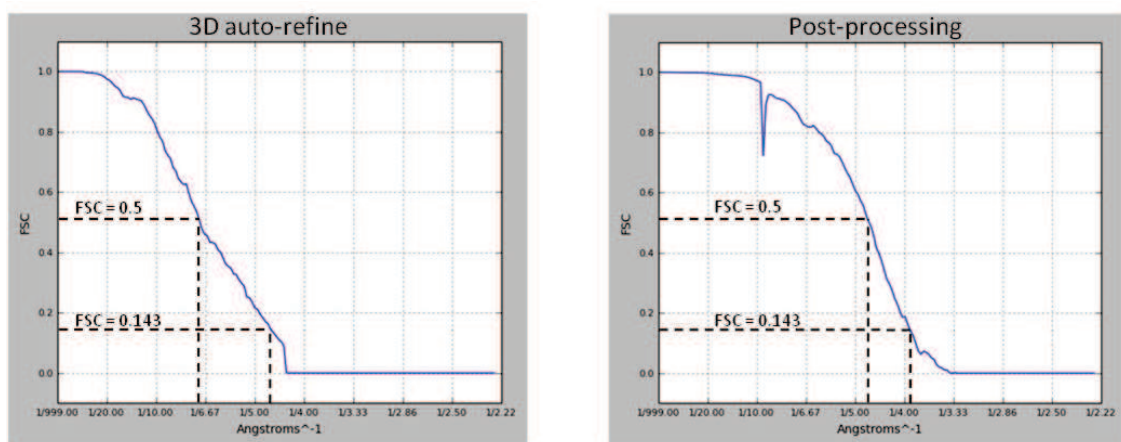


**Figure 29.** Resolution curve of cryo-EM structure reconstruction after 3D auto-refinement (left) and post-processing (right). Estimated resolution after course refinement was 4.7 Å using gold-standard FSC (0.143) and 6.9 Å at FSC=0.5. After refinement using the mask resolution increased to 3.9 Å using gold-standard FSC (0.143) and 4.7 Å at FSC=0.5.

### *Local resolution estimation*

Unlike crystal structures, cryo-EM structures have heterogeneous resolution in different regions, the core part of the molecule is usually better resolved than the periphery. This is because the periphery parts of the molecules are usually more flexible and also they move more during electron exposure in respect to the core part. Estimation of the local resolution is useful tool for

analysing the structure before modelling.

The local resolution was calculated using Resmap (Kucukelbir et al., 2014). Following parameters were used: box size 330 Å, resolution limit 3.0 – 8.0 Å, step size 0.35 Å. The results are shown in the Figure 30. The overall structure was around 3.5 – 4.5 Å resolution. However, the resolution at periphery dropped to 5.5 – 6.0 Å. As expected, the small subunit was less resolved due to its flexibility.

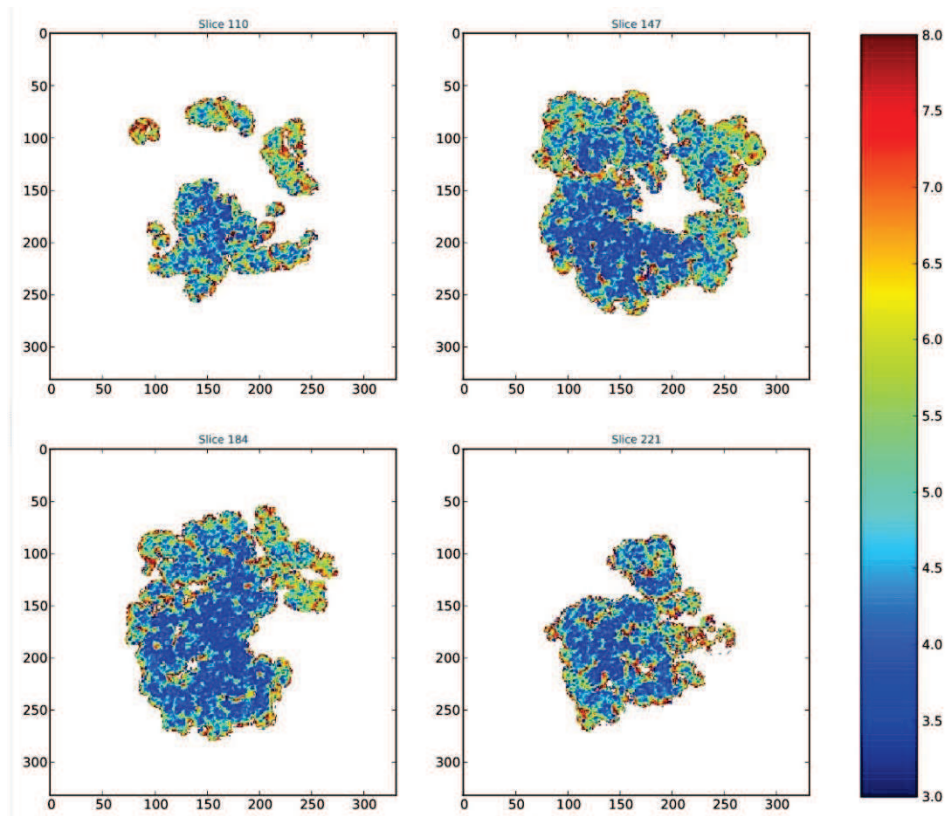


**Figure 30.** Local resolution map of *S. aureus* ribosome. The rainbow bar-legend corresponds to an estimated resolution of 3.0 – 8.0 Å.

### *Structure analysis*

The cryo-EM structure of *Staphylococcus aureus* 70S ribosome was visualised and analysed using UCSF Chimera package (University of California, San Francisco, USA; Pettersen et al., 2004).

The structure, solved at 3.9 Å resolution allows clear visualization of nucleotide-nucleotide interactions of the rRNA and proteins  $\beta$ -sheets (Figure 31). The side chains of the  $\alpha$ -helices can be traced in most regions closer to the core, but it can be problematic with some proteins that are very flexible or located on the periphery.

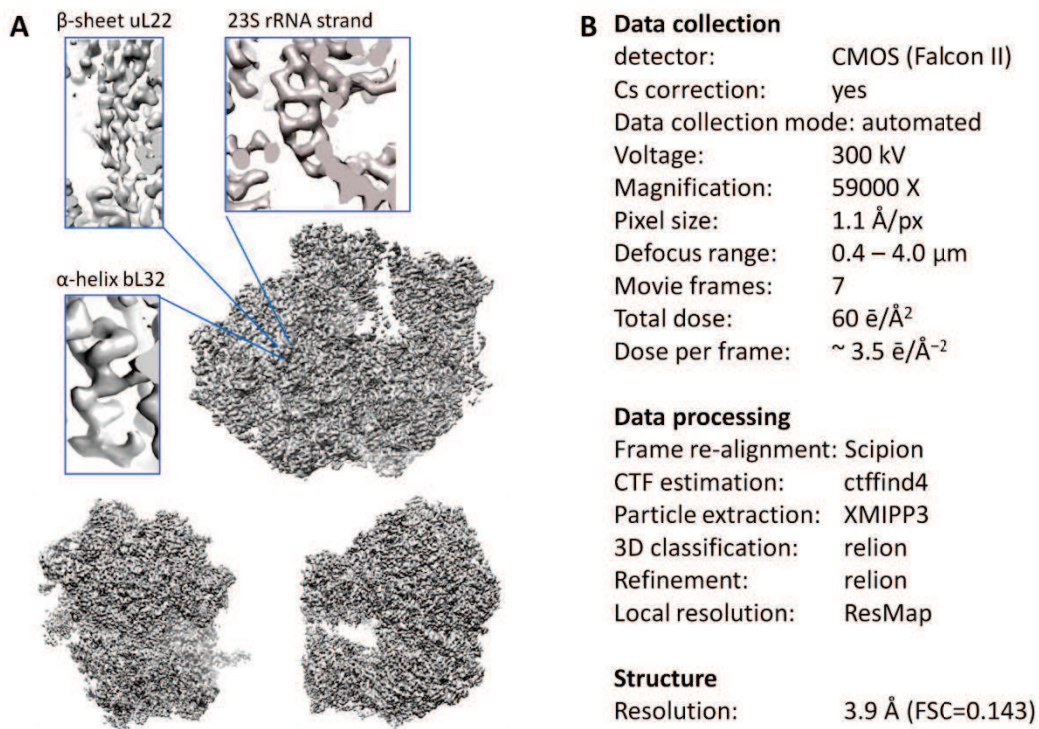


**Figure 31. A.** Cryo-EM structure of *S. aureus* ribosome. **B.** Settings of cryo-EM experiment.

We performed the comparative analysis of *S. aureus* ribosome using model objects: crystal structures of *T. thermophilus* (Jenner et al., 2010) and *E. coli* (Schuwirth et al., 2005) 70S ribosomes and cryo-EM structure of *B. subtilis* 70S ribosome (Sohmen et al., 2015). The *T. thermophilus* ribosome is the most structurally studied ribosome, the *E. coli* ribosome is the most biochemically studied and the mesophilic bacterium *Bacillus* is phylogenetically the closest organism to the genus *Staphylococci*.

The structure of *S. aureus* ribosome was compared to the structure of *B. subtilis* ribosome, the first Gram-positive bacterium ribosome structure solved by cryo-EM at high-resolution (3.5 – 3.9 Å) in the laboratories of D. Wilson and R. Beckmann (Sohmen et al., 2015). The qualities of both maps were very similar. Figure 32 (A and B) demonstrates part of PTC located on the intersubunit region, particularly nucleotides 2092-2097 of the 23S rRNA.

An overall comparison revealed almost no differences in the three-dimensional organisation of these two ribosomes. However, to study *B. subtilis* ribosome, the authors used a stalled model with tRNA in the P-site and peptide chain in the protein exit tunnel. Therefore, some differences between two ribosomes were found in the tRNA binding region, *e.g.* at nucleotide A2631 (A2602 in *E. coli*) of the 23S rRNA, which is located in the PTC. It is known to be conformationally the most flexible residue in PTC, however, in the presence of tRNAs, it is sandwiched between A- and P-tRNAs CCA ends (Nissen et al., 2000). We did not observe it in the structure of vacant *S. aureus* 70S

ribosome (Figure 32, E), but it was structurally stabilized in the *B. subtilis* structure by the CCA-end of the P-tRNA (Figure 32 D).

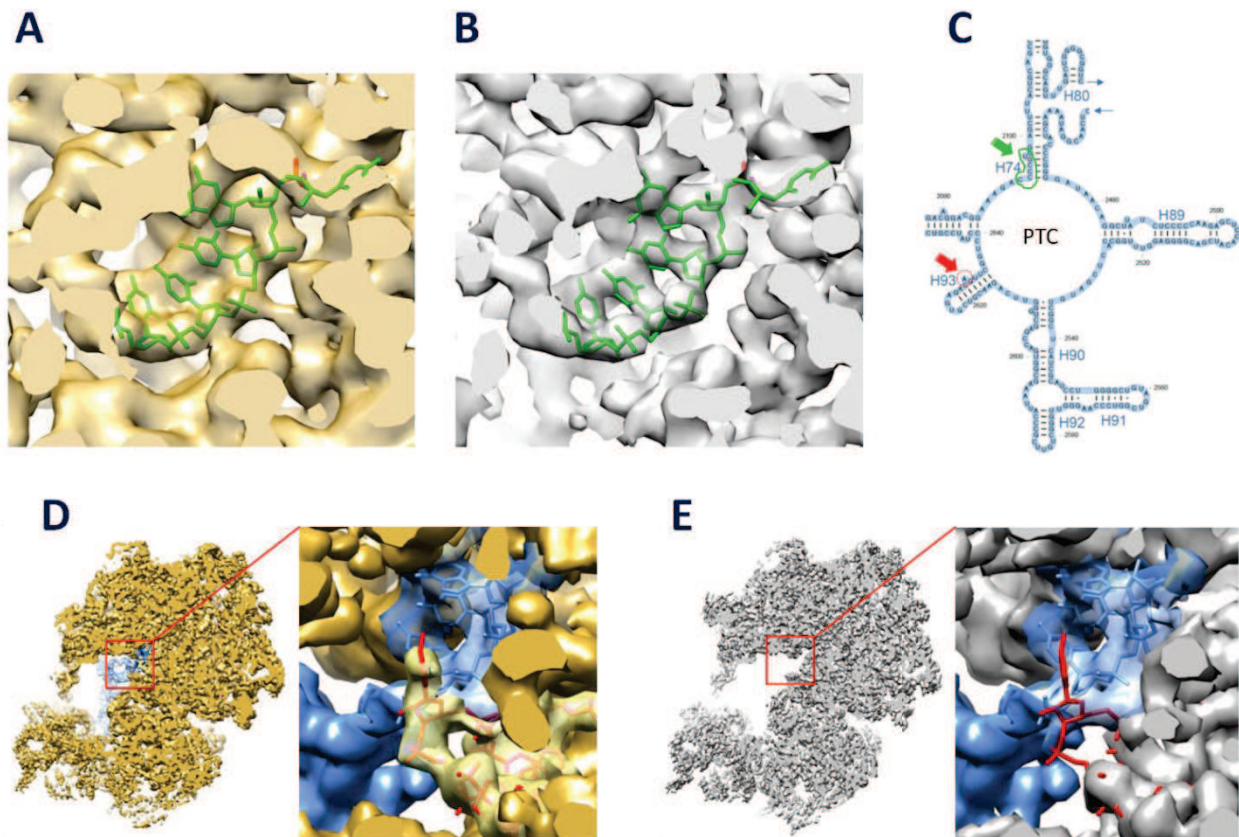


**Figure 32.** Comparison of cryo-EM structures of *B. subtilis* ribosome (gold) and *S. aureus* ribosome (grey). The model of *B. subtilis* (PDB code 3J9W) was fitted as rigid body into the *S. aureus* ribosome structure. P-tRNA is shown in blue, 23S rRNA nucleotides are shown in green and red. **A**, **B** – the intersubunit regions of two ribosomes; nucleotides 2092-2097 of 23S rRNA are colored in green. **C** – The secondary structure of PTC of *B. subtilis*. Arrows indicate the nucleotides highlighted on figures A-E. **D** – Position of nucleotide A2631 (red), fixed by the CCA-end (blue) of the P-tRNA bound to the *B. subtilis* ribosome. **E** – The nucleotide A2631 is not visible on the map of *S. aureus* ribosome due to its high flexibility.

One of the characteristic features of the ribosomes from mesophilic bacteria are the extensions of rRNAs. A comparison of the secondary structures of the 16S and 23S rRNA was performed using comparative RNA web (CRW) site (Cannone et al., 2002). For this analysis we chose one mesophilic Gram-positive bacterium (*S. aureus*), one mesophilic Gram-negative bacterium (*E. coli*) bacteria, one thermophilic Gram-negative bacterium (*T. thermophilus*) and one archaea (*Haloarcula marismortui*). Several rRNA helices were found to be extended in the structures of *S. aureus* and *E. coli* in contrast to *T. thermophilus* and *H. marismortui*. Some of them, are conserved with *E. coli* (h26, h44, H27, H68, H79), or *T. thermophilus* (h9, H15, H63), whereas others appear to be specific for the Gram-positive bacteria, *S. aureus* or *B. subtilis* (h6, h10, h17, H25, H54). Some of these helices are listed in Figure 33.

High-resolution crystal structures of 70S ribosomes have solved for *E. coli* and *T. thermophilus* and large 50S ribosomal subunit has only been solved for *H. marismortui*. Therefore, the same comparative analysis was performed using 3D models of these ribosomes. The results were consistent with secondary structure analysis and are shown in Figure 34. These extensions located mostly on the periphery, outside the functional sites of the ribosome and their exact role yet is unclear.

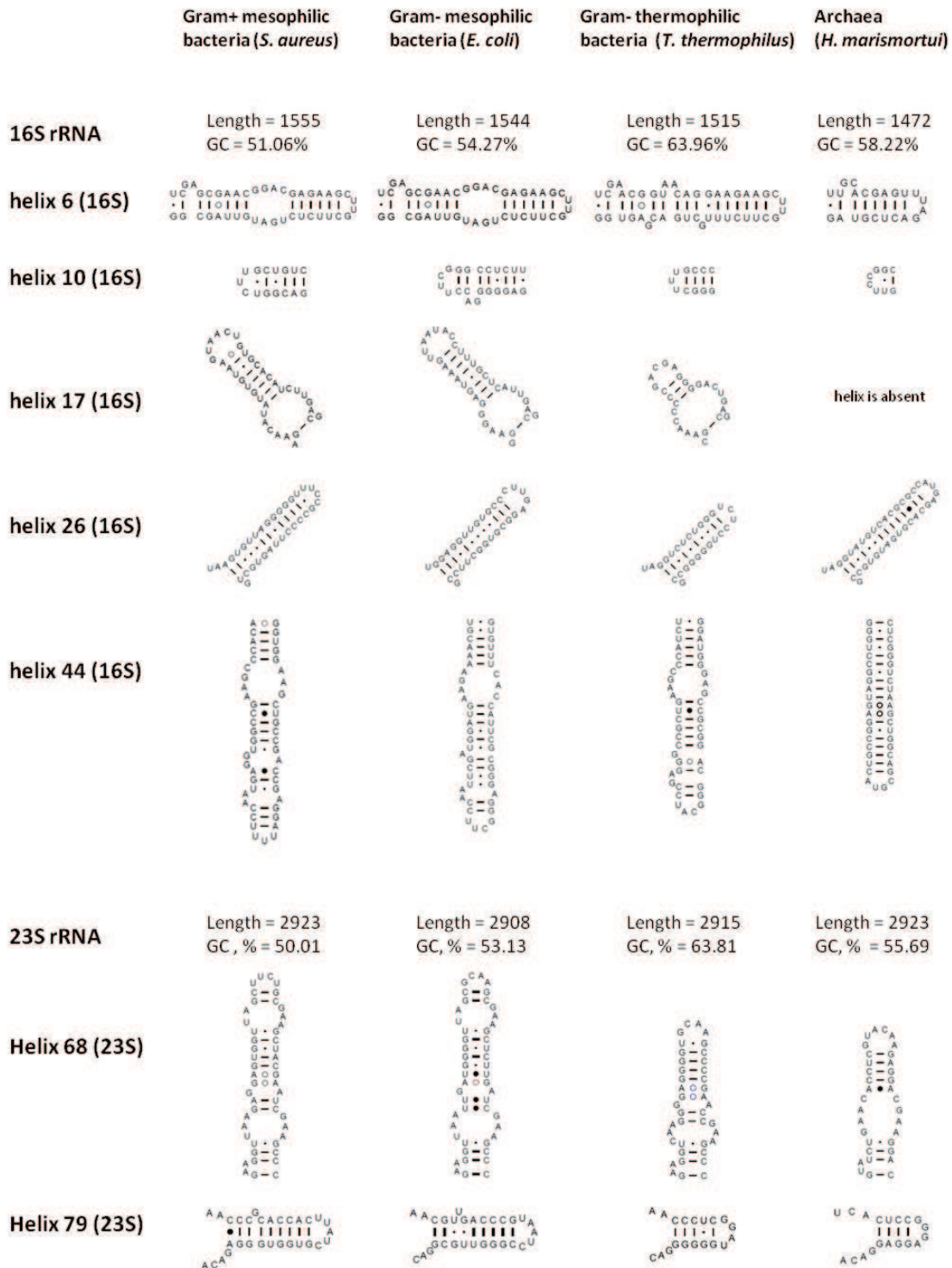


**Figure 33.** Examples of the comparative analysis of secondary structure elements of the rRNAs from different organisms.

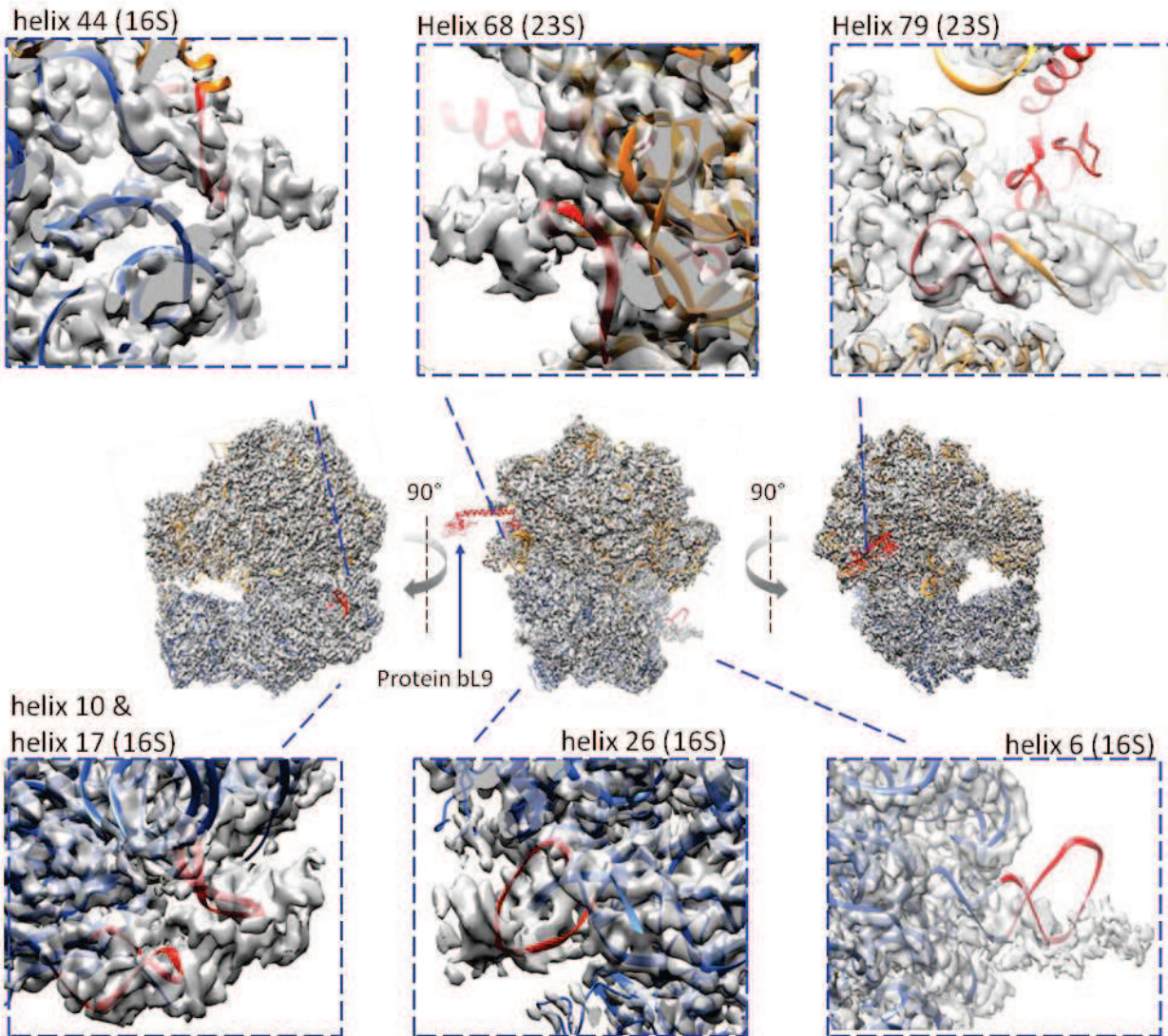


**Figure 34.** X-ray structure of *T. thermophilus* ribosome (PDB code 4V4F) fitted into *S. aureus* ribosome structure as rigid body: 30S subunit is colored in blue, 50S subunit is colored in gold. Extensions of some rRNA helices and ribosomal proteins are colored red.

One more important observation made in the sample of purified *S. aureus* 70S ribosome is the absence of the protein L9. The protein L9 is bacteria-specific ribosomal protein. It is located on the periphery very close to L1 stalk in domain V of the rRNA and protrudes at the side of bacterial ribosome. The protein is very weakly associated with the *S. aureus* ribosome and dissociated during ribosome purification procedure (Table 3).

## RESEARCH PROJECT 1: SUMMARY

Following results were obtained for the project of structure determination of *S. aureus* 70S ribosome:

- Growth of *Staphylococcus aureus* cells and their harvesting were adapted for purification of ribosomes for structural studies.
- The protocol of ribosome purification was established. The yield of material was sufficient to perform extensive search of crystallization conditions.
- Characterization of the ribosomes by different biochemical and biophysical methods proved their purity, stability and homogeneity.
- First crystals of *S. aureus* 70S ribosomes were obtained. Crystals were reproducible and reached appropriate size to perform diffraction experiments.
- The conditions of dehydration and cryo-cooling were optimized for obtained crystals.
- First diffraction data of *S. aureus* 70S ribosome crystals were collected. However, the resolution obtained was too low ( $\sim 18$  Å) for high-resolution structure determination.
- The appropriate conditions for cryo-EM grid preparation and data collection were found for *S. aureus* 70S ribosome sample.
- After the processing of the cryo-EM images, the structure of vacant *S. aureus* 70S ribosome was obtained at 3.9 Å resolution. The resolution will be further improved by performing several additional steps of image processing.
- First structure analysis revealed several features in ribosome structure unique for Gram-positive bacteria.

---

RESEARCH PROJECT 2:

**PURIFICATION AND CRYSTALLIZATION OF HUMAN eEF2**

---

## PURIFICATION AND CRYSTALLIZATION OF HUMAN eEF2 PROTEIN

One of the scientific goals of our laboratory is the crystal structure determination of the human 80S ribosome. For structure determination of human 80S ribosome the protocol of purification also have to be established. During our development of ribosome purifying protocols we discovered that most of the ribosomes co-purify with eEF2 protein. The most likely explanation for this observation is that eEF2 inactivates the ribosomes as a part of the physiological response of HeLa cells that were used for purification. The same observation was reported in the recent cryo-EM study of human 80S ribosome: the sample of vacant 80S ribosome contained some fraction of 80S ribosome complex with eEF2 (Anger, et al., 2013).

In general, any ribosome isolation protocol is based on the sedimentation properties and selection between ribosomal and protein fractions, and it can be achieved during the first steps of purification. In the preparation of the yeast 80S ribosome this selection occurs during the step of PEG precipitation where big complexes such as ribosome can be found in the insoluble fraction and proteins stay in the soluble fraction. Therefore, for purification of native eEF2 protein from HeLa cells we used the soluble fraction after PEG precipitation. Using this approach, we also made a selection between the free cytosolic eEF2 and ribosome-associated eEF2.

### HeLa cells preparation

HeLa cells were grown in suspension cultures in Minimal Essential Media Spinner Modification (S-MEM) (Sigma Aldrich) supplemented with 7% new-born calf serum, 2 mM Glutamine and 40 µg/ml gentamycin at 37 °C in 5% CO<sub>2</sub> environment. These cell cultures were maintained at the IGBMC HeLa cell facility.

### Purification of native eEF2

During purification of ribosomes from 3 – 6 liters of HeLa cell culture, the ribosome-free soluble fraction after PEG precipitation step was precipitated using (NH<sub>4</sub>)<sub>2</sub>SO<sub>4</sub> – salt powder was added to 80% saturation level, stirred for 1 hour and precipitated at 20000×g / 40 min. Pellet was dissolved in buffer I (20 mM Tris-HCl pH 7.5, 20 mM KCl, 5 mM MgCl<sub>2</sub>, 0.1 mM EDTA, 1 mM DTT) and dialysed overnight against buffer I. Sample was clarified by spinning at 20000×g / 30 min and loaded on HiTrap Q HP 5 ml anion exchange column (GE Healthcare Life Sciences). The column was

pre-equilibrated in buffer I and the sample was eluted using 0 – 100% gradient of buffer II (20 mM Tris-HCl pH 7.5, 500 mM KCl, 5 mM MgCl<sub>2</sub>, 0.1 mM EDTA, 1 mM DTT). Fractions containing eEF2 were pooled together, diluted with buffer I to give a KCl concentration of 30 – 40 mM and loaded on Heparin 5 ml column (GE Healthcare Life Sciences) pre-equilibrated in buffer I. Protein was eluted using 0 – 100% gradient of buffer II. Fractions containing eEF2 were pooled, and then by reducing the volume to 0.3 – 0.5 ml using Amicon Ultra centrifugal filter MWCO 50 kDa (Millipore) Centricons. These fractions were subsequently applied to a size exclusion chromatography column Superdex 200 10/300, 24 ml, pre-equilibrated with buffer III (20 mM Tris-HCl pH 7.5, 100 mM KCl, 5 mM MgCl<sub>2</sub>, 1 mM DTT). Pure protein containing fractions were pooled, concentrated using Amicon Ultra 50 kDa by reducing them to the least possible volume. Final concentrations were around 0.6 – 0.8 mg/ml (6.8 μM), and total amount around 30-60 μg. These yields are obviously too low for any crystallization experiments.

Another purification was carried out on a larger scale using  $900 \times 10^8$  cells. Frozen cells (235 ml of packed cell volume) were washed once in PBS buffer (137 mM NaCl, 2.7 mM KCl, 10 mM Na<sub>2</sub>HPO<sub>4</sub>, 1.8 mM KH<sub>2</sub>PO<sub>4</sub>, and re-suspended in 940 ml of re-suspension buffer (50 mM Tris-HCl pH 7.9, 1 mM EDTA, 1 mM DTT, 0.5 mM PMSF). After 30 min on ice, cells were lysed using tissue grinder with loose pestle “B” going 10 times up and down. After centrifugation 1200×g / 10 min supernatant was collected, KCl was adjusted to 250 mM and MgCl<sub>2</sub> was adjusted to 10 mM. Cell debris was removed by centrifugation 25000×g / 60 min, and the ribosome fraction removed by centrifugation 100000×g / 160 min. The supernatant aliquoted, ammonium sulfate powder was added to give 80% saturation, stirred for 1 hour on ice and then centrifuged at 20000×g / 40 min. Protein containing pellet was flash frozen in liquid nitrogen and stored at -20 °C. When needed, several aliquots were dissolved in buffer I and all further steps were identical to small-scale purification with only difference that due to limited capacity, the HiTrap Q HP 5 ml column was loaded 3 times in a row. Chromatography protocols, and results are summarized in Figure 35. Final yield was around 2 mg of pure eEF2 at a concentration of 8 mg/ml that was sufficient to perform some crystallization experiments.

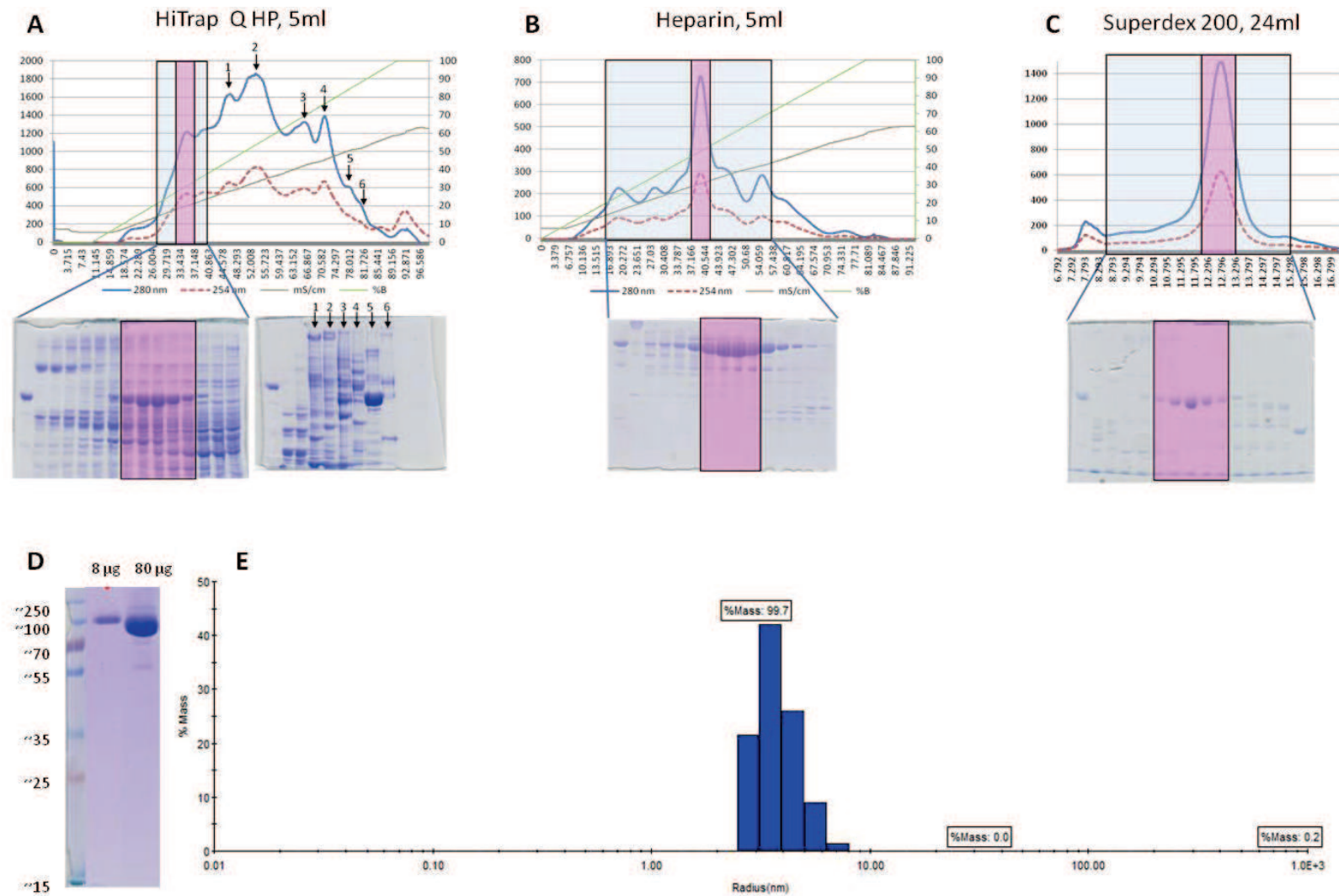


**Figure 35.** Purification of human eEF2 protein. A - C. Profiles after anion exchange (A), affinity (B) and size exclusion (C) chromatography. Absorbance units at 280 nm and 254 nm are presented at left Y-axis, percentage of elution buffer and conductivity values are presented at right Y-axis. SDS gels of highlighted fractions are shown below each respective chromatography profile. Pooled fraction containing eEF2 protein are shown in pink. D. 15 % SDS gel of purified eEF2 E. DLS profile of purified eEF2 protein.

## Characterization of human eEF2.

### *SDS-PAGE*

One dimensional SDS PAGE was used to evaluate the purity of the protein. Classic Tris-Glycine buffer was used to perform the experiments (Laemmli, 1970). The optimal amount of protein to load was 8 µg, which showed exact position of the protein compared to ladder. Overloads wells with 80 µg, revealed the presence of some impurities in the sample.

Purified eEF2 corresponded to the position around 100 kDa and the contamination and degradation of the protein visually were very minor, less than 5% (Figure 35 D).

### *Dynamic light scattering (DLS)*

DLS is the technique that can be used to determine the size distribution profile of proteins in solution (Berne and Pecora, 2000). This technique is very useful for detecting the aggregation of proteins. A light is passed through the sample, all the molecules scatter photons and scattering is detected. Small particles (single proteins) move very fast in solution and scatter in different directions within very short period of time, big particles (aggregates) move in solution slower and scattering does not change quickly. Observing this difference in scattering of the level of sample we may estimate the dispersity.

Measurements were performed using DynaPro NanoStar instrument (Wyatt Tech. Corp.) with following parameters: acquisition time – 7 sec, Number of acquisitions – 10, temperature – 25 °C. The data was analysed by Dynamics V7 software (Wyatt Tech. Corp.). DLS results revealed that percentage of polydispersity was very low; 99.7% of the eEF2 protein was in monomer form, while the remained was aggregated. The hydrodynamic radius estimated to be around 5 nm. The molecular mass was estimated to be around 80 kDa (95.3 kDa theoretical) which is acceptable for this method, taking in account that the DLS technique is calculating molecular weight by averaging measurements of hydrodynamic radius of the molecules; hence for elongated proteins as eEF2 this calculation won't be absolutely reliable. Distribution of the molecules in the solution measured by DLS is shown in Figure 35 E.

### *Multi-angle laser light scattering (MALLS)*

Size exclusion chromatography (SEC) column coupled with MALLS is a powerful technique to

determine molecular weight and homogeneity of a sample. A SEC column is connected with a refractive index measuring device and a lights scattering detector. When light passes through the fractions from the column, it is scattered depending on the interaction with the molecules. The intensity of light scattered is measured which determines the molar mass of protein. The eEF2 sample was analysed using Superdex 200 10/300 column connected with Dawn a DSP detector (Wyatt Tech. Corp.).

The system was operated at 20 °C, protein was eluted in the storage buffer with a flow rate of 0.5 ml/min. During the experiment molecular mass of the eEF2 was estimated more carefully and resulted in 91.1 kDa  $\pm$  0.1%, and the hydrodynamic radius was estimated to be 3.5 nm  $\pm$  10%. A single peak in SEC indicated presence of only monomer form of the protein (Figure 36).

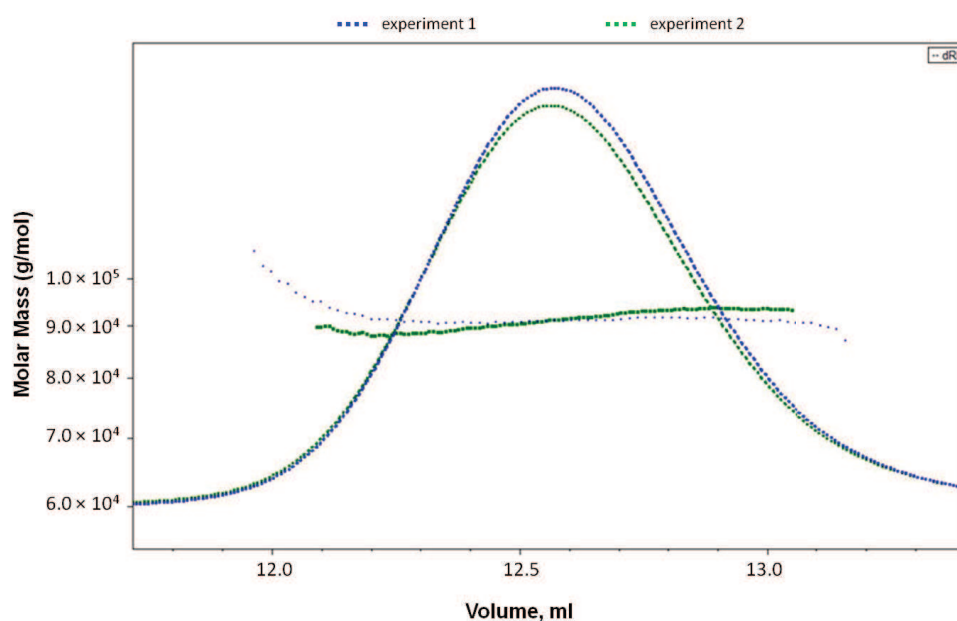


**Figure 36.** MALLS profiles of two independent experiments. Peak: refractive index recorded; horizontal lines: averaged MW estimation from different scattering angles.

### *Mass spectrometry*

Characterization of the protein by mass spectrometry was performed using MALDI and LC MS/MS analysis. All experiments were performed by Lauriane Kuhg, Johana Chicher and Phillippe Hammann at the proteomic platform at IBMC (Institut de Biologie Moléculaire et Cellulaire), Strasbourg, France. The major band from the SDS PAGE corresponding to the size of eEF2 was cut from the gel for analysis. Protein search was performed using HUMANunipro20121009 (HUMANuniprot\_20121009.fasta) protein database. The MALDI analysis identified the presence of the only human protein, eEF2 with a score of 154 and only 60 % sequence coverage. The molecular weight was determined as 95.2 kDa. In turn, LC MS/MS method estimated the majority of eEF2

protein with meta-score 15272 and 96.6 % sequence coverage. Molecular weight was determined to be 95.3 kDa. Traces of other human proteins were observed by LC MS/MS method. Estimated molecular weight of the proteins strongly corresponds to its theoretical value.

**Table 6.** Mass spectrometry results of eEF2 protein sample

Protein	Score	Covarage, %	MW [kDa]	Calc. pI
<b>MALDI results</b>				
Elongation factor 2 (Homo sapiens)	154	60	95.2	6.41
<b>LC MS/MS results</b>				
Elongation factor 2 (Homo sapiens )	15272.3	96.6	95.3	6.4
Gelsolin (Homo sapiens)	3883.8	63.6	81.4	5.5
Ribonucleoside-diphosphate reductase large subunit (Homo sapiens)	1712.9	46.5	90	6.9
Peptidyl-prolyl cis-trans isomerase FKBP4 (Homo sapiens)	936.8	38.3	51.8	5.2
Ribosomal protein S6 kinase alpha-3 (Homo sapiens)	41.5	1.5	80.5	6.7

## Crystallization of human eEF2.

To get crystals of human eEF2, two strategies were chosen. First, we searched for crystallization conditions similar to that published for yeast eEF2, 0.1 M Hepes pH 7.2, 5% EG, 3 mM DTT, 0.9 mM NaN<sub>3</sub>, 7 – 9% PEG 8000 (Jørgensen et al., 2002). Second, we searched for new crystallization conditions using all commercial screens from SIGMA, Hampton Research, Molecular dimensions, Quiagen: "Classics", "Protein complex", "Nucleix", "MPD", "JCSG+", "PEGs", "PEG ion pH", "Index", "Anions", "Cations", "Salt RX", "Wizard I" and "Wizard II" available at the IGBMC crystallization facility. Crystallization experiments were conducted at 20 °C, 100 nl of protein in buffer III were mixed with 100 nl of reservoir solution in MRC 2drop plates using the Mosquito robot.

Crystals appeared in several drops within a PEG ion pH commercial screen in wells containing Na<sub>2</sub>SO<sub>4</sub>, Na-citrate, bis-Tris propane pH 6.5 – 7.5 and 20% PEG 3350 (Figure 37 A). Needle-like crystals appeared in 6 hours and grew during the next 36 – 48 hours until they reached a maximum length of 30 µm. The same crystals appeared when hand-made solutions were used instead of commercial ones. Several optimization steps were performed, including: adjustment of concentrations of salt and precipitant, pH, temperature, a range of different additive compounds, varying drop volume, and introduction of seeding were performed. The best crystals were obtained in a 400 nl drop with 220 mM Na<sub>2</sub>SO<sub>4</sub>, 100 mM bis-Tris propane pH 7.0, 17.5% PEG 3350 with 1% 1,1,1,3,3,3-hexafluoro-2-propanol (Figure 37 D) or without it (Figure 37 C).

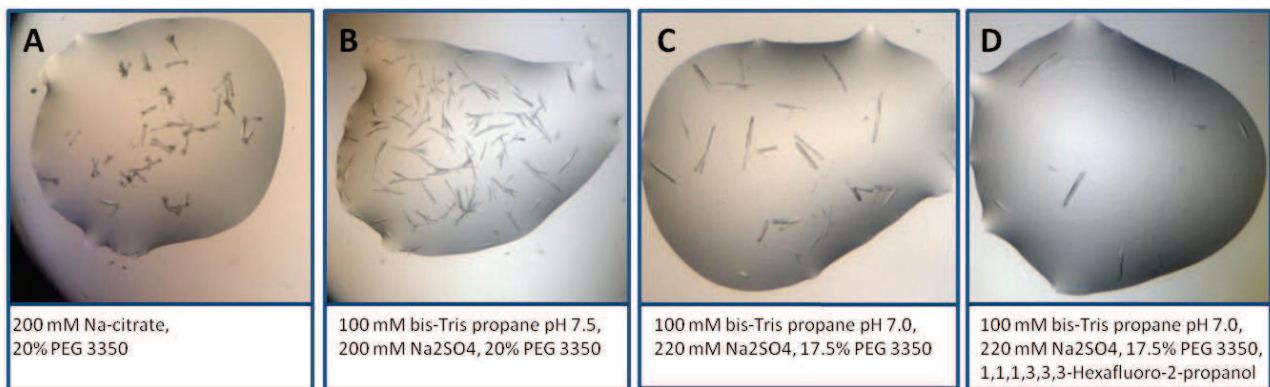


**Figure 37.** Crystals of eEF2 protein obtained by robotic screening.

Increasing the drop volume up to 1  $\mu$ l did not increase the size of crystals as expected. Micro-seeding technique gave the same crystals as before, sometimes even poorer, suggesting that if used, this method should be carefully optimized. Nevertheless, crystals obtained were large enough (100  $\mu$ m needles) to perform preliminary diffraction experiment.

## Diffraction experiment

The crystals were tested at PXI – X06SA beamline, at Swiss Light Source synchrotron by direct exposure of the crystallization plate to the x-rays. Rather poor diffraction pattern confirmed that it was not a salt crystal. The highest resolution spot was visible at the area around 30  $\text{\AA}$ . (Figure 38).

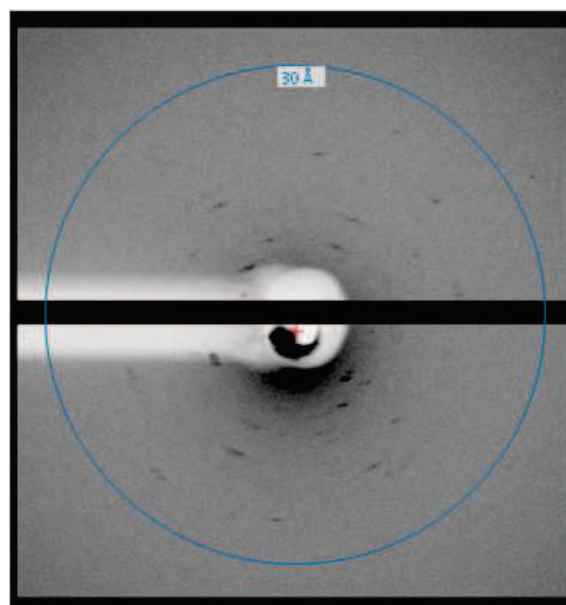


**Figure 38.** Diffraction pattern of eEF2 crystals in MRC 2drop crystallization plate.

## Cloning of human eEF2

Further optimization of crystallization of eEF2 was impossible due to the lack of material. Purification of the native protein required many human cells, which are expensive. We therefore decided to clone and express the protein heterologously. Initially, as it offers the easiest, cheapest and fastest expression system, *E. coli* was selected.

The plasmid pET-15b (His-tag, trombin cleavage site, ampicillin resistance, IPTG inducible) was chosen as expression vector. A human cDNA library was used as a template for amplification of eEF2 coding sequence. eEF2 cDNA is about 2.5 kb long can present difficulties. Therefore, two different strategies were used to clone the protein (Figure 39):

1. Amplification of the full fragment with following full gene ligation into the expression vector;

2a. Amplification of two halves of the gene separately with following fusion of two pcr fragments to reconstruct the full gene and then, ligation full gene into the expression vector;

2b. Amplification of two halves of the gene with following triple ligation into the expression vector.

### *Gene amplification*

Full gene coding human eEF2 or its fragments were amplified by the Polymerase Chain Reaction (PCR), using HeLa cDNA library incorporated into bacteriophage and proper DNA oligonucleotide primers (Figure 39). Primers were designed using Serial Cloner 2.6 software (© Franck Perez) with 20 – 25 nucleotides flanking the gene and six nucleotides of specific restriction sites linked with two or three nucleotide linkers. Table 7 lists the primers used in this study.

**Table 7.** Primers used for amplification of human eEF2. Restriction sites are highlighted in red, linkers are highlighted in blue.

Name	Sequence, 5' – 3'	Fragment length
F1	GCGC <b>CATATG</b> <b>GGA</b> ATGGTGAACCTCACGGTAGA	1.1 kb
R1	GGCAGGTCAGCCGGGTTCTTGG	
F2	GCGTCAGCCCTGTTGTCAGAGTGG	1.5 kb
R2	GCGC <b>GGATCC</b> <b>TA</b> CTACAATTTGTCCAGGAAGTTG	

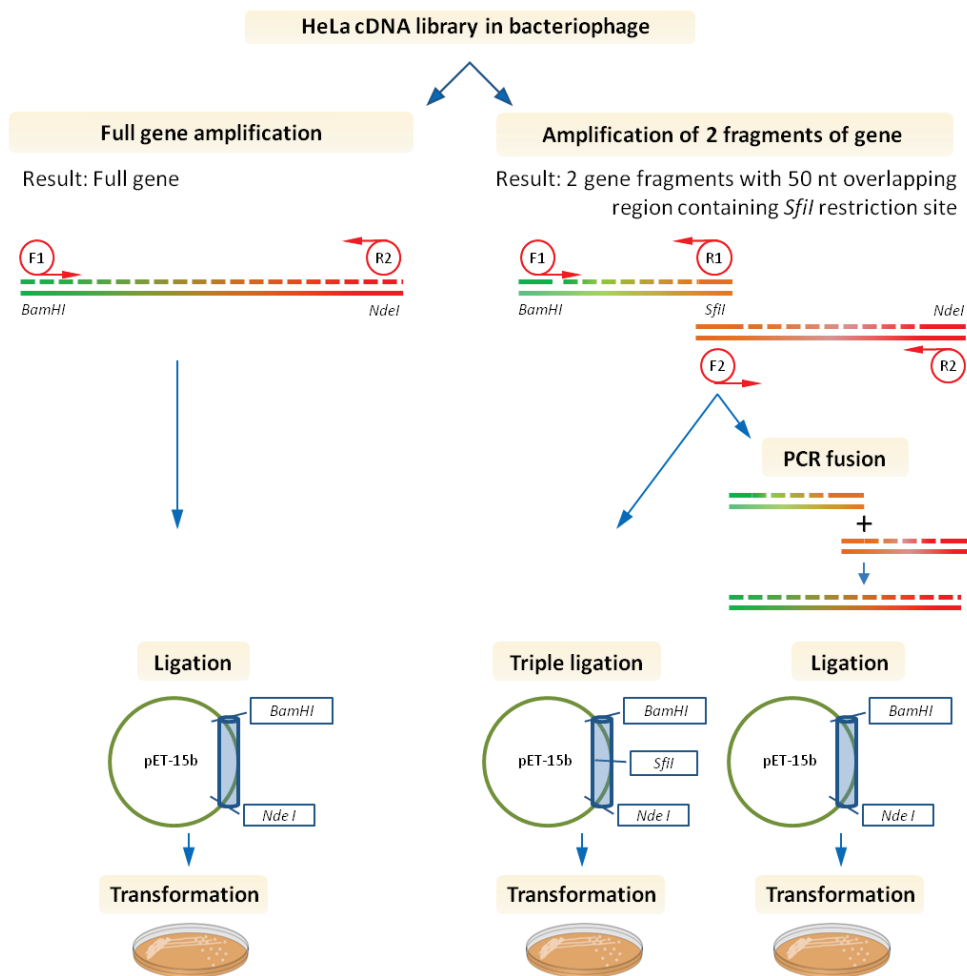


**Figure 39.** Two strategies of eEF2 cloning experiment.

PCR reactions were prepared as follows, in a final volume of 20  $\mu$ l:

- DNA: 1.5  $\mu$ l (HeLa cDNA library)
- Polymerase buffer: 2  $\mu$ l (10X)
- dNTP mix: 1  $\mu$ l (2.5 mM stock concentration)
- Primer forward: 1.25  $\mu$ l (10  $\mu$ M stock)
- Primer reverse: 1.25  $\mu$ l (10  $\mu$ M stock)
- Q5 High Fidelity Polymerase: 0.3  $\mu$ l (3.5 U/ $\mu$ l)
- Polymerase enhancer: 5  $\mu$ l
- H<sub>2</sub>O: 8  $\mu$ l

Reactions were carried out in a Thermocycler (Bio-Rad) using the following steps:

- |    |       |                     |       |
|----|-------|---------------------|-------|
| 1. | 95 °C | 2:00 minutes        | } 35X |
| 2. | 95 °C | 0:30 minutes        |       |
| 3. | 55 °C | 0:30 minutes        |       |
| 4. | 72 °C | 2:00 (3:00) minutes |       |
| 5. | 72 °C | 10:00 minutes       |       |

The temperature of annealing ( $T_A$ ; step 3) was optimized according to the melting temperature and the length of the primers. The elongation time (step 4) was optimised according to the length amplification fragment since the High Fidelity polymerase can synthesise  $\sim$ 1000 nt per minute. All

PCR products were analysed by using a 1% agarose gel (Figure 40 B) prepared in 1X TAE solution (40 mM Tris, 20 mM acetic acid, 1 mM EDTA pH 8.0). Amplification of the full gene of eEF2 straight from the cDNA library failed. Only a very faint band was visible at the position corresponding to 2.6 kb, which is the size of full gene of eEF2. Some methods of pcr optimization such as varying the time and temperature of elongation step of PCR, varying the primer constructs, and changing the polymerases used were tried. Unfortunately, none of them provided full-length gene amplification. Therefore, the work was continued using two small fragments only, which could be successfully amplified. After confirmation of the presence of PCR products with expected size, they were purified using NucleoSpin® Gel and PCR Clean-up kit (Machery Nagel).

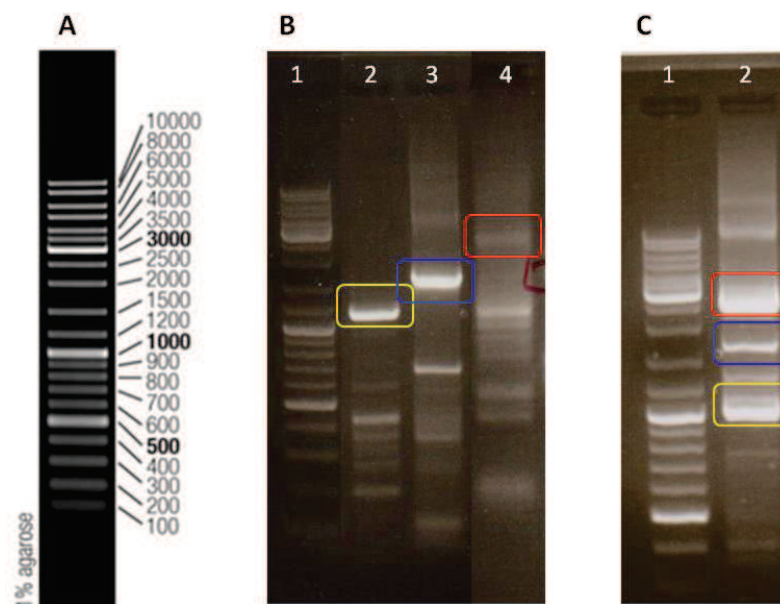


**Figure 40.** Agarose gel of amplified fragments of eEF2 DNA. **A.** DNA ladder #0331. **B.** Amplification of eEF2 from cDNA library 1 – DNA Ladder, 2 – amplification of small fragment of eEF2 gene, 3 – amplification of big fragment of eEF2 gene 4 – amplification of full eEF2 gene. **C.** Result of PCR fusion reaction. 1 – DNA ladder, 2 – fragments amplified during fusion of gene fragments. The yellow selection points the fragments that correspond to 1.1 kb fragment, the blue - 1.5 kb fragment of eEF2 gene. The red selection points the position of the full gene.

### *PCR fusion*

An additional PCR reaction was performed to fuse 1.1 and 1.5 kb fragments of the gene to obtain the full-size gene. First the PCR mixture was prepared without primers and

- DNA: 2  $\mu$ l (1  $\mu$ l of each purified fragment)
- Polymerase buffer: 3  $\mu$ l (10X)
- dNTP mix: 1  $\mu$ l (2.5 mM stock concentration)
- Q5 High Fidelity Polymerase: 0.3  $\mu$ l (3.5 U/ $\mu$ l)
- Polymerase enhancer: 6  $\mu$ l
- DMSO: 1.5  $\mu$ l (100%)
- H<sub>2</sub>O: 14  $\mu$ l

The reaction was carried out in a Thermocycler (Bio-Rad) using the following protocol:

1.	95 °C	2:00 minutes	} 10X (+ 25X)
2.	95 °C	0:30 minutes	
3.	55 °C	0:30 minutes	
4.	72 °C	1:30 (3:00) minutes	
5.	72 °C	10:00 minutes	

The first 10 cycles of reaction were run without primers, to allow the two fragments to anneal to each other and be extended by polymerase. Later 1 µl of each primer (F1 and R2) was added to the reaction and 25 more cycles were done with the elongation step prolonged to 3:00 min. Agarose gel showed that sufficient amount of fragments fused to form a full-length gene (Figure 40 C).

### *Restriction reaction*

Bands corresponding to the fragments of interest were carefully cut and DNA was extracted using QIAEX II Gel extraction kit (Qiagen). Restriction of the fragments and the vector was performed in the buffers recommended by manufacturers (New England Biolabs) for particular restriction enzyme combinations. Restriction of the full gene was performed using *BamHI* and *NdeI* incubated at 37 °C for 2 hours. For triple ligation technique fragments were additionally treated with *SfiI* enzyme at 50 °C for 1.5 hours.

### *Phenol-chloroform extraction of restricted fragments*

Upon dephosphorylation of the cleaved vector, all the fragments and vector were purified using phenol-chloroform extraction method. An equal volume of phenol was added into restriction reaction mixture, vortexed vigorously and centrifuged at 10000×g / 10 min. An Equal volume of chloroform:isoamyl alcohol (24:1) mixture was added to upper layer fraction, vortexed vigorously and centrifuged at 10000×g / 10 min. Ethanol (96%, 2.5 volumes) and 0.1 volume of 3 M sodium acetate were added to the upper layer, incubated 20 min / 20 °C and centrifuged at 13000×g / 10 min. The pellet was washed with 70% ethanol and dissolved in a minimal volume of water.

### *Ligation of DNA fragments with the vector*

The eEF2 gene and vector, both carrying sticky ends, were mixed in different ratios and incubated overnight at 16 °C together with DNA-ligase buffer and enzyme. The reaction with vector alone was used as a control for possibility of self-ligation.

### *Transformation of competent cells and control digestion of the plasmid.*

The products of the ligation reactions were then used for transformation of competent *E. coli* DH5 $\alpha$  cells. For each transformation, 100  $\mu$ l of cells were incubated on ice with 10 – 20  $\mu$ l of the cloning reaction for 5 minutes. A heat shock of 45 s at 42 °C was used for relaxing the cell membrane and allowing the vector to enter. Cells were placed for 5 min on ice and then supplemented with 1 ml  $\mu$ l of 2x LB medium (2% Bacto-tryptone, 1.5% yeast extract, 2 % NaCl, pH 7.0) and incubated for 1 hr at 37 °C. All the cells were subsequently plated on LB-agar plates with the appropriate selective antibiotic (in this specific case, ampicillin at 0.1 mg/ml) to allow for selection of recombinant clones. The plates were incubated at 37 °C for at least 12 – 18 hours until single colonies became visible.

The result of transformation was quite encouraging – control plates had 50 – 200 times less colonies than experimental plates. It means that the level of self-ligation was relatively low. Several randomly picked colonies were tested for the presence of the gene of interest.

#### *Detection of the insertion of the gene*

The first method we used to check for the presence of the insert was the so called colony PCR. Single colonies were transferred to 100  $\mu$ l of liquid LB medium and grew for 2 hours at 37 °C with shaking. To check the presence of the insertion in the vector we used these cells as the DNA template for the PCR reaction with primers F1 and R1 (Table 7). After 35 cycles of amplification, the reaction mix was subjected to agarose gel analysis.

Another method we used to detect gene insertion was digestion with restriction enzymes. Single colonies were transferred to 1 ml of liquid LB medium containing 0.1 mg/ml ampicillin and grown for 14 hours at 37 °C with shaking. Plasmids were purified using NucleoSpin® Plasmid kit (Machery Nagel), treated with *Sfi*I enzyme alone or *Bam*HI + *Nde*I enzymes together. After incubation, the reaction mix was subjected to agarose gel analysis.

Unfortunately, none of the colonies showed the presence of the gene insertion (gels not shown).

## RESEARCH PROJECT 2: SUMMARY

Following results were obtained for the project of purification and crystallization of eEF2 protein:

- The protocol of purification of native eEF2 protein from HeLa cells was established.
- The purity and homogeneity of the protein was proved by different biochemical and biophysical methods proved their purity, stability and homogeneity.
- First needle-like crystals of human native eEF2 protein were obtained. Crystals were reproducible, although required some optimization.
- The diffraction analysis of these crystals at the synchrotron proved them to be protein crystals. However, the quality of the diffraction was not enough to collect the data.
- As the part of recombinant eEF2 protein production work, the coding sequence of the eEF2 gene was successfully amplified, but not yet sub-cloned into bacterial expression vector.

---

Discussion

---

## DISCUSSION

Protein biosynthesis is a fundamental process found in every living cell, and it participates in the decoding of genetic information. While this process in general is highly conserved, ribosome composition and biogenesis, and the regulation of protein synthesis have evolved many adaptations and specializations within the various domains of living organisms. For example, the Gram-positive mesophilic pathogenic bacteria *Staphylococcus aureus* has specifics of translational machinery that differ in some respects to other bacteria that are Gram-negative, thermophilic and non-pathogenic.

The ribosome of *S. aureus* is structurally different from the ribosome of Gram-negative bacteria such as *Escherichia coli* or *Thermus thermophilus*. By comparative analysis of 3D structures of these bacteria several differences were found in their rRNA organisation. Results implied the presence of short extensions in the helices of 16S and 23S rRNA (Figure 34). All these extensions are located on the periphery of the ribosome, and their exact role in translation is yet unclear. Interestingly, most of them are consistent with expansion segments of *B. subtilis* rRNA and, to some extent, with the yeast ribosome (see Figure 41). From the evolutionary standpoint, it is uncertain whether Gram-negative or Gram-positive bacteria evolved first (see for review Koch, 2003). The divergence in secondary and tertiary structure of rRNA discussed here may support the theory that Gram-positive bacteria appeared after Gram-negative forms. This conclusion is consistent with classifications of the bacteria based on the sequence of the 16S rRNA coding genes (Woese, 1987).

Another important detail observed in the *S. aureus* ribosome structure is the absence of ribosomal proteins S1 and L9. Protein S1 is the largest and the most acidic ribosomal protein, and its role is to facilitate the accommodation of mRNA on the 30S subunit during the initiation of translation in bacteria. It is present in the cell in a non-stoichiometric ratio to the ribosomes, with approximately one protein occurring per seven ribosomes (Kurland et al., 1969). Protein S1 from *E. coli* or *T. thermophilus* consists of around 550 amino acids folded into six domains, and it binds to the ribosome relatively weakly. For example, S1 was not found in the crystal structures of *T. thermophilus* ribosome (Yusupov et al., 2001), but was present in sub-stoichiometric ratio in the sample of small 30S ribosomal subunit from *T. thermophilus* which was used for crystallization (Trakhanov et al., 1987), thus the sample of 30S was intentionally purified from S1 prior crystallization (Clemons et al., 2001). Protein S1 from *S. aureus* consists of 391 amino acids folded into 4 domains and it does not bind to the ribosome. The mechanism of the interaction of the S1 protein with the ribosome in *S. aureus* remains elusive.

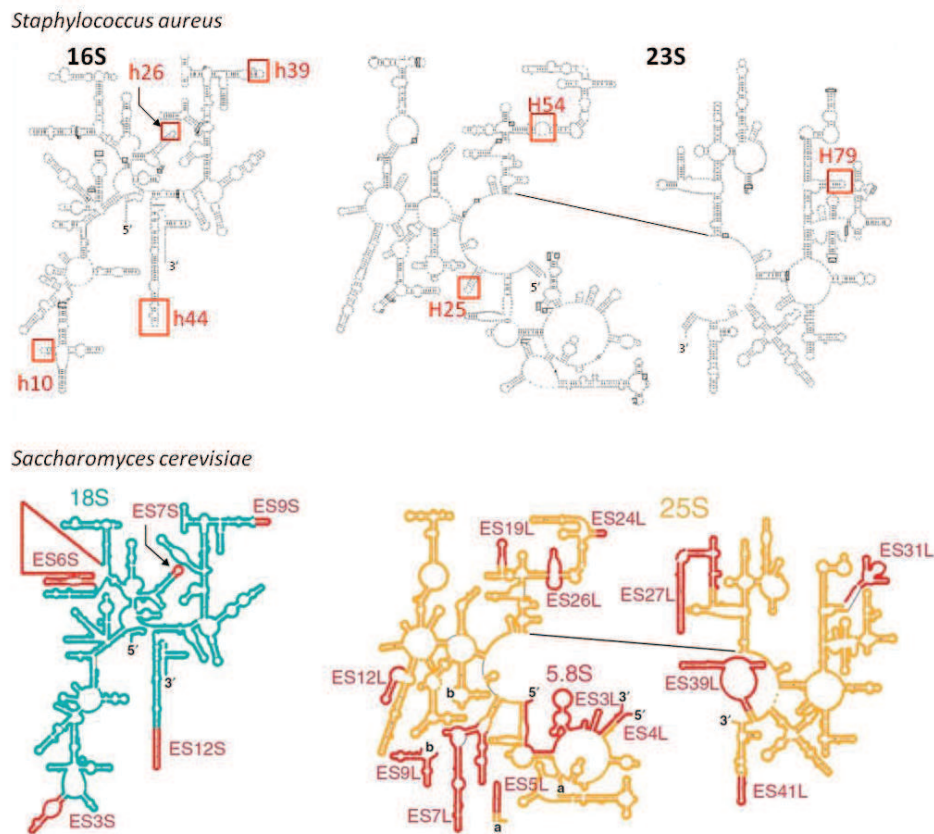


**Figure 41.** Secondary structures of *S. aureus* and *S. cerevisiae* rRNA (adapted from Jenner et al., 2012). Expansion segments are highlighted in red. Red squares indicate the expansion segments which are consistent with yeast ribosome.

Similarly, little is known about the role of protein L9 in bacterial translation. The crystal structure of this protein suggests the presence of two globular domains separated by a remarkably long  $\alpha$ -helix (Hoffman et al., 1994). Crystal structure of 70S ribosome from *T. thermophilus* demonstrated binding of L9 protein to 23S rRNA of the large ribosomal subunit at the base of the L1 stalk. Interestingly, L9 protein of one ribosome has occupied tRNA-binding sites of another ribosome, thus providing compact crystal packing (Yusupov et al., 2001). The position of the L9 protein near the neighbouring 5'-upstream ribosome in top-to-top polysomes suggests that it might contribute to inter-ribosome regulation. Protein L9 is likely to fluctuate between an extended and a compact arrangements within the ribosome, indicating that its contacts to preceding ribosome in a polysome may constrain ribosome dynamics transiently. Such transient contacts could increase with increasing temperature or other stress and thus constitute a ribosome pausing signal (Dunkle and Cate, 2011). On the other hand, ribosomal protein L9 is not essential in *E. coli* or *T. thermophilus*, yet it is conserved across bacteria.

Proteins S1 and L9 are similarly absent in the cryo-EM structure of the *B. subtilis* 70S ribosome (Sohmen et al., 2015). Based on these observations we can predict that Gram-positive bacteria will

be found to display distinctive features in the initiation steps of protein synthesis and in their polysome organization.

The resistance of a bacterium to antimicrobial compounds is based on its specialization (predator, mutualist, pathogen, etc). In pathogens, which often come to contact with antibacterial compounds, certain modifications of the ribosome (predominantly methylation of nucleotides in the antibiotic binding sites) may provide the resistance to antibiotics. Methylation is performed by specific enzymes, the methyltransferases, and these are often encoded by mobile genetic elements and therefore can be rapidly transferred from one cell to another. Our work on the structure of the ribosome from *S. aureus* aimed to provide structural information on the modifications that determine its resistance to most of commonly used ribosome-binding antibiotics. Current structure obtained by cryo-EM at 3.9 Å do not permit to distinguish modifications of rRNA, therefore further improvements in structure determination are required. Understanding the structural aspects of resistance will provide new perspectives for modifying existing or creating the new anti-staphylococcal compounds.

The natural environment of bacteria may influence the composition of the ribosomes, e.g. the G+C content of the rRNA. For most mesophilic bacteria, including *S. aureus* it is around 50%, which is relatively low in comparison with thermophilic organisms. The corresponding value for *T. thermophilus* is 64% and for *B. streathermophilus* it is 60%. A high G+C stabilizes the ribosome under extreme temperatures.

The natural habitat may also determine the ways bacteria regulate the protein synthesis. Bacteria often have to cope with various stresses; therefore, they have evolved various mechanisms of surviving under stress. These mechanisms include the formation of spores, dormant cells or persistent cells. *S. aureus* is known to form persistent cells, which are characterized by significantly decreased metabolic activity, energy consumption and sensitivity to antibiotics. Persistence is accompanied by alterations in ribosomal profile of the cells. It has been observed that when bacteria are stressed most but not all of the ribosomes form inactive dimers, also called 100S ribosomes. These 100S particles are thought to represent a protection and/or storage state, a phenomenon referred to as ribosome hibernation (Yoshida et al., 2002). Dimerization of ribosomes is reversible process which occurs upon binding of a small protein called the hibernation promoting factor (HPF). When bacteria are transferred to favourable conditions, the HPF dissociates, and the “rescued” ribosomes participate in translation. Such a defence mechanism provides a rapid response to a change in environmental conditions (reviewed in Starosta et al., 2014).

Many bacteria have been found to form ribosome dimers, although the number of proteins

involved may vary. Some bacteria (such as *E. coli*, *P. carotovorum*, *S. typhimurium* and *K. pneumonia*) express three different proteins: YfiA, RMF (ribosome modulation factor) and short HPF. Cooperative binding of RMF and short HPF proteins to the ribosomes leads to their dimerization, whereas binding of YfiA inhibits ribosome activity without dimerization. The other group of bacteria including *S. aureus*, *T. thermophilus*, *L. acidophilus* carry only one protein, long HPF. The long HPF protein combines the properties of all three proteins. It can dimerize ribosomes, thus behaving as the combination of short HPF + RMF; or, it may block translation without dimerization, thus behaving as the YfiA protein. There are no obvious criteria that delimit these two groups of bacteria. Each group includes Gram-positive and Gram-negative, thermophilic and mesophilic, pathogenic and non-pathogenic bacteria.

Recent structure of *T. thermophilus* 70S ribosome in complex with RMF and short HPF proteins from *E. coli* visualized the binding sites of two proteins and revealed conformational rearrangements of the head of 30S ribosomal subunit, which facilitate the dimerization of two ribosomes; and ribosome dimers were modelled (Polikanov et al., 2012). However, the structure of real ribosomal dimers is still missing.

Bacteria are known to form ribosome dimers upon transition to the stationary growth phase when the nutrients are limited. Unlike other bacteria, *S. aureus* was shown to keep part of its ribosomes in the dimerized form even during the exponential growth phase (Ueta et al., 2009). The peak of 100S ribosomes observed in sucrose density gradients during purification of *S. aureus* ribosomes in this study might be related to this phenomenon. Moreover, these dimers can withstand thorough pelleting through the high salt (0.5 M KCl) sucrose cushion, indicating that they have high stability and rigidity, and hence, they may be important in the physiology of *S. aureus*.

## PERSPECTIVES

The work described in this thesis was the first step in the context of future development of drugs against *Staphylococcus aureus*. Obtained structure of *S. aureus* ribosome is the first high-resolution ribosome structure from pathogenic bacteria obtained using cryo-EM. The modelling step is not performed yet, therefore it is not included in this thesis manuscript. Obtained model of *S. aureus* vacant ribosome will be used later on for solving structures of this ribosome in complex with different ligands. No structures of bacterial ribosome dimers containing long hibernation promoting factor (HPF) are known so far. One of the goal of our laboratory is to solve the structure of *S. aureus* ribosome dimers in complex with long HPF protein from *S. aureus*, also referred to as hibernating ribosomes. The structure will shed light on the organization of dimers and increase our knowledge about translation regulation in pathogenic bacteria.

All the results obtained in this work will help to describe *Staphylococcus aureus* ribosome and its functional complexes at the atomic level in the nearest future. The combination of methods of X-ray crystallography and cryo-electron microscopy will help to achieve this aim. Obtained results will provide a foundation for the development of new compounds against this pathogenic and extremely resistant bacterium.

**REFERENCES**

- Adrian, M., Dubochet, J., Lepault, J., and McDowell, A.W. (1984). Cryo-electron microscopy of viruses. *Nature* 308, 32–36.
- Agirrezabala, X., and Frank, J. (2010). From DNA to proteins via the ribosome: Structural insights into the workings of the translation machinery. *Hum. Genomics* 4, 226.
- \*\*Agirrezabala, X., Lei, J., Brunelle, J.L., Ortiz-Meoz, R.F., Green, R., and Frank, J. (2008). Visualization of the Hybrid State of tRNA Binding Promoted by Spontaneous Ratcheting of the Ribosome. *Mol. Cell* 32, 190–197.
- \*\*Agirrezabala, X., Liao, H.Y., Schreiner, E., Fu, J., Ortiz-Meoz, R.F., Schulten, K., Green, R., and Frank, J. (2012). Structural characterization of mRNA-tRNA translocation intermediates. *Proc. Natl. Acad. Sci.* 109, 6094–6099.
- Agrawal, R.K., and Sharma, M.R. (2012). Structural aspects of mitochondrial translational apparatus. *Curr. Opin. Struct. Biol.* 22, 797–803.
- Aldred, K.J., Kerns, R.J., and Osheroff, N. (2014). Mechanism of quinolone action and resistance. *Biochemistry* 53, 1565–1574.
- \*\*Amunts, A., Brown, A., Bai, X. -c., Llacer, J.L., Hussain, T., Emsley, P., Long, F., Murshudov, G., Scheres, S.H.W., and Ramakrishnan, V. (2014). Structure of the yeast mitochondrial large ribosomal subunit. *Science* (80-. ). 343, 1485–1489.
- \*\*Amunts, A., Brown, A., Toots, J., Scheres, S.H.W., and Ramakrishnan, V. (2015). The structure of the human mitochondrial ribosome. *Sci.* 348 , 95–98.
- Andriole, V.T. (2000). *The quinolones* (Academic Press).
- Anger, A.M., Armache, J.-P., Berninghausen, O., Habeck, M., Subklewe, M., Wilson, D.N., and Beckmann, R. (2013). Structures of the human and *Drosophila* 80S ribosome. *Nature* 497, 80–85.
- Armache, J.-P., Jarasch, A., Anger, A.M., Villa, E., Becker, T., Bhushan, S., Jossinet, F., Habeck, M., Dindar, G., Franckenberg, S., et al. (2010). Cryo-EM structure and rRNA model of a translating eukaryotic 80S ribosome at 5.5-Å resolution. *Proc. Natl. Acad. Sci. U. S. A.* 107, 19748–19753.
- Asherie, N. (2004). Protein crystallization and phase diagrams. *Methods* 34, 266–272.
- Bai, X.C., Fernandez, I.S., McMullan, G., and Scheres, S.H.W. (2013). Ribosome structures to near-atomic resolution from thirty thousand cryo-EM particles. *Elife* 2013.
- Baker, L.A., and Rubinstein, J.L. (2010). Radiation damage in electron cryomicroscopy.
- Ban, N. (2000). The complete atomic structure of the large ribosomal subunit at 2.4 Å



resolution. *Science* (80- ). 289, 905–920.

Baragaña, B., Hallyburton, I., Lee, M.C.S., Norcross, N.R., Grimaldi, R., Otto, T.D., Proto, W.R., Blagborough, A.M., Meister, S., and Wirjanata, G. (2015). A novel multiple-stage antimalarial agent that inhibits protein synthesis. *Nature* 522, 315–320.

Bartesaghi, A., Merk, A., Banerjee, S., Matthies, D., Wu, X., Milne, J.L.S., and Subramaniam, S. (2015). 2.2 Å resolution cryo-EM structure of  $\beta$ -galactosidase in complex with a cell-permeant inhibitor. *Sci.* 348 , 1147–1151.

Becker, K., Harmsen, D., Mellmann, A., Meier, C., Schumann, P., Peters, G., and Von Eiff, C. (2004). Development and evaluation of a quality-controlled ribosomal sequence database for 16S ribosomal DNA-based identification of *Staphylococcus* species. *J. Clin. Microbiol.* 42, 4988–4995.

\*\*Behrmann, E., Loerke, J., Budkevich, T.V., Yamamoto, K., Schmidt, A., Penczek, P.A., Vos, M.R., Bürger, J., Mielke, T., Scheerer, P., et al. (2015). structural snapshots of actively translating human ribosomes. *Cell* 161, 845–857.

Benito, Y., Kolb, F.A., Romby, P., Lina, G., Etienne, J., and Vandenesch, F. (2000). Probing the structure of RNAIII, the *Staphylococcus aureus* agr regulatory RNA, and identification of the RNA domain involved in repression of protein A expression. *RNA* 6, 668–679.

Ben-Shem, A., Garreau de Loubresse, N., Melnikov, S., Jenner, L., Yusupova, G., and Yusupov, M. (2011). The Structure of the Eukaryotic Ribosome at 3.0 Å Resolution. *Science* (80- ). 334, 1524–1529.

Bera, A., Herbert, S., Jakob, A., Vollmer, W., and Götz, F. (2005). Why are pathogenic staphylococci so lysozyme resistant? The peptidoglycan O-acetyltransferase OatA is the major determinant for lysozyme resistance of *Staphylococcus aureus*. *Mol. Microbiol.* 55, 778–787.

Berne, B.J., and Pecora, R. (2000). *Dynamic light scattering: with applications to chemistry, biology, and physics* (Courier Corporation).

Binshtein, E., and Ohi, M.D. (2015). Cryo-electron microscopy and the amazing race to atomic resolution. *biochemistry* 54, 3133–3141.

\*Blaha, G., Stanley, R.E., and Steitz, T.A. (2009). Formation of the first peptide bond: the structure of EF-P bound to the 70S ribosome. *Science* 325, 966–970.

Blaha, G.M., Polikanov, Y.S., and Steitz, T.A. (2012). Elements of ribosomal drug resistance and specificity. *Curr. Opin. Struct. Biol.* 22, 750–758.

Blow, D. (2002). *Outline of crystallography for biologists* (Oxford University Press).

Blundell, T.L., Cutfield, J.F., Cutfield, S.M., Dodson, E.J., Dodson, G.G., Hodgkin, D.C., Mercola, D.A., and Vijayan, M. (1971). Atomic positions in rhombohedral 2-zinc insulin crystals. *Nature* 231,

506–511.

Bodley, J.W., Zieve, F.J., Lin, L., and Zieve, S.T. (1969). Formation of the ribosome-G factor-GDP complex in the presence of fusidic acid. *Biochem. Biophys. Res. Commun.* 37, 437–443.

Bondi, A., and Dietz, C.C. (1945). Penicillin Resistant Staphylococci. *Exp. Biol. Med.* 60 , 55–58.

Brilot, A.F., Chen, J.Z., Cheng, A., Pan, J., Harrison, S.C., Potter, C.S., Carragher, B., Henderson, R., and Grigorieff, N. (2012). Beam-induced motion of vitrified specimen on holey carbon film. *J. Struct. Biol.* 177, 630–637.

\*\*Brilot, A.F., Korostelev, A.A., Ermolenko, D.N., and Grigorieff, N. (2013). Structure of the ribosome with elongation factor G trapped in the pretranslocation state. *Proc. Natl. Acad. Sci. U. S. A.* 110, 20994–20999.

Brodersen, D.E., Clemons, W.M., Carter, A.P., Morgan-Warren, R.J., Wimberly, B.T., and Ramakrishnan, V. (2000). The structural basis for the action of the antibiotics tetracycline, pactamycin, and hygromycin B, on the 30S ribosomal subunit. *Cell* 103, 1143–1154.

Bronner, S., Monteil, H., and Prévost, G. (2004). Regulation of virulence determinants in *Staphylococcus aureus*: Complexity and applications. *FEMS Microbiol. Rev.* 28, 183–200.

\*\*Brown, A., Amunts, A., Bai, X., Sugimoto, Y., Edwards, P.C., Murshudov, G., Scheres, S.H.W., and Ramakrishnan, V. (2014). Structure of the large ribosomal subunit from human mitochondria. *Sci.* 346, 718–722.

\*\*Budkevich, T., Giesebrecht, J., Altman, R.B., Munro, J.B., Mielke, T., Nierhaus, K.H., Blanchard, S.C., and Spahn, C.M.T. (2011). Structure and dynamics of the mammalian ribosomal pretranslocation complex. *Mol. Cell* 44, 214–224.

\*\*Budkevich, T. V., Giesebrecht, J., Behrmann, E., Loerke, J., Ramrath, D.J.F., Mielke, T., Ismer, J., Hildebrand, P.W., Tung, C.S., Nierhaus, K.H., et al. (2014). Regulation of the mammalian elongation cycle by subunit rolling: A eukaryotic-specific ribosome rearrangement. *Cell* 158, 121–131.

Calvori C, Frontali L, Leoni L, T.G. (1965). Effect of rifamycin on protein synthesis. *Nature* 207, 417–418.

Campbell, M.G., Cheng, A., Brilot, A.F., Moeller, A., Lyumkis, D., Veessler, D., Pan, J., Harrison, S.C., Potter, C.S., Carragher, B., et al. (2012). Movies of ice-embedded particles enhance resolution in electron cryo-microscopy. *Structure* 20, 1823–1828.

Cannone, J.J., Subramanian, S., Schnare, M.N., Collett, J.R., D'Souza, L.M., Du, Y., Feng, B., Lin, N., Madabusi, L. V, and Müller, K.M. (2002). The comparative RNA web (CRW) site: an online database of comparative sequence and structure information for ribosomal, intron, and other RNAs.

BMC Bioinformatics 3, 2.

Chambers, H.F. (1997). Methicillin resistance in staphylococci: molecular and biochemical basis and clinical implications. *Clin. Microbiol. Rev.* 10, 781–791.

Chan, P.F., and Foster, S.J. (1998). Role of SarA in virulence determinant production and environmental signal transduction in *Staphylococcus aureus*. *J. Bacteriol.* 180, 6232–6241.

Chayen, N.E., Stewart, P.D.S., and Blow, D.M. (1992). Microbatch crystallization under oil—a new technique allowing many small-volume crystallization trials. *J. Cryst. Growth* 122, 176–180.

Chen, C.M., and Behringer, R.R. (2004). *Ovca1* regulates cell proliferation, embryonic development, and tumorigenesis. *Genes Dev.* 18, 320–332.

Chen, J.Y.C., and Bodley, J.W. (1988). Biosynthesis of diphthamide in *Saccharomyces cerevisiae*. Partial purification and characterization of a specific S-adenosylmethionine:elongation factor 2 methyltransferase. *J. Biol. Chem.* 263, 11692–11696.

Chen, C., Tang, J., Dong, W., Wang, C., Feng, Y., Wang, J., Zheng, F., Pan, X., Liu, D., Li, M., et al. (2007). A glimpse of streptococcal toxic shock syndrome from comparative genomics of *S. suis* 2 chinese isolates. *PLoS One* 2, e315.

Chen, Y., Feng, S., Kumar, V., Ero, R., and Gao, Y.-G. (2013). Structure of EF-G-ribosome complex in a pretranslocation state. *Nat. Struct. Mol. Biol.* 20, 1077–1084.

Cheng, Y., Grigorieff, N., Penczek, P.A., and Walz, T. (2015). A primer to single-particle cryo-electron microscopy. *Cell* 161, 438–449.

Cheung, A.L., Koomey, J.M., Butler, C.A., Projan, S.J., and Fischetti, V.A. (1992). Regulation of exoprotein expression in *Staphylococcus aureus* by a locus (*sar*) distinct from *agr*. *Proc. Natl. Acad. Sci. U. S. A.* 89, 6462–6466.

Cheung, A.L., Eberhardt, K.J., Chung, E., Yeaman, M.R., Sullam, P.M., Ramos, M., and Bayer, A.S. (1994). Diminished virulence of a *sar-lagr-* mutant of *Staphylococcus aureus* in the rabbit model of endocarditis. *J. Clin. Invest.* 94, 1815–1822.

Chevalier, C. (2009). Function and mechanism of action of RNAIII and new ncRNAs in *Staphylococcus aureus* (Doctoral thesis, University of Strasbourg, Strasbourg, France). Retrieved from: <http://scd-theses.u-strasbg.fr/1714/>

Cimolai, N. (2008). MRSA and the environment: Implications for comprehensive control measures. *Eur. J. Clin. Microbiol. Infect. Dis.* 27, 481–493.

Clemons, W.M., Brodersen, D.E., McCutcheon, J.P., May, J.L.C., Carter, A.P., Morgan-Warren, R.J., Wimberly, B.T., and Ramakrishnan, V. (2001). Crystal structure of the 30 S ribosomal subunit from *Thermus thermophilus*: purification, crystallization and structure determination. *J. Mol. Biol.*



310, 827–843.

Cole, A.M., Tahk, S., Oren, A., Yoshioka, D., Kim, Y.H., Park, A., and Ganz, T. (2001). Determinants of *Staphylococcus aureus* nasal carriage. *Clin. Diagn. Lab. Immunol.* 8, 1064–1069.

\*Colussi, T.M., Costantino, D.A., Zhu, J., Donohue, J.P., Korostelev, A.A., Jaafar, Z.A., Plank, T.-D.M., Noller, H.F., and Kieft, J.S. (2015). Initiation of translation in bacteria by a structured eukaryotic IRES RNA. *Nature* 519, 110–113.

Cosgrove, S.E., Sakoulas, G., Perencevich, E.N., Schwaber, M.J., Karchmer, A.W., and Carmeli, Y. (2003). Comparison of mortality associated with methicillin-resistant and methicillin-susceptible *Staphylococcus aureus* bacteremia: a meta-analysis. *Clin. Infect. Dis.* 36, 53–59.

Crossley, K.B., Archer, G., Jefferson, K., and Fowler, V. (2009). *Staphylococci in human disease* (Wiley Online Library).

Crowfoot, D., Bunn, C.W., Rogers-Low, B.W., and Turner-Jones, A. (1949). *The chemistry of penicillin*. Princet. Univ. Press, New Jersey.

Cruz, J.W., Rothenbacher, F.P., Maehigashi, T., Lane, W.S., Dunham, C.M., and Woychik, N.A. (2014). Doc toxin is a kinase that inactivates elongation factor Tu. *J. Biol. Chem.* 289, 7788–7798.

Czworkowski, J., Wang, J., Steitz, T.A., and Moore, P.B. (1994). The crystal structure of elongation factor G complexed with GDP, at 2.7 Å resolution. *EMBO J.* 13, 3661–3668.

D’Arcy, A., Elmore, C., Stihle, M., and Johnston, J.E. (1996). A novel approach to crystallising proteins under oil. *J. Cryst. Growth* 168, 175–180.

David, M.D., Kearns, A.M., Gossain, S., Ganner, M., and Holmes, A. (2006). Community-associated methicillin-resistant *Staphylococcus aureus*: nosocomial transmission in a neonatal unit.

\*Demeshkina, N., Jenner, L., Westhof, E., Yusupov, M., and Yusupova, G. (2012). A new understanding of the decoding principle on the ribosome. *Nature* 484, 256–259.

Deora, R., and Misra, T.K. (1996). Characterization of the primary sigma factor of *Staphylococcus aureus*. *J Biol Chem* 271, 21828–21834.

Deora, R., Tseng, T., and Misra, T.K. (1997). Alternative transcription factor sigma<sup>SB</sup> of *Staphylococcus aureus*: characterization and role in transcription of the global regulatory locus *sar*. *J. Bacteriol.* 179, 6355–6359.

Dubochet, J., Lepault, J., Freeman, R., Berriman, J.A., and Homo, J.-C. (1982). Electron microscopy of frozen water and aqueous solutions. *J. Microsc.* 128, 219–237.

Dunkle, J., and Cate, J.D. (2011). The packing of ribosomes in crystals and polysomes. In *Ribosomes SE - 6*, M. Rodnina, W. Wintermeyer, and R. Green, eds. (Springer Vienna), pp. 65–73.

Eisenstein, B.E. (2008). Treatment challenges in the management of complicated skin and soft-

tissue infections. In *Clinical Microbiology and Infection*, pp. 17–25.

Faruqi, A.R., and McMullan, G. (2011). Electronic detectors for electron microscopy. *Q. Rev. Biophys.* 44, 357–390.

\*\*Fernández, I.S., Bai, X.-C., Hussain, T., Kelley, A.C., Lorsch, J.R., Ramakrishnan, V., and Scheres, S.H.W. (2013). Molecular architecture of a eukaryotic translational initiation complex. *Science* 342, 1240585.

\*\*Fernández, I.S., Bai, X.C., Murshudov, G., Scheres, S.H.W., and Ramakrishnan, V. (2014). Initiation of translation by cricket paralysis virus IRES requires its translocation in the ribosome. *Cell* 157, 823–831.

Fiaux, J., Bertelsen, E.B., Horwich, A.L., and Wüthrich, K. (2002). NMR analysis of a 900K GroEL GroES complex. *Nature* 418, 207–211.

Fischer, N., Neumann, P., Konevega, A.L., Bock, L. V, Ficner, R., Rodnina, M. V, and Stark, H. (2015). Structure of the E. coli ribosome-EF-Tu complex at <3 Å resolution by Cs-corrected cryo-EM. *Nature* 520, 567–570.

Fleming, A. (1929). On the Antibacterial Action of Cultures of a *Penicillium*, with Special Reference to their Use in the Isolation of *B. influenzae*. *Br. J. Exp. Pathol.* 10, 226–236.

Foster, T., O'Reilly, M., and Bramley, A.J. (1990). Genetic studies of *Staphylococcus aureus* virulence factors. in *pathogenesis of wound and biomaterial-associated infections* SE - 4, T. Wadström, I. Eliasson, I. Holder, and Å. Ljungh, eds. (Springer London), pp. 35–46.

Frank, J. (2006). *Three-dimensional electron microscopy of macromolecular assemblies: visualization of biological molecules in their native state* (Oxford University Press).

Fridkin, S.K., Hageman, J.C., Morrison, M., Sanza, L.T., Como-Sabetti, K., Jernigan, J.A., Harriman, K., Harrison, L.H., Lynfield, R., and Farley, M.M. (2005). Methicillin-resistant *Staphylococcus aureus* disease in three communities. *N. Engl. J. Med.* 352, 1436–1444.

Gabashvili, I.S., Agrawal, R.K., Spahn, C.M., Grassucci, R.A., Svergun, D.I., Frank, J., and Penczek, P. (2000). Solution structure of the E. coli 70S ribosome at 11.5 Å resolution. *Cell* 100, 537–549.

\*Gagnon, M.G., Seetharaman, S. V., Bulkley, D., and Steitz, T.A. (2012). structural basis for the rescue of stalled ribosomes: structure of YaeJ bound to the ribosome. *Science* (80- ). 335, 1370–1372.

\*Gagnon, M.G., Lin, J., Bulkley, D., and Steitz, T. a. (2014). Crystal structure of elongation factor 4 bound to a clockwise ratcheted ribosome. *Science* (80- ). 345, 684–687.

Gao, Y.-G., Selmer, M., Dunham, C.M., Weixlbaumer, A., Kelley, A.C., and Ramakrishnan, V.

(2009). The structure of the ribosome with elongation factor G trapped in the posttranslocational state. *Science* 326, 694–699.

García-Ruiz, J.M. (2003). Counterdiffusion methods for macromolecular crystallization. *Methods Enzymol.* 368, 130–154.

Garman, E.F., and Schneider, T.R. (1997). Macromolecular Cryocrystallography. *J. Appl. Crystallogr.* 30, 211–237.

Garreau de Loubresse, N., Prokhorova, I., Holtkamp, W., Rodnina, M. V, Yusupova, G., and Yusupov, M. (2014). Structural basis for the inhibition of the eukaryotic ribosome. *Nature* 513, 517–522.

\*\*des Georges, A., Hashem, Y., Unbehaun, A., Grassucci, R.A., Taylor, D., Hellen, C.U.T., Pestova, T. V., and Frank, J. (2014). Structure of the mammalian ribosomal pre-termination complex associated with eRF1•eRF3•GDPNP. *Nucleic Acids Res.* 42, 3409–3418.

Gertz, S., Engelmann, S., Schmid, R., Ziebandt, A.K., Tischer, K., Scharf, C., Hacker, J., and Hecker, M. (2000). Characterization of the sigma(B) regulon in *Staphylococcus aureus*. *J. Bacteriol.* 182, 6983–6991.

Ghuysen, J.M. (1994). Molecular structures of penicillin-binding proteins and beta-lactamases. *Trends Microbiol.* 2, 372–380.

Giraud, A.T., Raspanti, C.G., Calzolari, A., and Nagel, R. (1994). Characterization of a Tn551-mutant of *Staphylococcus aureus* defective in the production of several exoproteins. *Can. J. Microbiol.* 40, 677–681.

Giraud, A.T., Cheung, A.L., and Nagel, R. (1997). The sae locus of *Staphylococcus aureus* controls exoprotein synthesis at the transcriptional level. *Arch. Microbiol.* 168, 53–58.

Glaeser, R.M., Typke, D., Tiemeijer, P.C., Pulokas, J., and Cheng, A. (2011). Precise beam-tilt alignment and collimation are required to minimize the phase error associated with coma in high-resolution cryo-EM. *J. Struct. Biol.* 174, 1–10.

Gogia, Z. V, Yusupov, M.M., and Spirina, T.N. (1986). Structure of *Thermus thermophilus* ribosomes. I. Method of isolation and purification of ribosomes. *MOL. BIOL.(MOSCOW)*. 20, 519–526.

Goldstein, B.P. (2014). Resistance to rifampicin: a review. *J Antibiot* 67, 625–630.

Gourse, R.L., Gaal, T., Bartlett, M.S., Appleman, J.A., and Ross, W. (1996). rRNA transcription and growth rate-dependent regulation of ribosome synthesis in *Escherichia coli*. *Annu. Rev. Microbiol.* 50, 645–677.

Greber, B.J., Boehringer, D., Leibundgut, M., Bieri, P., Leitner, A., Schmitz, N., Aebersold, R.,

and Ban, N. (2014). The complete structure of the large subunit of the mammalian mitochondrial ribosome. *Nature advance on*.

Greber, B.J., Bieri, P., Leibundgut, M., Leitner, A., Aebersold, R., Boehringer, D., and Ban, N. (2015). The complete structure of the 55S mammalian mitochondrial ribosome. *Sci.* 348, 303–308.

\*Guo, Z., and Noller, H.F. (2012). Rotation of the head of the 30S ribosomal subunit during mRNA translocation. *Proc. Natl. Acad. Sci. U. S. A.* 109, 20391–20394.

Hapke, B., and Noll, H. (1976). Structural dynamics of bacterial ribosomes: IV. Classification of ribosomes by subunit interaction. *J. Mol. Biol.* 105, 97–109.

Hardy, S.J.S., Kurland, C.G., Voynow, P., and Mora, G. (1969). Ribosomal proteins of *Escherichia coli*. I. Purification of the 30 S ribosomal proteins. *Biochemistry* 8, 2897–2905.

Harms, J., Schlutzen, F., Zarivach, R., Bashan, A., Gat, S., Agmon, I., Bartels, H., Franceschi, F., and Yonath, A. (2001). High resolution structure of the large ribosomal subunit from a mesophilic eubacterium. *Cell* 107, 679–688.

Harris, L.G., Foster, S.J., Richards, R.G., Lambert, P., Stickler, D., and Eley, A. (2002). An introduction to *Staphylococcus aureus*, and techniques for identifying and quantifying *S. aureus* adhesins in relation to adhesion to biomaterials: Review. *Eur. Cells Mater.* 4, 39–60.

Hartman, B.J., and Tomasz, A. (1984). Low-affinity penicillin-binding protein associated with beta-lactam resistance in *Staphylococcus aureus*. *J. Bacteriol.* 158, 513–516.

Hartmann G, Honikel KO, Knüsel F, N.J. (1967). The specific inhibition of the DNA-directed RNA synthesis by rifamycin. *Biochim Biophys Acta* 145, 843–844.

\*\*Hashem, Y., Des Georges, A., Dhote, V., Langlois, R., Liao, H.Y., Grassucci, R.A., Hellen, C.U.T., Pestova, T. V., and Frank, J. (2013a). XStructure of the mammalian ribosomal 43S preinitiation complex bound to the scanning factor DHX29. *Cell* 153.

\*\*Hashem, Y., des Georges, A., Dhote, V., Langlois, R., Liao, H.Y., Grassucci, R. a, Pestova, T. V, Hellen, C.U.T., and Frank, J. (2013b). Hepatitis-C-virus-like internal ribosome entry sites displace eIF3 to gain access to the 40S subunit. *Nature* 503, 539–543.

\*\*Hashem, Y., des Georges, A., Fu, J., Buss, S.N., Jossinet, F., Jobe, A., Zhang, Q., Liao, H.Y., Grassucci, R. a, Bajaj, C., et al. (2013c). High-resolution cryo-electron microscopy structure of the *Trypanosoma brucei* ribosome. *Nature* 494, 385–389.

Van Heel, M., Gowen, B., Matadeen, R., Orlova, E. V, Finn, R., Pape, T., Cohen, D., Stark, H., Schmidt, R., Schatz, M., et al. (2000). Single-particle electron cryo-microscopy: towards atomic resolution. *Q. Rev. Biophys.* 33, 307–369.

Heras, B., and Martin, J.L. (2005). Post-crystallization treatments for improving diffraction



quality of protein crystals. *Acta Crystallogr. Sect. D Biol. Crystallogr.* 61, 1173–1180.

Hermann, T. (2005). Drugs targeting the ribosome. *Curr. Opin. Struct. Biol.* 15, 355–366.

Hodgkin, D.C. (1949). The X-ray analysis of the structure of penicillin. *Adv. Sci.* 6, 85–89.

Hodgkin DC, Kamper J, Mackay M, Pickworth J, Trueblood KN, W.J. (1956). Structure of vitamin B12. *Nature* 178, 64–66.

Hoffman, D.W., Davies, C., Gerchman, S.E., Kycia, J.H., Porter, S.J., White, S.W., and Ramakrishnan, V. (1994). Crystal structure of prokaryotic ribosomal protein L9: a bi-lobed RNA-binding protein. *EMBO J.* 13, 205.

Honjo, T., Nishizuka, Y., and Hayaishi, O. (1968). Diphtheria toxin-dependent adenosine diphosphate ribosylation of aminoacyl transferase II and inhibition of protein synthesis. *J. Biol. Chem.* 243, 3553–3555.

Hooper, D.C. (1999). Mode of action of fluoroquinolones. In *Drugs*, pp. 6–10.

Horsburgh, M.J., Aish, J.L., White, I.J., Shaw, L., Lithgow, J.K., and Foster, S.J. (2002). *??b* modulates virulence determinant expression and stress resistance: Characterization of a functional *rsbU* strain derived from *Staphylococcus aureus* 8325-4. *J. Bacteriol.* 184, 5457–5467.

\*\*Hussain, T., Ll acer, J.L., Fern andez, I.S., Munoz, A., Martin-Marcos, P., Savva, C.G., Lorsch, J.R., Hinnebusch, A.G., and Ramakrishnan, V. (2015). Structural changes enable start codon recognition by the eukaryotic translation initiation complex. *Cell* 159, 597–607.

Infante, A.A., and Baierlein, R. (1971). Pressure-induced dissociation of sedimenting ribosomes: effect on sedimentation patterns. *Proc. Natl. Acad. Sci.* 68, 1780–1785.

Ito, K., Fujiwara, T., Toyoda, T., and Nakamura, Y. (2002). Elongation factor G participates in ribosome disassembly by interacting with ribosome recycling factor at their tRNA-mimicry domains. *Mol. Cell* 9, 1263–1272.

Jacoby, G.A., and Munoz-Price, L.S. (2005). The new beta-lactamases. *N. Engl. J. Med.* 352, 380–391.

Janzon, L., and Arvidson, S. (1990). The role of the delta-lysin gene (*hld*) in the regulation of virulence genes by the accessory gene regulator (*agr*) in *Staphylococcus aureus*. *EMBO J.* 9, 1391.

\*Jenner, L., Demeshkina, N., Yusupova, G., and Yusupov, M. (2010a). Structural aspects of messenger RNA reading frame maintenance by the ribosome. *Nat. Struct. Mol. Biol.* 17, 555–560.

\*Jenner, L., Demeshkina, N., Yusupova, G., and Yusupov, M. (2010b). Structural rearrangements of the ribosome at the tRNA proofreading step. *Nat. Struct. Mol. Biol.* 17, 1072–1078.

Jenner, L., Melnikov, S., de Loubresse, N.G., Ben-Shem, A., Iskakova, M., Urzhumtsev, A.,



Meskauskas, A., Dinman, J., Yusupova, G., and Yusupov, M. (2012). Crystal structure of the 80S yeast ribosome. *Curr. Opin. Struct. Biol.* 22, 759–767.

Jin, T., Bokarewa, M., Foster, T., Mitchell, J., Higgins, J., and Tarkowski, A. (2004). *Staphylococcus aureus* resists human defensins by production of staphylokinase, a novel bacterial evasion mechanism. *J. Immunol.* 172, 1169–1176.

Johanson, U., Aevansson, A., Liljas, A., and Hughes, D. (1996). The dynamic structure of EF-G studied by fusidic acid resistance and internal revertants. *J. Mol. Biol.* 258, 420–432.

Johnson, M.D., and Decker, C.F. (2008). Antimicrobial agents in treatment of MRSA infections. *Disease-a-Month* 54, 793–800.

Jorgensen, R., Carr-Schmid, A., Ortiz, P.A., Kinzy, T.G., and Andersen, G.R. (2002). Purification and crystallization of the yeast elongation factor eEF2. *Acta Crystallogr. Sect. D Biol. Crystallogr.* 58, 712–715.

Jørgensen, R., Ortiz, P.A., Carr-Schmid, A., Nissen, P., Kinzy, T.G., and Andersen, G.R. (2003). Two crystal structures demonstrate large conformational changes in the eukaryotic ribosomal translocase. *Nat. Struct. Biol.* 10, 379–385.

Jørgensen, R., Merrill, A.R., Yates, S.P., Marquez, V.E., Schwan, A.L., Boesen, T., and Andersen, G.R. (2005). Exotoxin A-eEF2 complex structure indicates ADP ribosylation by ribosome mimicry. *Nature* 436, 979–984.

Junecko JM, Zielinska AK, Mrak LN, Ryan DC, Graham JW, Smeltzer MS, L.C. (2012). Transcribing virulence in *Staphylococcus aureus*. *World J Clin Infect Dis* 2, 63–76.

Kaliner, M.A. (1991). Human nasal respiratory secretions and host defense. *Am. Rev. Respir. Dis.* 144, S52–S56.

Kaltschmidt, E., and Wittmann, H.G. (1970). Ribosomal proteins. XII. Number of proteins in small and large ribosomal subunits of *Escherichia coli* as determined by two-dimensional gel electrophoresis. *Proc. Natl. Acad. Sci. U. S. A.* 67, 1276–1282.

Kashchiev, D. (2000). *Nucleation* (Butterworth-Heinemann).

Kastner, B., Stöffler-Meilicke, M., and Stöffler, G. (1981). Arrangement of the subunits in the ribosome of *Escherichia coli*: demonstration by immunoelectron microscopy. *Proc. Natl. Acad. Sci.* 78, 6652–6656.

Kaushal, P.S., Sharma, M.R., Booth, T.M., Haque, E.M., Tung, C.-S., Sanbonmatsu, K.Y., Spremulli, L.L., and Agrawal, R.K. (2014). Cryo-EM structure of the small subunit of the mammalian mitochondrial ribosome. *Proc. Natl. Acad. Sci. U. S. A.* 111, 7284–7289.

Kernodle, DS (2000). Mechanisms of resistance to beta-lactam antibiotics. In *Gram-positive*



pathogens, (Washington, DC, USA: American Society for Microbiology), pp. 609–620.

Khatter, H., Myasnikov, A.G., Natchiar, S.K., and Klaholz, B.P. (2015). Structure of the human 80S ribosome. *Nature* 520, 640–645.

Kluytmans, J., Van Belkum, A., and Verbrugh, H. (1997). Nasal carriage of *Staphylococcus aureus*: Epidemiology, underlying mechanisms, and associated risks. *Clin. Microbiol. Rev.* 10, 505–520.

Knox, K.W., and Wicken, A.J. (1973). Immunological properties of teichoic acids. *Bacteriol. Rev.* 37, 215–257.

Koch, A.L. (2003). Were Gram-positive rods the first bacteria? *Trends Microbiol.* 11, 166–170.

\*Korostelev, A.A. (2011). Structural aspects of translation termination on the ribosome. *RNA* 17, 1409–1421.

Korostelev, A., Trakhanov, S., Laurberg, M., and Noller, H.F. (2006). Crystal Structure of a 70S Ribosome-tRNA Complex Reveals Functional Interactions and Rearrangements. *Cell* 126, 1065–1077.

Korostelev, A., Asahara, H., Lancaster, L., Laurberg, M., Hirschi, A., Zhu, J., Trakhanov, S., Scott, W.G., and Noller, H.F. (2008). Crystal structure of a translation termination complex formed with release factor RF2. *Proc. Natl. Acad. Sci. U. S. A.* 105, 19684–19689.

Kucukelbir, A., Sigworth, F.J., and Tagare, H.D. (2014). Quantifying the local resolution of cryo-EM density maps. *Nat. Methods* 11, 63–65.

Kühlbrandt, W. (2014a). The Resolution Revolution. *Science* (80-. ). 343, 1443–1444.

Kühlbrandt, W. (2014b). Cryo-EM enters a new era. *Elife* 3, e03678.

Kurland, C.G., Voynow, P., Hardy, S.J.S., Randall, L., and Lutter, L. (1969). Physical and functional heterogeneity of *E. coli* ribosomes. In *Cold Spring Harbor Symposia on Quantitative Biology*, (Cold Spring Harbor Laboratory Press), pp. 17–24.

Laemmli, U.K. (1970). Cleavage of structural proteins during the assembly of the head of bacteriophage T4. *Nature* 227, 680–685.

Lagerkvist, U., Rymo, L., Lindqvist, O., and Andersson, E. (1972). Appendix SOME PROPERTIES OF CRYSTALS OF LYSINE TRANSFER RIBONUCLEIC ACID LIGASE FROM YEAST. *J. Biol. Chem.* 247, 3897–3899.

Lake, J.A. (1976). Ribosome structure determined by electron microscopy of *Escherichia coli* small subunits, large subunits and monomeric ribosomes. *J. Mol. Biol.* 105, 131–159.

\*Laurberg, M., Asahara, H., Korostelev, A., Zhu, J., Trakhanov, S., and Noller, H.F. (2008). Structural basis for translation termination on the 70S ribosome. *Nature* 454, 852–857.

- Lee, S.S.J., and Cudney, R. (2004). A modified microdialysis button for use in protein crystallization. *J. Appl. Crystallogr.* 37, 504–505.
- Leeds, J.A., LaMarche, M.J., Brewer, J.T., Bushell, S.M., Deng, G., Dewhurst, J.M., Dzink-Fox, J., Gangl, E., Jain, A., Lee, L., et al. (2011). In vitro and in vivo activities of novel, semisynthetic thiopeptide inhibitors of bacterial elongation factor Tu. *Antimicrob. Agents Chemother.* 55, 5277–5283.
- Lee-Huang, S., Lee, H., and Ochoa, S. (1974). Inhibition of polypeptide chain initiation in *Escherichia coli* by elongation factor G. *Proc. Natl. Acad. Sci. U. S. A.* 71, 2928–2931.
- Li, X., Mooney, P., Zheng, S., Booth, C.R., Braunfeld, M.B., Gubbens, S., Agard, D.A., and Cheng, Y. (2013). Electron counting and beam-induced motion correction enable near-atomic-resolution single-particle cryo-EM. *Nat. Methods* 10, 584–590.
- Lim, D., and Strynadka, N.C.J. (2002). Structural basis for the beta-lactam resistance of PBP2a from methicillin-resistant *Staphylococcus aureus*. *Nat. Struct. Biol.* 9, 870–876.
- \*Lin, J., Gagnon, M.G., Bulkeley, D., and Steitz, T.A. (2015). Conformational changes of elongation factor G on the ribosome during tRNA translocation. *Cell* 160, 219–227.
- Lindberg, M., Jönsson, K., Müller, H.-P., Signäs, C., and Höök, M. (1990). Fibronectin Binding Proteins from *Staphylococcus aureus*. In *Pathogenesis of Wound and Biomaterial-Associated Infections* SE - 6, T. Wadström, I. Eliasson, I. Holder, and Å. Ljungh, eds. (Springer London), pp. 55–63.
- Lippmann, C., Betzel, C., Dauter, Z., Wilson, K., and Erdmann, V.A. (1988). Crystallization and preliminary X-ray diffraction studies of intact EF-Tu from *Thermus aquaticus* YT-1. *FEBS Lett.* 240, 139–142.
- Liu, S., Milne, G.T., Kuremsky, J.G., Fink, G.R., and Leppla, S.H. (2004). Identification of the proteins required for biosynthesis of diphthamide, the target of bacterial ADP-ribosylating toxins on translation elongation factor 2. *Mol. Cell. Biol.* 24, 9487–9497.
- Liu, S., Wiggins, J.F., Sreenath, T., Kulkarni, A.B., Ward, J.M., and Leppla, S.H. (2006). Dph3, a small protein required for diphthamide biosynthesis, is essential in mouse development. *Mol. Cell. Biol.* 26, 3835–3841.
- Liu, S., Bachran, C., Gupta, P., Miller-Randolph, S., Wang, H., Crown, D., Zhang, Y., Wein, A.N., Singh, R., Fattah, R., et al. (2012). Diphthamide modification on eukaryotic elongation factor 2 is needed to assure fidelity of mRNA translation and mouse development. *Proc. Natl. Acad. Sci.* 109, 13817–13822.
- Le Loir, Y., Baron, F., and Gautier, M. (2003). *Staphylococcus aureus* and food poisoning.

Genet. Mol. Res. 2, 63–76.

Lowy, F.D. (1998). Medical progress - Staphylococcus aureus infections. *N. Engl. J. Med.* 339, 520–532.

Lowy, F.D. (2000). Is Staphylococcus aureus an intracellular pathogen? *Trends Microbiol.* 8, 341–343.

Luft, J.R., Newman, J., and Snell, E.H. (2014). Crystallization screening: The influence of history on current practice. *Acta Crystallogr. Sect. FStructural Biol. Commun.* 70, 835–853.

Luong, T.T., Sau, K., Roux, C., Sau, S., Dunman, P.M., and Lee, C.Y. (2011). Staphylococcus aureus ClpC divergently regulates capsule via sae and codY in strain Newman but activates capsule via codY in strain UAMS-1 and in strain Newman with repaired saeS. *J. Bacteriol.* 193, 686–694.

Lyon, B.R., Iuorio, J.L., May, J.W., and Skurray, R.A. (1984). Molecular epidemiology of multiresistant Staphylococcus aureus in Australian hospitals. *J. Med. Microbiol.* 17, 79–89.

Lyumkis, D., Moeller, A., Cheng, A., Herold, A., Hou, E., Irving, C., Jacovetty, E.L., Lau, P.W., Mulder, A.M., Pulokas, J., et al. (2010). Automation in Single-Particle Electron Microscopy. *Connecting the Pieces.*

Mainiero, M., Goerke, C., Geiger, T., Gonser, C., Herbert, S., and Wolz, C. (2010). Differential target gene activation by the Staphylococcus aureus two-component system saeRS. *J. Bacteriol.* 192, 613–623.

Manuell, A.L., Quispe, J., and Mayfield, S.P. (2007). Structure of the chloroplast ribosome: Novel domains for translation regulation. *PLoS Biol.* 5, 1785–1797.

Mateyak, M.K., and Kinzy, T.G. (2010). eEF1A: Thinking outside the ribosome. *J. Biol. Chem.* 285, 21209–21213.

McClure, W.R., and Cech, C.L. (1978). On the mechanism of rifampicin inhibition of RNA synthesis. *J. Biol. Chem.* 253, 8949–8956.

McManus, M.C. (1997). Mechanisms of bacterial resistance to antimicrobial agents. *Am. J. Health. Syst. Pharm.* 54, 1420–1433; quiz 1444–1446.

McMullan, G., Chen, S., Henderson, R., and Faruqi, A.R. (2009a). Detective quantum efficiency of electron area detectors in electron microscopy. *Ultramicroscopy* 109, 1126–1143.

McMullan, G., Clark, A.T., Turchetta, R., and Faruqi, A.R. (2009b). Enhanced imaging in low dose electron microscopy using electron counting. *Ultramicroscopy* 109, 1411–1416.

McPherson, A. (2004). Introduction to protein crystallization. *Methods* 34, 254–265.

Melnikov, S., Ben-Shem, A., Garreau de Loubresse, N., Jenner, L., Yusupova, G., and Yusupov, M. (2012). One core, two shells: bacterial and eukaryotic ribosomes. *Nat. Struct. Mol. Biol.* 19, 560–



567.

Melnikov, S., Mailliot, J., Byung-Sik S., Rigger L., Neuner S., Dever T., Micura R., Yusupova G. and Yusupov M. (2015). Insights into the hypusine-induced peptide-bond formation by the eukaryotic ribosome. *Nature*.

Mikol, V., Hirsch, E., and Giege, R. (1990). Diagnostic of precipitant for biomacromolecule crystallization by quasi-elastic light-scattering. *J. Mol. Biol.* 213, 187–195.

Milazzo, A.-C., Cheng, A., Moeller, A., Lyumkis, D., Jacovetty, E., Polukas, J., Ellisman, M.H., Xuong, N.-H., Carragher, B., and Potter, C.S. (2011). Initial evaluation of a direct detection device detector for single particle cryo-electron microscopy. *J. Struct. Biol.* 176, 404–408.

Mindell, J.A., and Grigorieff, N. (2003). Accurate determination of local defocus and specimen tilt in electron microscopy. *J. Struct. Biol.* 142, 334–347.

Moesby, L., Hansen, E.W., Christensen, J.D., Høyer, C.H., Juhl, G.L., and Olsen, H.B. (2005). Dry and moist heat sterilisation cannot inactivate pyrogenicity of Gram positive microorganisms. *Eur. J. Pharm. Sci.* 26, 318–323.

Mohan, S., Donohue, J.P., and Noller, H.F. (2014). Molecular mechanics of 30S subunit head rotation. *Proc. Natl. Acad. Sci. U. S. A.* 111, 13325–13330.

Moran Jr, C.P. (1993). RNA polymerase and transcription factors. *Bacillus Subtilis Other Gram-Positive Bact. Biochem. Physiol. Mol. Genet. Am. Soc. Microbiol. Washington, DC* 653–667.

Morfeltdt, E., Janzou, L., Arvidson, S., and Löfdahl, S. (1988). Cloning of a chromosomal locus (exp) which regulates the expression of several exoprotein genes in *Staphylococcus aureus*. *MGG Mol. Gen. Genet.* 211, 435–440.

Morgan, M. (2011). Treatment of MRSA soft tissue infections: An overview. *Injury* 42, S11–S17.

Morita, Y., Kodama, K., Shiota, S., Mine, T., Kataoka, A., Mizushima, T., and Tsuchiya, T. (1998). NorM, putative multidrug efflux protein, of *Vibrio parahaemolyticus* and its homolog in *Escherichia coli*. *Antimicrob. Agents Chemother.* 42, 1778–1782.

\*\*Muhs, M., Hilal, T., Mielke, T., Skabkin, M.A., Sanbonmatsu, K.Y., Pestova, T. V, and Spahn, C.M.T. (2015). Cryo-EM of ribosomal 80S complexes with termination factors reveals the translocated cricket paralysis virus IRES. *Mol. Cell* 57, 422–432.

Neely, A.N., and Maley, M.P. (2000). Survival of enterococci and staphylococci on hospital fabrics and plastic. *J. Clin. Microbiol.* 38, 724–726.

Neu, H.C. (1992). The crisis in antibiotic resistance. *Science* 257, 1064–1073.

Newman, J. (2006). A review of techniques for maximizing diffraction from a protein crystal in



stilla. In *Acta Crystallographica Section D: Biological Crystallography*, pp. 27–31.

Nissen, P., Hansen, J., Ban, N., Moore, P.B., and Steitz, T.A. (2000). The structural basis of ribosome activity in peptide bond synthesis. *Science* (80- ). 289, 920–930.

Noll, M., and Noll, H. (1976). Structural dynamics of bacterial ribosomes: V. Magnesium-dependent dissociation of tight couples into subunits: Measurements of dissociation constants and exchange rates. *J. Mol. Biol.* 105, 111–127.

Norvick, R.P., and Jiang, D. (2003). The staphylococcal *saeRS* system coordinates environmental signals agr quorum sensing. *Microbiology* 149, 2709–2717.

Novick, R.P., Ross, H.F., Projan, S.J., Kornblum, J., Kreiswirth, B., and Moghazeh, S. (1993). Synthesis of staphylococcal virulence factors is controlled by a regulatory RNA molecule. *EMBO J.* 12, 3967–3975.

O'Farrell, P.H. (1975). High resolution two-dimensional electrophoresis of proteins. *J. Biol. Chem.* 250, 4007–4021.

O'Riordan, K., and Lee, J.C. (2004). *Staphylococcus aureus* capsular polysaccharides. *Clin. Microbiol. Rev.* 17, 218–234.

Ortiz, P.A., Ulloque, R., Kihara, G.K., Zheng, H., and Kinzy, T.G. (2006). Translation elongation factor 2 anticodon mimicry domain mutants affect fidelity and diphtheria toxin resistance. *J. Biol. Chem.* 281, 32639–32648.

Ovchinnikov, L.P., Motuz, L.P., Natapov, P.G., Averbuch, L.J., Wettenhall, R.E.H., Szyszka, R., Kramer, G., and Hardesty, B. (1990). Three phosphorylation sites in elongation factor 2. *FEBS Lett.* 275, 209–212.

\*\*Pallesen, J., Hashem, Y., Korkmaz, G., Koripella, R.K., Huang, C., Ehrenberg, M., Sanyal, S., and Frank, J. (2013). Cryo-EM visualization of the ribosome in termination complex with apo-RF3 and RF1. *Elife* 2013.

Park, J.H., Johansson, H.E., Aoki, H., Huang, B., Kim, H.Y., Ganoza, M.C., and Park, M.H. (2012). Post-translational modification by beta-lysylation is required for the activity of *E. coli* Elongation Factor P (EF-P). *J Biol Chem* 287, 2579–2590.

Pearson, M. (2011) Crystal structures of naturally inhibited ribosomes (Doctoral thesis, University of California, Santa Cruz). Retrieved from: <http://gradworks.umi.com/34/52/3452518.html>

Penczek, P.A. (2010). Image restoration in cryo-electron microscopy. *Methods Enzymol.* 482, 35–72.

Perutz, M.F., Rossmann, M.G., Cullis, A.N.N.F., Muirhead, H., WILL, G., and North, A.C.T.



(1960). Structure of Haemoglobin: A Three-Dimensional Fourier Synthesis at 5.5- $\text{\AA}$  Resolution, Obtained by X-Ray Analysis. *Nature* 185, 416–422.

Peschel, A., Jack, R.W., Otto, M., Collins, L. V, Staubitz, P., Nicholson, G., Kalbacher, H., Nieuwenhuizen, W.F., Jung, G., Tarkowski, A., et al. (2001). Staphylococcus aureus resistance to human defensins and evasion of neutrophil killing via the novel virulence factor MprF is based on modification of membrane lipids with l-lysine. *J. Exp. Med.* 193, 1067–1076.

\*Petry, S., Brodersen, D.E., Murphy IV, F. V., Dunham, C.M., Selmer, M., Tarry, M.J., Kelley, A.C., and Ramakrishnan, V. (2005). Crystal structures of the ribosome in complex with release factors RF1 and RF2 bound to a cognate stop codon. *Cell* 123, 1255–1266.

Pettersen, E.F., Goddard, T.D., Huang, C.C., Couch, G.S., Greenblatt, D.M., Meng, E.C., and Ferrin, T.E. (2004). UCSF Chimera—A visualization system for exploratory research and analysis. *J. Comput. Chem.* 25, 1605–1612.

Poehlsgaard, J., and Douthwaite, S. (2003). Macrolide antibiotic interaction and resistance on the bacterial ribosome. *Curr. Opin. Investig. Drugs* 4, 140–148.

Polacek, N., and Mankin, A.S. (2005). The ribosomal peptidyl transferase center: structure, function, evolution, inhibition. *Crit. Rev. Biochem. Mol. Biol.* 40, 285–311.

\*Polikanov, Y.S., Blaha, G.M., and Steitz, T.A. (2012). How Hibernation Factors RMF, HPF, and YfiA Turn Off Protein Synthesis. *Science* (80- ). 336, 915–918.

Poole, K. (2004). Resistance to  $\beta$ -lactam antibiotics. *Cell. Mol. Life Sci.* 61, 2200–2223.

Pootoolal, J., Neu, J., and Wright, G.D. (2002). Glycopeptide antibiotic resistance. *Annu. Rev. Pharmacol. Toxicol.* 42, 381–408.

Price, N.T., Redpath, N.T., Severinov, K. V, Campbell, D.G., Russell, J.M., and Proud, C.G. (1991). Identification of the phosphorylation sites in elongation factor-2 from rabbit reticulocytes. *FEBS Lett.* 282, 253–258.

\*Pulk, A., and Cate, J.H.D. (2013). Control of ribosomal subunit rotation by elongation factor G. *Science* 340, 1235970.

Qin, Y., Polacek, N., Vesper, O., Staub, E., Einfeldt, E., Wilson, D.N., and Nierhaus, K.H. (2006). The Highly Conserved LepA Is a Ribosomal Elongation Factor that Back-Translocates the Ribosome. *Cell* 127, 721–733.

\*Qu, X., Wen, J.-D., Lancaster, L., Noller, H.F., Bustamante, C., and Tinoco, I. (2011). The ribosome uses two active mechanisms to unwind messenger RNA during translation. *Nature* 475, 118–121.

Ramakrishnan, V., and Moore, P.B. (2001). Atomic structures at last: The ribosome in 2000.

Curr. Opin. Struct. Biol. 11, 144–154.

Rammelkamp, C.H., and Maxon, T. (1942). Resistance of *Staphylococcus aureus* to the Action of Penicillin. *Exp. Biol. Med.* 51, 386–389.

\*\*Ramrath, D.J.F., Lancaster, L., Sprink, T., Mielke, T., Loerke, J., Noller, H.F., and Spahn, C.M.T. (2013). Visualization of two transfer RNAs trapped in transit during elongation factor G-mediated translocation. *Proc. Natl. Acad. Sci. U. S. A.* 110, 20964–20969.

Rayner, C., and Munckhof, W.J. (2005). Antibiotics currently used in the treatment of infections caused by *Staphylococcus aureus*. *Intern. Med. J.* 35 Suppl 2, S3–S16.

Recsei, P., Kreiswirth, B., O'Reilly, M., Schlievert, P., Gruss, A., and Novick, R.P. (1986). Regulation of exoprotein gene expression in *Staphylococcus aureus* by *agr*. *MGG Mol. Gen. Genet.* 202, 58–61.

Robertson, E.S., Aggison, L.A., and Nicholson, A.W. (1994). Phosphorylation of elongation factor G and ribosomal protein S6 in bacteriophage T7-infected *Escherichia coli*. *Mol. Microbiol.* 11, 1045–1057.

Rodnina, M. V, Savelsbergh, A., Katunin, V.I., and Wintermeyer, W. (1997). Hydrolysis of GTP by elongation factor G drives tRNA movement on the ribosome. *Nature* 385, 37–41.

Rohou, A., and Grigorieff, N. (2015). CTFFIND4: Fast and accurate defocus estimation from electron micrographs. *J. Struct. Biol.*

Rosenthal, P.B., and Henderson, R. (2003). Optimal Determination of Particle Orientation, Absolute Hand, and Contrast Loss in Single-particle Electron Cryomicroscopy. *J. Mol. Biol.* 333, 721–745.

Roy, H., Zou, S.B., Bullwinkle, T.J., Wolfe, B.S., Gilreath, M.S., Forsyth, C.J., Navarre, W.W., and Ibba, M. (2011). The tRNA synthetase paralog PoxA modifies elongation factor-P with (R)- $\beta$ -lysine. *Nat. Chem. Biol.* 7, 667–669.

\*Rozov, A., Demeshkina, N., Westhof, E., Yusupov, M., and Yusupova, G. (2015). Structural insights into the translational infidelity mechanism. *Nat Commun* 6.

Rubinstein, J.L., and Brubaker, M.A. (2015). Alignment of cryo-EM movies of individual particles by optimization of image translations. *J. Struct. Biol.*

Russo, C.J., and Passmore, L.A. (2014). Ultrastable gold substrates for electron cryomicroscopy. *Sci.* 346, 1377–1380.

Salemme, F.R. (1972). A free interface diffusion technique for the crystallization of proteins for x-ray crystallography. *Arch. Biochem. Biophys.* 151, 533–539.

Sambrook, J; Fritsch, E.F.M.T. (1989). *Molecular Cloning: A laboratory manual*. In Cold Spring



Harbour,.

Sanchez-Weatherby, J., Bowler, M.W., Huet, J., Gobbo, A., Felisaz, F., Lavault, B., Moya, R., Kadlec, J., Ravelli, R.B.G., and Cipriani, F. (2009). Improving diffraction by humidity control: A novel device compatible with X-ray beamlines. *Acta Crystallogr. Sect. D Biol. Crystallogr.* 65, 1237–1246.

Saridakis, E., and Chayen, N.E. (2003). Systematic improvement of protein crystals by determining the supersolubility curves of phase diagrams. *Biophys. J.* 84, 1218–1222.

Savelsbergh, A., Matassova, N.B., Rodnina, M. V, and Wintermeyer, W. (2000). Role of domains 4 and 5 in elongation factor G functions on the ribosome. *J. Mol. Biol.* 300, 951–961.

Scheres, S.H. (2014). Beam-induced motion correction for sub-megadalton cryo-EM particles. *Elife* 3, e03665.

Scheres, S.H.W. (2012). RELION: implementation of a Bayesian approach to cryo-EM structure determination. *J. Struct. Biol.* 180, 519–530.

Scheres, S.H.W., and Chen, S. (2012). Prevention of overfitting in cryo-EM structure determination. *Nat Meth* 9, 853–854.

Schlunzen, F., Tocilj, A., Zarivach, R., Harms, J., Gluehmann, M., Janell, D., Bashan, A., Bartels, H., Agmon, I., Franceschi, F., et al. (2000). Structure of functionally activated small ribosomal subunit at 3.3 angstroms resolution. *Cell* 102, 615–623.

Schlünzen, F., Pyetan, E., Fucini, P., Yonath, A., and Harms, J.M. (2004). Inhibition of peptide bond formation by pleuromutilins: The structure of the 50S ribosomal subunit from *Deinococcus radiodurans* in complex with tiamulin. *Mol. Microbiol.* 54, 1287–1294.

Schuwirth, B.S., Borovinskaya, M.A., Hau, C.W., Zhang, W., Vila-Sanjurjo, A., Holton, J.M., and Cate, J.H.D. (2005). Structures of the bacterial ribosome at 3.5 Å resolution. *Science* 310, 827–834.

Selmer, M., Dunham, C.M., Murphy, F. V, Weixlbaumer, A., Petry, S., Kelley, A.C., Weir, J.R., and Ramakrishnan, V. (2006). Structure of the 70S ribosome complexed with mRNA and tRNA. *Science* 313, 1935–1942.

Shigematsu, H., and Sigworth, F.J. (2013). Noise models and cryo-EM drift correction with a direct-electron camera. *Ultramicroscopy* 131, 61–69.

Shockman, G.D., and Barren, J.F. (1983). Structure, function, and assembly of cell walls of gram-positive bacteria. *Annu. Rev. Microbiol.* 37, 501–527.

Shockman, G.D., Daneo-Moore, L., Kariyama, R., and Massidda, O. (1996). Bacterial walls, peptidoglycan hydrolases, autolysins, and autolysis. *Microb. Drug Resist.* 2, 95–98.

Shoham, M., Müssig, J., Shevack, A., Arad, T., Wittmann, H.G., and Yonath, A. (1986). A new crystal form of large ribosomal subunits from *Halobacterium marismortui*. *FEBS Lett.* 208, 321–324.

- Sitikov, A.S., Davydova, E.K., Bezlepina, T.A., Ovchinnikov, L.P., and Spirin, A.S. (1984). Eukaryotic elongation factor 2 loses its non-specific affinity for RNA and leaves polyribosomes as a result of ADP-ribosylation. *FEBS Lett.* 176, 406–410.
- Sohmen, D., Harms, J.M., Schlünzen, F., and Wilson, D.N. (2009). of Protein Synthesis I.
- Sohmen, D., Chiba, S., Shimokawa-Chiba, N., Innis, C.A., Berninghausen, O., Beckmann, R., Ito, K., and Wilson, D.N. (2015). Structure of the *Bacillus subtilis* 70S ribosome reveals the basis for species-specific stalling. *Nat Commun* 6.
- Song, M.D., Wachi, M., Doi, M., Ishino, F., and Matsushashi, M. (1987). Evolution of an inducible penicillin-target protein in methicillin-resistant *Staphylococcus aureus* by gene fusion. *FEBS Lett.* 221, 167–171.
- Sorzano, C.O.S., Marabini, R., Velázquez-Muriel, J., Bilbao-Castro, J.R., Scheres, S.H.W., Carazo, J.M., and Pascual-Montano, A. (2004). XMIPP: a new generation of an open-source image processing package for electron microscopy. *J. Struct. Biol.* 148, 194–204.
- \*\*Spahn, C.M.T., Gomez-Lorenzo, M.G., Grassucci, R.A., Jørgensen, R., Andersen, G.R., Beckmann, R., Penczek, P.A., Ballesta, J.P.G., and Frank, J. (2004a). Domain movements of elongation factor eEF2 and the eukaryotic 80S ribosome facilitate tRNA translocation. *EMBO J.* 23, 1008–1019.
- \*\*Spahn, C.M.T., Jan, E., Mulder, A., Grassucci, R.A., Sarnow, P., and Frank, J. (2004b). Cryo-EM visualization of a viral internal ribosome entry site bound to human ribosomes: The IRES functions as an RNA-based translation factor. *Cell* 118, 465–475.
- Spirin, A.S., Sabo, B., and Kovalenko, V.A. (1971). Dependence of dissociation—association of uncharged ribosomes of *Escherichia coli* on the Mg<sup>2+</sup> concentration, ionic strength, pH and temperature. *FEBS Lett.* 15, 197–200.
- Spirin, A.S., Belitsina, N. V, and Lishnevskaya, E.B. (1972). On some artifacts of sucrose gradient sedimentation of ribosomes. *FEBS Lett.* 24, 219–224.
- Stahli, C., and Noll, H. (1977). Structural dynamics of bacterial ribosomes. *Mol. Gen. Genet.* MGG 153, 159–168.
- Stark, H., Mueller, F., Orlova, E. V, Schatz, M., Dube, P., Erdemir, T., Zemlin, F., Brimacombe, R., and van Heel, M. (1995). The 70S *Escherichia coli* ribosome at 23 Å resolution: fitting the ribosomal RNA. *Structure* 3, 815–821.
- Starosta, A.L., Lassak, J., Jung, K., and Wilson, D.N. (2014). The bacterial translation stress response. *FEMS Microbiol. Rev.* 38, 1172–1201.
- Sun, F., Li, C., Jeong, D., Sohn, C., He, C., and Bae, T. (2010). In the *Staphylococcus aureus* two-



component system *sae*, the response regulator SaeR Binds to a direct repeat sequence and DNA binding requires phosphorylation by the sensor kinase SaeS. *J. Bacteriol.* 192, 2111–2127.

\*\*Svidritskiy, E., Brilot, A.F., Koh, C.S., Grigorieff, N., and Korostelev, A.A. (2014). Structures of yeast 80S ribosome-tRNA complexes in the rotated and nonrotated conformations. *Structure* 22, 1210–1218.

\*\*Taylor, D., Unbehauen, A., Li, W., Das, S., Lei, J., Liao, H.Y., Grassucci, R.A., Pestova, T. V., and Frank, J. (2012). Cryo-EM structure of the mammalian eukaryotic release factor eRF1-eRF3-associated termination complex. *Proc. Natl. Acad. Sci.*

Teng, T.Y. (1990). Mounting of crystals for macromolecular crystallography in a free-standing thin film. *J. Appl. Crystallogr.* 23, 387–391.

Tenson, T., and Mankin, A. (2006). Antibiotics and the ribosome. *Mol Microbiol* 59, 1664–1677.

Tong, Y., Park, I., Hong, B.S., Nedyalkova, L., Tempel, W., and Park, H.W. (2009). Crystal structure of human eIF5A1: Insight into functional similarity of human eIF5A1 and eIF5A2. *Proteins Struct. Funct. Bioinforma.* 75, 1040–1045.

\*Tourigny, D.S., Fernández, I.S., Kelley, A.C., and Ramakrishnan, V. (2013). Elongation factor G bound to the ribosome in an intermediate state of translocation. *Science* 340, 1235490.

Trakhanov, S.D., Yusupov, M.M., Agalarov, S.C., Garber, M.B., Ryazantsev, S.N., Tischenko, S.V., and Shirokov, V.A. (1987). Crystallization of 70 S ribosomes and 30 S ribosomal subunits from *Thermus thermophilus*. *FEBS Lett.* 220, 319–322.

Tran, J.H., Jacoby, G.A., and Hooper, D.C. (2005a). Interaction of the plasmid-encoded quinolone resistance protein Qnr with *Escherichia coli* DNA gyrase. *Antimicrob. Agents Chemother.* 49, 118–125.

Tran, J.H., Jacoby, G.A., and Hooper, D.C. (2005b). Interaction of the plasmid-encoded quinolone resistance protein QnrA with *Escherichia coli* topoisomerase IV. *Antimicrob. Agents Chemother.* 49, 3050–3052.

Ueta, M., Wada, C., and Wada, A. (2010). Formation of 100S ribosomes in *Staphylococcus aureus* by the hibernation promoting factor homolog SaHPF. *Genes to Cells* 15, 43–58.

Utsui, Y., and Yokota, T. (1985). Role of an altered penicillin-binding protein in methicillin- and cephem-resistant *Staphylococcus aureus*. *Antimicrob. Agents Chemother.* 28, 397–403.

VandenBergh, M.F.Q., Yzerman, E.P.F., Van Belkum, A., Boelens, H.A.M., Sijmons, M., and Verbrugh, H.A. (1999). Follow-up of *Staphylococcus aureus* nasal carriage after 8 years: Redefining the persistent carrier state. *J. Clin. Microbiol.* 37, 3133–3140.



Vasiliev, V.D. (1974). Morphology of the ribosomal 30S subparticle according to electron microscopic data. *Acta Biol. Med. Ger.* 33, 779.

Vasiliev, V.D., Selivanova, O.M., Baranov, V.I., and Spirin, A.S. (1983). Structural study of translating 70 S ribosomes from *Escherichia coli*. I. Electron microscopy. *FEBS Lett.* 155, 167–172.

Vila-Sanjurjo, A., Ridgeway, W.K., Seymaner, V., Zhang, W., Santoso, S., Yu, K., and Cate, J.H.D. (2003). X-ray crystal structures of the WT and a hyper-accurate ribosome from *Escherichia coli*. *Proc. Natl. Acad. Sci. U. S. A.* 100, 8682–8687.

Vogele, L., Palm, G.J., Mesters, J.R., and Hilgenfeld, R. (2001). Conformational change of elongation factor Tu (EF-Tu) induced by antibiotic binding. Crystal structure of the complex between EF-Tu??GDP and aurodox. *J. Biol. Chem.* 276, 17149–17155.

Voorhees, R.M., Fernández, I.S., Scheres, S.H.W., and Hegde, R.S. (2014). Structure of the mammalian ribosome-Sec61 complex to 3.4 Å resolution. *Cell* 157, 1632–1643.

Voyich, J.M., Vuong, C., DeWald, M., Nygaard, T.K., Kocianova, S., Griffith, S., Jones, J., Iverson, C., Sturdevant, D.E., Braughton, K.R., et al. (2009). The SaeR/S gene regulatory system is essential for innate immune evasion by *Staphylococcus aureus*. *J. Infect. Dis.* 199, 1698–1706.

Wade, R.H. (1992). A brief look at imaging and contrast transfer. *Ultramicroscopy* 46, 145–156.

Wagenknecht, T., Carazo, J.M., Radermacher, M., and Frank, J. (1989). Three-dimensional reconstruction of the ribosome from *Escherichia coli*. *Biophys. J.* 55, 455–464.

Waldvogel, F.A. (1995). *Staphylococcus aureus* (including toxic shock syndrome). *Princ. Pract. Infect. Dis.* Churchill Livingstone, New York, NY 1754–1777.

Wang, L., and Sigworth, F.J. (2006). Cryo-EM and single particles. *Physiology (Bethesda)*. 21, 13–18.

Washburn, M.P., Wolters, D., and Yates, J.R. (2001). Large-scale analysis of the yeast proteome by multidimensional protein identification technology. *Nat. Biotechnol.* 19, 242–247.

Watson, J.D., and Crick, F.H. (1953). Molecular structure of nucleic acids. *Nature* 171, 737–738.

\*Weixlbaumer, A., Jin, H., Neubauer, C., Voorhees, R.M., Petry, S., Kelley, A.C., and Ramakrishnan, V. (2008). Insights into translational termination from the structure of RF2 bound to the ribosome. *Science* 322, 953–956.

World Health Organization. 2015. Drug resistance. Worldwide country situation analysis: response to antimicrobial resistance. Web. Publication date: 29 April 2015, ISBN: 978 92 4 156494 6, WHO reference number: WHO/HSE/PED/AIP/2015.1

Wilkinson, B.J. (1997). The staphylococci in human disease. Biology (Basel).

Williamson, M.P., Havel, T.F., and Wüthrich, K. (1985). Solution conformation of proteinase inhibitor IIA from bull seminal plasma by <sup>1</sup>H nuclear magnetic resonance and distance geometry. *J. Mol. Biol.* 182, 295–315.

Wilson, D.N. (2011). On the specificity of antibiotics targeting the large ribosomal subunit. *Ann. N. Y. Acad. Sci.* 1241, 1–16.

Wilson, D.N. (2014). Ribosome-targeting antibiotics and mechanisms of bacterial resistance. *Nat. Rev. Microbiol.* 12, 35–48.

Wimberly, B.T., Brodersen, D.E., Clemons, W.M., Morgan-Warren, R.J., Carter, A.P., Vornrhein, C., Hartsch, T., and Ramakrishnan, V. (2000). Structure of the 30S ribosomal subunit. *Nature* 407, 327–339.

Woese, C.R. (1987). Bacterial evolution. *Microbiol. Rev.* 51, 221–271.

Wolf, H., Chinali, G., and Parmeggiani, A. (1974). Kirromycin, an inhibitor of protein biosynthesis that acts on elongation factor Tu. *Proc. Natl. Acad. Sci. U. S. A.* 71, 4910–4914.

\*\*Wong, W., Bai, X., Brown, A., Fernandez, I.S., Hanssen, E., Condrón, M., Tan, Y.H., Baum, J., and Scheres, S.H.W. (2014). Cryo-EM structure of the *Plasmodium falciparum* 80S ribosome bound to the anti-protozoan drug emetine. *Elife* 3.

Yamaguchi, K., and Subramanian, A.R. (2000). The plastid ribosomal proteins. Identification of all the proteins in the 50 S subunit of an organelle ribosome (chloroplast). *J. Biol. Chem.* 275, 28466–28482.

Yanagisawa, T., Sumida, T., Ishii, R., Takemoto, C., and Yokoyama, S. (2010). A paralog of lysyl-tRNA synthetase aminoacylates a conserved lysine residue in translation elongation factor P. *Nat. Struct. Mol. Biol.* 17, 1136–1143.

Yonath, A., Bartunik, H.D., Bartels, K.S., and Wittmann, H.G. (1984). Some X-ray diffraction patterns from single crystals of the large ribosomal subunit from *Bacillus stearothermophilus*. *J. Mol. Biol.* 177, 201–206.

Yonath, A., Saper, M.A., Makowski, I., Müssig, J., Piefke, J., Bartunik, H.D., Bartels, K.S., and Wittmann, H.G. (1986). Characterization of single crystals of the large ribosomal particles from *Bacillus stearothermophilus*. *J. Mol. Biol.* 187, 633–636.

Yoshida, H., Maki, Y., Kato, H., Fujisawa, H., Izutsu, K., Wada, C., and Wada, A. (2002). The ribosome modulation factor (RMF) binding site on the 100S ribosome of *Escherichia coli*. *J. Biochem.* 132, 983–989.

Yusupov, M.M., Trakhanov, S.D., Barynin, V. V., Boroviagin, V.L., and Garber, M.B. (1987).

Crystallization of 30S subparticles from *Thermus thermophilus* ribosomes (Kristallizatsiia 30 S subchastits ribosom *Thermus thermophilus*). In *Doklady Akad Nauk (USSR)*, pp. 1271–1274.

Yusupov, M.M., Yusupova, G.Z., Baucom, a, Lieberman, K., Earnest, T.N., Cate, J.H., and Noller, H.F. (2001). Crystal structure of the ribosome at 5.5 Å resolution. *Science* 292, 883–896.

Yusupova, G.Z., Yusupov, M.M., Cate, J.H.D., and Noller, H.F. (2001). The path of messenger RNA through the ribosome. *Cell* 106, 233–241.

Zeppezauer, M., Eklund, H., and Zeppezauer, E.S. (1968). Micro diffusion cells for the growth of single protein crystals by means of equilibrium dialysis. *Arch. Biochem. Biophys.* 126, 564–573.

Zhang, W., Dunkle, J.A., and Cate, J.H.D. (2009). Structures of the ribosome in intermediate states of ratcheting. *Science* 325, 1014–1017.

\*Zhou, J., Korostelev, A., Lancaster, L., and Noller, H.F. (2012). Crystal structures of 70S ribosomes bound to release factors RF1, RF2 and RF3. *Curr. Opin. Struct. Biol.* 22, 733–742.

\*Zhou, J., Lancaster, L., Donohue, J.P., and Noller, H.F. (2013). Crystal structures of EF-G-ribosome complexes trapped in intermediate states of translocation. *Science* 340, 1236086.

\*Zhou, J., Lancaster, L., Donohue, J.P., and Noller, H.F. (2014). How the ribosome hands the A-site tRNA to the P site during EF-G-catalyzed translocation. *Sci.* 345, 1188–1191.

# Structural studies of the *Staphylococcus aureus* ribosome

## Résumé

Le ribosome est une machinerie cellulaire importante impliquée dans la synthèse protéique de toute cellule vivante. Par conséquent, le ribosome est l'une des principales cibles des antibiotiques naturels, qui sont capables de tuer les cellules bactériennes en bloquant la synthèse protéique. Toutefois, certaines bactéries sont résistantes à ces antibiotiques en raison de petites modifications au niveau de leurs ribosomes. Entre autres, *Staphylococcus aureus* (*S. aureus*) est un agent pathogène responsable de nombreuses infections graves chez l'Homme. Les structures cristallines d'antibiotiques en complexe avec des ribosomes de bactéries non-résistantes, non-pathogènes, Gram négatives ont fourni un aperçu sans précédent des mécanismes d'action de ces antibiotiques. Cependant, aucune structure de ribosome de bactéries pathogènes, hautement résistantes, Gram positives telles que *S. aureus* n'a encore été identifiée.

Dans cette étude, nous présentons la première structure de ribosome de *S. aureus* à haute résolution (3.9 Å) résolue par cryo-microscopie électronique (cryo-ME). Nous mettons en évidence plusieurs caractéristiques de l'organisation des ribosomes spécifiques des bactéries Gram-positives. Nous décrivons également le protocole de purification et de cristallisation du ribosome de *S. aureus* pour de futures études de cryo-ME et de cristallographie aux rayons X.

Tous les résultats obtenus dans ces travaux, faciliteront la description à l'échelle atomique du ribosome de *S. aureus* et ses complexes fonctionnels dans un futur proche. La combinaison des méthodes de cristallographie aux rayons X et de cryo-ME aidera à atteindre cet objectif. Les résultats obtenus serviront de base pour le développement de nouveaux composés contre la bactérie pathogène et extrêmement résistante qu'est *S. aureus*.

Mots clés: *Staphylococcus aureus*, traduction, ribosome, structure, cristallographie, cryo-ME

## Summary

The ribosome is a large cellular machinery that performs the protein synthesis in every living cell. Therefore, the ribosome is one of the major targets of naturally produced antibiotics, which can kill bacterial cells by blocking protein synthesis. However, some bacteria are resistant to these antibiotics due to small modifications of their ribosomes. Among them, *Staphylococcus aureus* (*S. aureus*), a severe pathogen that causes numerous infections in humans. The crystal structures of complexes of antibiotics with ribosomes from Gram-negative non-pathogenic non-resistant bacteria have provided unparalleled insight into mechanisms of antibiotics action and promoted the development of new semi-synthetic and synthetic antibiotics. However, the structure of the ribosome from Gram-positive pathogenic and highly resistant bacteria such as *S. aureus* was still unidentified.

In this study we present the first high resolution structure of the ribosome from *S. aureus* solved at 3.9 Å by cryo-electron microscopy (cryo-EM). We demonstrate several features of the ribosome organization which are unique for Gram-positive bacteria. We also describe the protocol of purification and crystallization of *S. aureus* ribosome for future cryo-EM and X-ray crystallography studies.

All the results obtained in this work will help to describe *S. aureus* ribosome and its functional complexes at the atomic level in the nearest future. The combination of X-ray crystallography and cryo-EM methods will help to achieve this aim. The obtained results will provide a foundation for the development of new compounds against pathogenic and extremely resistant bacteria *S. aureus*.

Key words: *Staphylococcus aureus*, translation, ribosome, structure, crystallography, cryo-EM